HIGH-ORDER DISCONTINUOUS GALERKIN METHODS FOR INCOMPRESSIBLE FLOWS

Adeline de Montlaur

Doctoral Thesis
Advisors: Antonio Huerta and Sonia Fernández-Méndez
Barcelona, September 2009

Escola Politècnica Superior de Castelldefels
Programa de Doctorat en Ciència i Tecnologia Aerospacial

Abstract

High-order Discontinuous Galerkin methods for incompressible flows

Adeline de Montlaur

This PhD thesis proposes divergence-free Discontinuous Galerkin formulations providing high orders of accuracy for incompressible viscous flows.

A new Interior Penalty Discontinuous Galerkin (IPM-DG) formulation is developed, leading to a symmetric and coercive bilinear weak form for the diffusion term, and achieving high-order spatial approximations. It is applied to the solution of the Stokes and Navier-Stokes equations. The velocity approximation space is decomposed in every element into a solenoidal part and an irrotational part. This allows to split the IPM weak form in two uncoupled problems. The first one solves for velocity and hybrid pressure, and the second one allows the evaluation of pressures in the interior of the elements. This results in an important reduction of the total number of degrees of freedom for both velocity and pressure. The introduction of an extra penalty parameter leads to an alternative DG formulation for the computation of solenoidal velocities with no presence of pressure terms. Pressure can then be computed as a post-process of the velocity solution. Other DG formulations, such as the Compact Discontinuous Galerkin method, are contemplated and compared to IPM-DG.

High-order Implicit Runge-Kutta methods are then proposed to solve transient incompressible problems, allowing to obtain unconditionally stable schemes with high orders of accuracy in time. For this purpose, the unsteady incompressible Navier-Stokes equations are interpreted as a system of Differential Algebraic Equations, that is a system of ordinary differential equations corresponding to the conservation of momentum equation, plus algebraic constraints corresponding to the incompressibility condition.

Numerical examples demonstrate the applicability of the proposed methodologies and compare their efficiency and accuracy.

Resumen

Métodos de Galerkin discontinuo de alto orden para flujos incompresibles

Adeline de Montlaur

Esta tesis doctoral propone formulaciones de Galerkin discontinuo (DG) de alto orden para flujos viscosos incompresibles.

Un nuevo método de DG con penalti interior (IPM-DG) se desarrolla, conduciendo a una forma débil simétrica y coerciva para el término de difusión, y logrando aproximación espacial de alto orden. Se aplica para resolver las ecuaciones de Stokes y Navier-Stokes. El espacio de aproximación de la velocidad se descompone en cada elemento en una parte solenoidal y otra irrotacional, permitiendo dividir la forma débil IPM-DG en dos problemas desacoplados. El primero proporciona las velocidades y presiones híbridas, mientras el segundo calcula la presión en el interior de los elementos. Este desacoplamiento representa una reducción importante del número de grados de libertad tanto para velocidad como para presión. La introducción de un parámetro extra penalti resulta en una formulación DG alternativa, involucrando exclusivamente a las velocidades solenoidales. Las presiones se pueden calcular como un post-proceso de la solución de las velocidades. Se contemplan otras formulaciones DG, como por ejemplo el método Compact Discontinuous Galerkin, y se comparan con el método IPM-DG.

Se proponen métodos implícitos de Runge-Kutta de alto orden para problemas incompresibles transitorios, permitiendo obtener esquemas incondicionalmente estables y con alto orden de precisión temporal. Las ecuaciones de Navier-Stokes incompresibles transitorias se interpretan como un sistema de Ecuaciones Algebraicas Diferenciales, es decir un sistema de ecuaciones diferenciales ordinarias correspondiendo a la ecuación de conservación del momento, más las restricciones algebraicas correspondiendo a la condición de incompresibilidad.

Ejemplos numéricos muestran la aplicabilidad de los métodos propuestos y comparan su eficiencia y su precisión.

Acknowledgments

This thesis all began a few years ago, when I first entered Antonio Huerta's office and met with Sonia Fernández. They both opened me the doors of the LaCàN (Laboratori de Càlcul Numèric) group research and gave me the greatest opportunity to develop my PhD thesis with them. Thanks Sonia for helping me to solve the numerous doubts I had all along these years and for always being so available. Thanks Antonio for always helping me to get back to the correct trail and for the numerous suggestions and constructive ideas. Many thanks to both of you for your continuous support during the last 4/5 years and for helping me to become a better researcher.

Though I was always like a free electron wandering between Castelldefels and the North Campus of the UPC, where most of my colleagues of LaCàN are located, each visit at North Campus came along with long and interesting conversations with LaCàN members. Special thanks to Antonio R., Pedro, Marino and Pep, who at some point gave me some interesting feedback and ideas on my research or teaching. Thanks to Esther, Eva, Eloi, Rubén and Xevi, we have had parallel PhD trajectories and have shared some of the good but also harder moments of a PhD thesis. Thanks to David for the help with the cluster and to Sergio for sharing some of his C routines. And many thanks to Imma for solving any administrative task that kept on appearing during the thesis.

I also had the chance to spend nine months in the Aerospace Computational Design Laboratory at the Massachusetts Institute of Technology, working with Jaume Peraire. Many thanks Jaume, thanks for welcoming me there, and for giving me a chance to work with fantastic people. Special thanks to Per and Alejandra, always willing to give me a hand when needed, to Karen for getting me into the touch rugby gang, and also to Xesús and Luis, we shared good moments at work as well as during our Bostonian social life.

A foot in North Campus and the other one in Castelldefels. These years of teaching have been intense, full of surprises and represent an incredible experience. Thanks to Miguel and Eduard for giving me a chance to enter the Escola Politècnica Superior

de Castelldefels, believing in my teaching skills before I even did. Thanks to the *aero* group: Dago, Jorge, Luis, Pep, Santi and Xevi. These years would not have been the same without the endless lunch conversations, the Monday or birthday cakes, the shared awareness that 'PhD thesis should be our absolute priority no matter what'. Thanks also to the *physics* group and especially to Cesca, David, Pere, and Ricard. Thanks to Daniel for giving me the opportunity to work on the vertical wind tunnel project, which launched me on the CFD path.

And since PhD is not always a long quiet river, in the busiest moments, I could always count on getting back to normal life or at least life outside PhD, thanks to numerous actors. I have been playing rugby in the CEU team since my first days in Barcelona and no matter what, Tuesdays and Fridays have always been rugby days and always managed to clear my head from matrices and solenoidal spaces. Thanks to my teammates, coaches and friends for the great times playing, for the laughing during *tercer, cuarto o quinto tiempo* and for the great conversations anytime about anything. Thanks to the Catalano-Irish squad of the Barcelona Gaelettes and Gaels for having me discover that round balls can also generate fun games.

And because I was never really able to stay quiet in one place of the world, huge thanks to those of you in Barcelona/Lleida, Vincennes/Paris, Strasbourg, Toulouse, Cardiff, Boston and also to those of you dispatched everywhere else, for the great moments together and for being there even being far away.

Final thanks to my family, especially to my parents and my brothers, thanks for supporting any decision I had to take, as long as I was not going much further than 1000 km from Paris, and then for being so positive and encouraging during all this adventurous trip toward the PhD defense.

Contents

List of Figures

List of Tables

Chapter 1

Introduction

Aerodynamics – branch of fluid dynamics studying gas flows – has numerous applications, from predicting aerodynamic forces on aircraft or other vehicle designs, including automobiles, to predicting forces and moments in sailing or the ones applied on buildings. It studies flows around solid objects of various shapes as well as flows through solid objects. It can be classified depending on the speed of the flow, relative to the speed of sound, and also depending on its viscosity. In this work, incompressible viscous flows are considered, examples of application being amongst others light aircraft dynamics, car and Formula One designs, or low speed wind tunnels.

There are two main ways of studying the aerodynamic properties of an object: an experimental one, using for example wind tunnel testing, and a numerical one, using the so-called Computational Fluid Dynamics (CFD), science of predicting fluid flow, heat and mass transfer, and related phenomena, by solving numerically a set of governing mathematical equations. The results of CFD analysis are relevant in studies of new designs and product development as well as in troubleshooting and redesign. Though it does not completely eliminate experimental testing, it complements it, reducing the total effort required in the experiment design and data acquisition. A critical step for a good CFD analysis is to properly model the flow to be studied.

Back to our problem, the mathematical equations describing viscous flows are composed by a set of partial differential equations, the Navier-Stokes equations, which describe the physics of a large number of phenomena such as ocean currents, water flow in a pipe, flow around an airfoil, etc. They establish that changes in momentum

of the particles of a fluid are simply the product of changes in pressure and dissipative viscous forces acting inside the fluid. Incompressible Navier-Stokes problems are a subset of the Navier-Stokes models, adding to the momentum conservation equation the incompressibility constraint. The Navier-Stokes equations are usually not amenable to analytical solutions, except for very simple cases. Therefore, flow problems have to be solved numerically. To this end, flow domains to be studied have to be split into smaller subdomains and discretized governing equations are solved inside each of these portions of the domain. Each portion is known as element, and the collection of all elements is known as mesh. Typical methods used to solve the approximate version of the system of equations are finite volumes, finite elements, or finite differences. As usual in CFD problems, great care must be taken to impose continuity of the solution across the common interfaces between two subdomains, so that the approximate solutions inside the elements can be put together to give a complete description of the fluid flow in the entire domain.

Obtaining a good level of precision in numerical results is highly interesting in CFD, especially when dealing with zones such as boundary layers, around an airfoil, a car aileron or on the wall of a wind tunnel. Spatial accuracy is needed to correctly describe the changes in velocity and pressure and then to calculate for example lift, drag or other aerodynamic coefficients of an object. One way of increasing the precision in these zones is to use a finer mesh, of characteristic size h. This is usually the strategy chosen in commercial CFD software and it is referred to as *h-refinement*. Another alternative, used in the context of Finite Element Methods (FEM), is to define high-order approximations of degree p in the mesh elements, using for instance a Discontinuous Galerkin (DG) formulation.

DG methods use element-by-element discontinuous approximations. Continuity between elements is weakly imposed introducing numerical fluxes through element sides or faces. The attractiveness of DG is mainly due to its stability properties in convection dominated problems and its efficiency for high-order computations, which allows *hp*-adaptive refinement. Also, the element-by-element formulation leads to efficient explicit time integration with straight-forward parallel implementation. En-

hancing the flexibility given by DG, high-order divergence-free DG formulations for incompressible flows are developed in this thesis.

Clearly, for the same mesh, the cost of a DG formulation is higher than a continuous formulation because of the duplication of the degrees of freedom at the boundaries of the elements. Nevertheless, this increment in degrees of freedom is less significant for high-order approximations, which are desired here to obtain high orders of accuracy. Moreover, divergence-free approximations can be easily defined in a DG formulation and allow to reduce the number of degrees of freedom. In a solenoidal formulation, incompressible flows are first solved for velocity and only part of the pressure's degrees of freedom, reducing the overall size of the system to be solved. The rest of pressure's degrees of freedom is computed as a post-process. This results in a competitive code that can be used for steady or unsteady flows.

In the past, special emphasis has been made in solving stationary flows, because of the constraints of computing costs. Nevertheless, lots of physical phenomena of interest are inherently unsteady, as for example, separated flows or wake flows. An efficient temporal method is then needed to solve these problems. Since high orders of accuracy are obtained in space with the divergence-free DG formulation proposed in this thesis, same levels of precision are desired for time integration. Furthermore, since lots of physical situations require large variations in element size, as boundary layers or high Reynolds number flows, implicit time integration is considered to obtain an unconditionally stable formulation. To satisfy these requirements, high order Implicit Runge-Kutta methods are proposed in this thesis to solve incompressible unsteady flows.

1.1 Objectives

The main objective of this PhD thesis is to propose a divergence-free Discontinuous Galerkin (DG) formulation providing high orders of accuracy both in space and in time for unsteady incompressible viscous flows. To reach this objective, various partial objectives have to be accomplished:

- to derive DG formulations, providing symmetric and coercive bilinear weak forms for the diffusion term, and achieving high-order spatial approximations,
- to introduce solenoidal approximations in order to reduce the total number of degrees of freedom of velocity and pressure,
- to explore possibilities of getting a formulation where velocity and pressure are completely decoupled, reducing even more the total number of degrees of freedom,
- to develop a Matlab code, in order to solve numerical examples demonstrating the applicability of the proposed formulations,
- to analyze and study the behavior of the proposed methods,
- to critically compare different DG formulations with solenoidal approximations,

these partial objectives are achieved for the steady incompressible Stokes and Navier-Stokes equations by Montlaur et al. (2008, 2009) and in Chapter 2;

- to propose high-order and unconditionally stable time integration methods for unsteady incompressible flows,

this objective is developed in Chapter 3.

1.2 State of the art

Research in FEM for the numerical solution of problems with incompressibility constraints has been very active in the last decades. These problems have a large number of applications ranging from the simulation of incompressible fluids to the solution of the Maxwell's equations in electrodynamics problems. Classical strategies to treat incompressible flows include velocity-pressure pairs satisfying the LBB stability condition, stabilized formulations for velocity-pressure pairs that are not stable in standard

Galerkin formulation, or penalizing the incompressibility by means of a slightly compressible formulation. Another possibility, which is the one chosen in this thesis, is to use solenoidal basis functions, whose implementation for high-order approximations is made easier by using *Discontinuous Galerkin* (DG) interpolations. Some of the solutions proposed for this approach, are commented next.

1.2.1 Discontinuous Galerkin method

The DG method, which has first been proposed and analysed by Reed and Hill (1973), has recently been receiving great attention by several authors, with examples of application in CFD (Cockburn, 2004), and in particular for the Stokes equations (Baker et al., 1990; Cockburn and Gopalakrishnan, 2005; Toselli, 2002). Among the advantages of DG discretization are its compactness (coupling is restricted to the elements sharing a face) and the possibility to accommodate elements of varying order of accuracy within the same grid without difficulty, opening the way to a straightforward implementation of *hp*-adaptive methods. The drawback of a DG formulation is that for the same mesh, its cost is, in general, higher than the one of a continuous formulation because of the duplication of the degrees of freedom at the elements' boundaries. However, on the one hand this increment in degrees of freedom is less significant for high-order approximations. On the other hand, the following will show that using divergence-free approximations allows to decrease the total number of degrees of freedom and thus to reduce the computational cost.

Originally conceived for purely advective problems, the DG method has then been extended to treat advection-diffusion problems and was very successful in the numerical solution of the Navier-Stokes equations. Several schemes for the discretization of the viscous terms have been proposed in the literature, such as, among the many available, Bassi and Rebay (2001) for the compressible Navier-Stokes equations, or the *Local Discontinuous Galerkin* (LDG) formulation introduced by Cockburn and Shu (1998) for convection-diffusion problems.

LDG has been successfully analyzed and applied to Stokes, Oseen and Navier-

Stokes equations, see for instance Cockburn et al. (2005a). Lifting operators are introduced to substitute vorticity, leading to a velocity-pressure formulation, with an approximate orthogonality property. However, one major drawback of LDG is the loss of compactness due to the introduction of lifting factors. That is, the LDG stencil goes beyond immediate neighbors, in front of the usual DG stencil where degrees of freedom in one element are connected only to those in the neighboring elements.

To avoid this loss of compactness, *Compact Discontinuous Galerkin* (CDG) was introduced by Peraire and Persson (2008) with application to elliptic problems. CDG is very similar to LDG but it eliminates coupling between degrees of freedom of non-neighboring elements by means of alternative local lifting operators, recovering the compactness lost with LDG.

Another interesting feature of DG is that for incompressible problems, divergence-free high-order DG approximations can be easily defined as it will be seen in the following section.

1.2.2 Spatial discretizations for incompressible flows

To solve problems with incompressibility, an interesting alternative to velocity-pressure approximations satisfying the LBB condition consists in using explicit divergence-free bases. Crouzeix and Raviart (1973) constructed divergence-free elements for incompressible flows, in order to eliminate pressure in the final equation. They analyzed several combinations of conforming and non-conforming velocity elements and discontinuous pressure elements.

Some of these elements are briefly recalled here. The following discrete finite element spaces for velocity and pressure are defined

$$\begin{aligned} \boldsymbol{\mathcal{V}}^h &= \{\boldsymbol{v} \in [\mathcal{L}_2(\Omega)]^{\mathtt{n_{sd}}} \; ; \; \boldsymbol{v}|_{\Omega_i} \in [\mathcal{P}^k(\Omega_i)]^{\mathtt{n_{sd}}} \quad \forall \Omega_i\} \\ \mathcal{Q}^h &= \{q \in [\mathcal{L}_2(\Omega)] \; ; \; q|_{\Omega_i} \in [\mathcal{P}^{k-1}(\Omega_i)] \quad \forall \Omega_i\} \end{aligned} \tag{1.1}$$

where $\mathcal{P}^k(\Omega_i)$ is the space of polynomial functions of degree at most $k \geq 1$ in Ω_i. Solenoidal basis functions are considered that approximately satisfy the incompress-

ibility condition

$$\boldsymbol{\mathcal{S}}^h_{CR} = \{\boldsymbol{v}_h \in \boldsymbol{\mathcal{V}}^h \mid \int_{\Omega_i} q\, \boldsymbol{\nabla}\cdot\boldsymbol{v}_h \, d\Omega = 0 \quad \forall q \in \mathcal{Q}^h \},$$

and irrotational basis functions are then used to calculate the pressure once the velocity has been computed. Note that the irrotational space $\boldsymbol{\mathcal{I}}^h_{CR}$ is such that $\boldsymbol{\mathcal{V}}^h = \boldsymbol{\mathcal{S}}^h_{CR} \oplus \boldsymbol{\mathcal{I}}^h_{CR}$. This allows to split the Stokes problem $a\big(\boldsymbol{u}_h, \boldsymbol{v}\big) + b(\boldsymbol{v}, p_h) = l\big(\boldsymbol{v}\big)$, where $a\big(\boldsymbol{u}, \boldsymbol{v}\big) = \int_\Omega \boldsymbol{\nabla u} : \boldsymbol{\nabla v} d\Omega$, $b(\boldsymbol{v}, p) = \int_\Omega p \boldsymbol{\nabla}\cdot\boldsymbol{v}\, d\Omega$ and $l\big(\boldsymbol{v}\big) = \int_\Omega \boldsymbol{f}\cdot\boldsymbol{v}\, d\Omega$ in two uncoupled problems: first, find $\boldsymbol{u}_h \in \boldsymbol{\mathcal{S}}^h_{CR}$ such that

$$a\big(\boldsymbol{u}_h, \boldsymbol{v}\big) = l\big(\boldsymbol{v}\big) \quad \text{for all } \boldsymbol{v} \in \boldsymbol{\mathcal{S}}^h_{CR}. \tag{1.2}$$

Then, given $\boldsymbol{u}_h$ solution of (1.2), find $p_h \in \mathcal{Q}^h$ such that

$$b(\boldsymbol{v}, p_h) = a\big(\boldsymbol{u}_h, \boldsymbol{v}\big) - l\big(\boldsymbol{v}\big) \quad \text{for all } \boldsymbol{v} \in \boldsymbol{\mathcal{I}}^h_{CR}. \tag{1.3}$$

For example, the simplest Crouzeix-Raviart element, P_1-P_0 non-conforming element, shown in Figure 1.1, uses linear velocity, with continuity ensured at the middle points of the sides, and constant pressure.

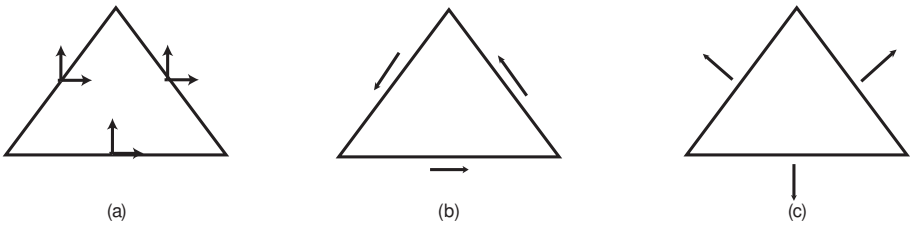

Figure 1.1: Crouzeix-Raviart P_1-P_0 element (a). Decomposition into elements from $\boldsymbol{\mathcal{S}}^h_{CR}$ (b) and $\boldsymbol{\mathcal{I}}^h_{CR}$ (c). Arrows indicate nodes for the velocity in the directions shown.

Griffiths (1981) also proposed an element level divergence-free basis for several finite element schemes on triangular and quadrilateral elements. The main advantage of both methods is that they compute velocity separately from pressure for the Stokes problem and calculate pressure afterwards, reducing the number of degrees

of freedom. Nevertheless, a major limitation of these techniques is that continuous and *weakly divergence-free* (or discretely divergence-free, following the notation of Gunzburger (1989)) approximation spaces are difficult to generalize for higher order approximations. New solenoidal and pressure spaces must be computed for each kind of element: there is no simple rule to construct these spaces for a higher polynomial order from the one of a lower polynomial order. Furthermore, it is very difficult to obtain such a formulation for high-order interpolation, that is for third or higher order. Because of the difficulties to construct them, these spaces of weak incompressibility have never been very popular.

On the other hand, in a Discontinuous Galerkin framework, divergence-free high-order approximations can easily be defined. An element by element discontinuous approximation with a divergence-free polynomial basis in each element can be considered, with a straightforward definition for high-order approximations, see Baker et al. (1990) or Cockburn and Gopalakrishnan (2005). For instance, a solenoidal basis in a 2D triangle for an approximation of degree $k = 2$ is

$$\boldsymbol{\mathcal{S}}^h = \left\langle \begin{pmatrix} 1 \\ 0 \end{pmatrix}, \begin{pmatrix} 0 \\ 1 \end{pmatrix}, \begin{pmatrix} 0 \\ x \end{pmatrix}, \begin{pmatrix} x \\ -y \end{pmatrix}, \begin{pmatrix} y \\ 0 \end{pmatrix}, \begin{pmatrix} 0 \\ x^2 \end{pmatrix}, \begin{pmatrix} 2xy \\ -y^2 \end{pmatrix}, \begin{pmatrix} x^2 \\ -2xy \end{pmatrix}, \begin{pmatrix} y^2 \\ 0 \end{pmatrix} \right\rangle \quad (1.4)$$

and an irrotational base for $k = 2$ is

$$\boldsymbol{\mathcal{I}}^h = \left\langle \begin{pmatrix} x \\ 0 \end{pmatrix}, \begin{pmatrix} x^2 \\ 0 \end{pmatrix}, \begin{pmatrix} 0 \\ y^2 \end{pmatrix} \right\rangle, \quad (1.5)$$

see for example Baker et al. (1990) for the construction of this basis.

Due to the important costs of DG methods, the reduction in degrees of freedom (both in velocity and pressure) induced by a divergence-free approach is very interesting from a computational point of view. Nevertheless the resulting formulation does not completely eliminate the degrees of freedom of the pressure. Thus, either a

non-consistent penalty term must be used to penalize the normal component of the velocity between elements and then completely eliminates pressure or, *hybrid pressure*, that is pressure on the side/face of the elements, has to be introduced. Methods using solenoidal DG formulations are commented next.

In the 90's, Baker et al. (1990) and Karakashian and Jureidini (1998) developed and analyzed a DG formulation with piecewise polynomial divergence-free velocity, which can be used for any order of the approximation and with optimal error bounds. However, this formulation has some limitations: it requires the use of continuous pressure approximations, only Dirichlet boundary conditions are considered (in fact, natural boundary conditions cannot be easily imposed), and different computational meshes (with different mesh sizes) must be considered for velocity and pressure to ensure stability (usually a finer mesh is used for the velocity).

A DG method for the Stokes equations with piecewise polynomial approximations was also proposed and analyzed by Toselli (2002), but without the point-wise imposition of the divergence-free condition. This DG formulation shows better stability properties than continuous Galerkin approximations and uniform divergence stability is proven when velocity is approximated one or two degrees higher than pressure. In fact, for equal order interpolation, numerical results show no spurious pressure modes although no uniform stability properties are proven. Unfortunately, the bilinear form related with velocities is non-symmetric, and the DG advantages for the definition of piecewise solenoidal approximations are not exploited.

Recently, Cockburn et al. (2005b, 2007) propose a DG formulation with solenoidal piecewise polynomial approximations. It is derived from a LDG rationale based on a mixed formulation of the problem (with velocity, vorticity and pressure), and with the introduction of numerical traces. Hybrid pressures are used, and pressures in the interior of the elements are computed as a postprocess of the LDG solution, see for example Cockburn and Gopalakrishnan (2005) and Carrero et al. (2005). As usual in LDG, lifting operators are introduced, leading to an approximate orthogonality property and a lost of consistency.

Note that divergence-free DG formulations are not limited to fluid problems, but

have also been used to solve the Maxwell equations (Cockburn et al., 2004) or in elasticity problems (Hansbo and Larson, 2003).

1.2.3 Interior Penalty Method

The Interior Penalty Method (IPM) is a compact formulation used to treat second order derivative, enhancing the flexibility given by discontinuous elements. In the case of Dirichlet boundary conditions, Nitsche (1971) first introduced penalty terms on the boundary of the domain in order to penalize the deviation between the values of approximate and true solutions. Similar rationale was followed by Arnold (1982) formulating a new finite element method for second-order parabolic equations where discontinuous piecewise polynomial functions were used over general meshes. Approximate continuity between elements was obtained adding consistent penalty terms. IPM leads to a symmetric and coercive bilinear weak form. There is no need to write the problem as a first order partial derivative equation and no additional variables or lifting operators have to be introduced. While other discontinuous methods, such as LDG, were first thought for hyperbolic problems and then applied to elliptic problems, IPM was originally formulated for second-order parabolic equations and thus especially conceived for self-adjoint operators as the diffusion operator. This is why in this thesis, taking advantage of the good properties of IPM for self-adjoint operators, a new consistent IPM-DG formulation is developed for incompressible flows.

Another penalty DG formulation has been proposed by Hansbo and Larson (2008) for the computation of solenoidal velocities with no presence of pressure terms. In this case normal discontinuities of the velocity are further penalized, allowing the elimination of the pressure's degrees of freedom, but leading to a non-consistent formulation. Different alternatives for this approximation, based on the definition of piecewise continuous stream function spaces, are proposed and analyzed and have inspired several authors, see for instance Mozolevsky et al. (2007) for the solution of the Navier-Stokes equations, or Montlaur et al. (2008) for the Stokes problem.

Interior Penalty Method has also been used for other kinds of problems as discon-

tinuities in solid mechanics (Hansbo and Hansbo, 2004), or Maxwell equations (Grote et al., 2008).

1.2.4 Time integrators for incompressible flows

Due to constraints of computing costs, in the past, the development of numerical techniques for fluid flow simulations has focused mainly on steady state calculations. However, many physical phenomena of interest are inherently unsteady, creating the need for efficient numerical formulation for unsteady flows, a few examples being separated flows, wake flows, fluid actuators and maneuvering. Good stability properties and high orders of accuracy in time as well as in space are critical requirements, especially when studying boundary layers or high Reynolds number flows. This section reviews the principal time integrators proposed for incompressible flows.

An important difficulty for the numerical simulation of incompressible flows is that velocity and pressure are coupled by the incompressibility constraint. The interest in using projection methods to overcome this difficulty in time-dependent viscous incompressible flows started with the introduction of fractional steps methods for incompressible Navier-Stokes equations by Chorin (1968) and Temam (2001). Following the original ideas of Chorin and Temam, numerous authors have successfully used fractional step methods for incompressible flows, among them Donea et al. (1981), Kim and Moin (1985), Guermond et al. (2006), Houzeaux et al. (2009). Fractional step method is a method of approximation of the unsteady equations based on a decomposition of the operators: the pressure/incompressibility terms are treated implicitly while the remaining terms, viscous and convective, can be treated either explicitly, semi-implicitly or fully implicitly. The most attractive feature of projection methods is thus that, at each time step, a sequence of decoupled elliptic equations are solved for velocity and pressure, making the method very efficient for large scale numerical simulations. Note that the treatment of boundary conditions is critical and depends on the chosen derivation of the fractional step method. A time discretization can be performed first, followed by a space discretization. A controversy arises then about

what boundary conditions are to be imposed at each step, so that the intermediate semi-discrete problems are well-posed. Alternatively space discretization can be performed prior to the fractional step time discretization; in that case, boundary conditions are fixed from the start. Another important feature of fractional step methods is their overall order of accuracy with respect to time discretization. Most methods are first-order-accurate, or at most second-order-accurate.

While explicit schemes are used at much lower cost, the number of realistic problems that are amenable to explicit formulation is very small. In common situations, large variations in element size, required to solve multiple spatial scales occurring in high Reynolds number flow or in boundary layers, make the use of explicit time integration techniques impractical. In such cases, implicit schemes have to be considered. Unconditionally stable schemes can then be used, as for example the multistep methods as Crank-Nicolson (Kim et al., 2002), or generalized-α methods (Jansen et al., 2000), which have both been applied to the incompressible Navier-Stokes equations. They reach second-order accuracy in time and complete the numerous low order temporal schemes available for incompressible flows.

High-order time integrators are widely used for compressible flows. For example, Persson and Peraire (2008) apply a backward difference approximation of time derivative to the compressible Navier-Stokes equations, leading to an optimal third-order accuracy in time. Higher orders can be obtained with backward difference approximation, but the higher the order the smaller the stability region. Furthermore because these methods are multistep and the value calculated at each time depends on values from previous time steps, a variable time step can not be easily used. These two drawbacks are avoided when using Runge-Kutta methods, which are one-step method, allowing the use of variable time step and whose stability regions increase with the order of the method. High-order Runge-Kutta methods are successfully applied to compressible flow problems, whose finite element or finite volume discretization leads to a system of Ordinary Differential Equations (ODEs), see Bassi and Rebay (1997), Wang and Mavriplis (2007). Explicit Runge-Kutta methods have also been used to solve incompressible flows, see for example Pereira et al. (2001) for an application

to a constrained ODE, or Linnick and Fasel (2005), Liu and Shu (2000) for vorticity stream-function formulations.

In this thesis, the space discretization of incompressible flow equations is interpreted as a system of Differential Algebraic Equations (DAE) (Hairer and Wanner, 1991), that is, a system of ODEs corresponding to the conservation of momentum equation, plus algebraic constraints corresponding to the incompressibility condition. High-order Implicit Runge-Kutta (IRK) methods are considered to solve this DAE system (Hairer et al., 1989). IRK methods are of special interest because high orders of accuracy can be obtained (Butcher, 1987) and they are unconditionally stable for an incompressible Navier-Stokes problem. However, since they have a higher cost than explicit methods or low-order implicit methods, it is necessary to balance the benefits obtained in stability and accuracy with the extra needed cost.

1.3 Overview

The thesis is divided in three main parts: the exposition, the appendices referring to the exposition and finally some of the main contributions of the thesis enclosed in form of a published paper and a paper accepted for publication.

The exposition part is divided in three chapters. Chapter 2 presents the main ideas and core concepts of the Discontinuous Galerkin (DG) formulations with solenoidal approximations proposed in this thesis for the simulation of incompressible flows, with applications to the steady Stokes and Navier-Stokes equations. The full details of the deduction and implementation of the proposed methodologies are appended either in appendices A and B, or in the final papers. Chapter 3 is concerned with obtaining unconditionally stable and high-order time integration methods, so that the resulting scheme proposed in this thesis has high order properties both in time and space. Explicit Runge-Kutta time integrators for constrained problems are commented in Appendix C. Finally Chapter 4 presents the conclusions and future developments.

The two appended papers correspond to references Montlaur et al. (2008) and Montlaur et al. (2009). Throughout the thesis these papers are cited using the corre-

sponding references.

Chapter 2

Discontinuous Galerkin Interior Penalty Method for incompressible flows

In this chapter, a new solenoidal Discontinuous Galerkin (DG) formulation for incompressible flows is built up and applied to Stokes and Navier-Stokes problems. An Interior Penalty Method (IPM) DG formulation is developed in Section 2.1.1 for the incompressible Stokes equations. Interelement continuity is enforced approximatively by means of penalties, leading to a symmetric and coercive bilinear form for the diffusion term. In a DG context, high-order piecewise solenoidal approximations are easily defined, with an important reduction in the number of degrees of freedom (Baker et al., 1990; Cockburn et al., 2005b; Montlaur et al., 2008). Thus, in Section 2.1.2, the approximation space for the velocity field is decomposed in every element as direct sum of solenoidal and irrotational polynomial spaces. This allows to split the IPM weak form in two uncoupled problems. The first one solves for velocity and hybrid pressure (i.e. pressure on elements' sides/faces), and the second one allows the evaluation of pressure in the interior of the elements as a post-process. Error bounds are given for the Stokes IPM formulation in Section 2.1.3. This new solenoidal IPM-DG method was proposed by Montlaur et al. (2008).

Other DG techniques, such as Local Discontinuous Galerkin (LDG) or Compact Discontinuous Galerkin (CDG), can also be used with solenoidal approximations to solve incompressible flow problems. A CDG formulation with solenoidal velocities was

developed for the incompressible Navier-Stokes equations by Montlaur et al. (2009) and is recalled for the Stokes problem in Section 2.1.5. CDG and IPM have many points in common: both methods lead to symmetric and coercive bilinear forms for self-adjoint operators and induce compact formulations, to the difference of LDG. Moreover, though CDG and IPM are derived from different rationales, CDG can be written as the IPM weak form plus some extra terms, including lifting operators. A deeper comparison of these methods is presented by Montlaur et al. (2009) and summarized in Sections 2.1.5 and 2.3.2.

In Section 2.1.6, the Stokes weak form with solenoidal velocities is reformulated as a minimization problem subject to the constraint of normal continuity of the velocity field. The solution of this optimization problem introducing a non-consistent penalty leads to an alternative DG formulation for the computation of velocities with no presence of pressure terms, with an important save in the number of degrees of freedom. Pressure is also computed as a post-process of the velocity solution.

Finally IPM with solenoidal approximation is extended to the Navier-Stokes equations in Section 2.2. Numerical examples show the applicability and accuracy of the proposed methods in Section 2.3.

2.1 DG formulations for Stokes

Let $\Omega \subset \mathbb{R}^{\mathtt{n_{sd}}}$ be an open bounded domain with boundary $\partial\Omega$ and $\mathtt{n_{sd}}$ the number of spatial dimensions. Suppose that Ω is partitioned in $\mathtt{n_{el}}$ disjoint subdomains Ω_i, which for example correspond to different materials, with boundaries $\partial\Omega_i$ that define an internal interphase Γ; the following definitions and notation are used

$$\overline{\Omega} = \bigcup_{i=1}^{\mathtt{n_{el}}} \overline{\Omega}_i, \quad \Omega_i \cap \Omega_j = \emptyset \text{ for } i \neq j,$$

$$\widehat{\Omega} := \bigcup_{i=1}^{\mathtt{n_{el}}} \Omega_i, \quad \text{and} \quad \Gamma := \bigcup_{\substack{i,j=1 \\ i \neq j}}^{\mathtt{n_{el}}} \overline{\Omega}_i \cap \overline{\Omega}_j = \left[\bigcup_{i=1}^{\mathtt{n_{el}}} \partial\Omega_i\right] \backslash \partial\Omega.$$

The strong form for the steady incompressible Stokes problem can be written as

$$-\boldsymbol{\nabla}\cdot\boldsymbol{\sigma} = \boldsymbol{s} \qquad \text{in } \widehat{\Omega}, \tag{2.1a}$$

$$\boldsymbol{\nabla}\cdot\boldsymbol{u} = 0 \qquad \text{in } \widehat{\Omega}, \tag{2.1b}$$

$$\boldsymbol{u} = \boldsymbol{u}_D \qquad \text{on } \Gamma_D, \tag{2.1c}$$

$$\boldsymbol{n}\cdot\boldsymbol{\sigma} = \boldsymbol{t} \qquad \text{on } \Gamma_N, \tag{2.1d}$$

$$[\![\boldsymbol{n}\otimes\boldsymbol{u}]\!] = \mathbf{0} \qquad \text{on } \Gamma, \tag{2.1e}$$

$$[\![\boldsymbol{n}\cdot\boldsymbol{\sigma}]\!] = \mathbf{0} \qquad \text{on } \Gamma, \tag{2.1f}$$

where $\partial\Omega = \overline{\Gamma}_D \cup \overline{\Gamma}_N$, $\Gamma_D \cap \Gamma_N = \emptyset$, $\boldsymbol{s} \in \mathcal{L}_2(\Omega)$ is a source term, $\boldsymbol{\sigma}$ is the ("dynamic" or "density-scaled") Cauchy stress, which is related to velocity $\boldsymbol{u}$, and pressure p, by the linear Stokes' law

$$\boldsymbol{\sigma} = -p\,\mathbf{I} + 2\nu\,\boldsymbol{\nabla}^{\mathtt{S}}\boldsymbol{u}, \tag{2.2}$$

with ν being the kinematic viscosity and $\boldsymbol{\nabla}^{\mathtt{S}} = \frac{1}{2}(\boldsymbol{\nabla} + \boldsymbol{\nabla}^T)$. Here unitary density is considered.

The *jump* $[\![\cdot]\!]$ and *mean* $\{\cdot\}$ operators are defined along the interface Γ using values from the elements to the left and to the right of the interface (say, Ω_i and Ω_j) and are also extended along the exterior boundary (only values in Ω are employed), namely

$$[\![\circledcirc]\!] = \begin{cases} \circledcirc_i + \circledcirc_j & \text{on } \Gamma, \\ \circledcirc & \text{on } \partial\Omega, \end{cases} \quad \text{and} \quad \{\circledcirc\} = \begin{cases} \kappa_i\,\circledcirc_i + \kappa_j \circledcirc_j & \text{on } \Gamma, \\ \circledcirc & \text{on } \partial\Omega. \end{cases}$$

Usually $\kappa_i = \kappa_j = 1/2$ but, in general, these two scalars are only required to verify $\kappa_i + \kappa_j = 1$, see for instance Hansbo and Hansbo (2004). The major difference between the mean and the jump operator is that the latter always involves the normal to the interface or to the domain. For instance, given two contiguous subdomains Ω_i and Ω_j their exterior unit normals are denoted respectively $\boldsymbol{n}_i$ and $\boldsymbol{n}_j$ (recall that $\boldsymbol{n}_i = -\boldsymbol{n}_j$)

and along $\partial\Omega$ the exterior unit normal is denoted by $\boldsymbol{n}$; the jump is then

$$[\![p\,\boldsymbol{n}]\!] = \begin{cases} p_i\,\boldsymbol{n}_i + p_j\,\boldsymbol{n}_j = \boldsymbol{n}_i(p_i - p_j) & \text{on } \Gamma \\ p\,\boldsymbol{n} & \text{on } \partial\Omega \end{cases}$$

for scalars, see Montlaur et al. (2008) for vectors or tensors.

Finally, in the following equations $(\cdot,\cdot)$ denotes the $\mathcal{L}_2$ scalar product in Ω, that is

$$\begin{aligned} (p,q) &= \int_\Omega p\,q\,d\Omega && \text{for scalars,} \\ (\boldsymbol{u},\boldsymbol{v}) &= \int_\Omega \boldsymbol{u}\cdot\boldsymbol{v}\,d\Omega && \text{for vectors,} \\ (\boldsymbol{\sigma},\boldsymbol{\tau}) &= \int_\Omega \boldsymbol{\sigma}:\boldsymbol{\tau}\,d\Omega && \text{for second order tensors.} \end{aligned}$$

Analogously, $(\cdot,\cdot)_\Upsilon$ denotes the $\mathcal{L}_2$ scalar product in any domain $\Upsilon \subset \Gamma \cup \partial\Omega$. For instance,

$$(p,q)_\Upsilon = \int_\Upsilon p\,q\,d\Gamma$$

for scalars.

2.1.1 IPM formulation

Following the standard approach of Interior Penalty Method, introduced by Arnold (1982) for second order parabolic equations, the Interior Penalty approach developed by Montlaur et al. (2008) for the Stokes equations is: find $\boldsymbol{u}_h \in \boldsymbol{\mathcal{V}}^h$ and $p_h \in \mathcal{Q}^h$ such that

$$\begin{aligned} a_{\mathtt{IP}}(\boldsymbol{u}_h,\boldsymbol{v}) + b(\boldsymbol{v},p_h) + \big(\{p_h\},[\![\boldsymbol{n}\cdot\boldsymbol{v}]\!]\big)_{\Gamma\cup\Gamma_D} &= l_{\mathtt{IP}}(\boldsymbol{v}) && \forall\,\boldsymbol{v}\in\boldsymbol{\mathcal{V}}^h, \\ b(\boldsymbol{u}_h,q) + \big(\{q\},[\![\boldsymbol{n}\cdot\boldsymbol{u}_h]\!]\big)_{\Gamma\cup\Gamma_D} &= \big(q,\boldsymbol{n}\cdot\boldsymbol{u}_D\big)_{\Gamma_D} && \forall\,q\in\mathcal{Q}^h, \end{aligned} \tag{2.3}$$

where $\boldsymbol{\mathcal{V}}^h$ and $\mathcal{Q}^h$ are defined in (1.1) and

$$a_{\mathtt{IP}}(\boldsymbol{u},\boldsymbol{v}) := \big(2\nu\boldsymbol{\nabla}^{\mathtt{S}}\boldsymbol{u},\boldsymbol{\nabla}^{\mathtt{S}}\boldsymbol{v}\big) + \frac{\gamma}{h}\big([\![\boldsymbol{n}\otimes\boldsymbol{u}]\!],[\![\boldsymbol{n}\otimes\boldsymbol{v}]\!]\big)_{\Gamma\cup\Gamma_D} - \big(2\nu\{\boldsymbol{\nabla}^{\mathtt{S}}\boldsymbol{u}\},[\![\boldsymbol{n}\otimes\boldsymbol{v}]\!]\big)_{\Gamma\cup\Gamma_D} - \big([\![\boldsymbol{n}\otimes\boldsymbol{u}]\!],2\nu\{\boldsymbol{\nabla}^{\mathtt{S}}\boldsymbol{v}\}\big)_{\Gamma\cup\Gamma_D}, \quad (2.4a)$$

$$l_{\mathtt{IP}}(\boldsymbol{v}) := \big(\boldsymbol{f},\boldsymbol{v}\big) + \big(\boldsymbol{t},\boldsymbol{v}\big)_{\Gamma_N} + \frac{\gamma}{h}\big(\boldsymbol{u}_D,\boldsymbol{v}\big)_{\Gamma_D} - \big(\boldsymbol{n}\otimes\boldsymbol{u}_D,2\nu\boldsymbol{\nabla}^{\mathtt{S}}\boldsymbol{v}\big)_{\Gamma_D}, \quad (2.4b)$$

$$b(\boldsymbol{v},p) := -\int_\Omega q\,\boldsymbol{\nabla}\cdot\boldsymbol{v}\,d\Omega. \quad (2.4c)$$

The penalty parameter, a positive scalar γ, must be large enough to ensure coercivity of the symmetric bilinear form $a_{\mathtt{IP}}$, see Montlaur et al. (2008). The characteristic mesh size is denoted by h. For instance, following Hansbo and Larson (2002), for a 2D mesh of straight edges, the mesh parameter h can be defined by

$$h_{|\partial\Omega_i} = \begin{cases} 2\left(\frac{\text{length}(\partial\Omega_i)}{\text{area}(\Omega_i)} + \frac{\text{length}(\partial\Omega_i)}{\text{area}(\Omega_j)}\right)^{-1} & \text{for } \partial\Omega_i \text{ on } \Gamma, \\ \frac{\text{area}(\Omega_i)}{\text{length}(\partial\Omega_i)} & \text{for } \partial\Omega_i \text{ on } \partial\Omega. \end{cases} \quad (2.5)$$

2.1.2 IPM with solenoidal approximations

The velocity space $\boldsymbol{\mathcal{V}}^h$ is now split into direct sum of a solenoidal part and an irrotational part, see Cockburn and Gopalakrishnan (2005), Carrero et al. (2005), Montlaur et al. (2008) for details, that is $\boldsymbol{\mathcal{V}}^h = \boldsymbol{\mathcal{S}}^h \oplus \boldsymbol{\mathcal{I}}^h$, where

$$\begin{aligned} \boldsymbol{\mathcal{S}}^h &= \big\{\boldsymbol{v}\in[\mathcal{L}_2(\Omega)]^{\mathtt{n_{sd}}} \mid \boldsymbol{v}|_{\Omega_i}\in[\mathcal{P}^k(\Omega_i)]^{\mathtt{n_{sd}}},\ \boldsymbol{\nabla}\cdot\boldsymbol{v}|_{\Omega_i}=0 \text{ for } i=1,\ldots,\mathtt{n_{el}}\big\}, \\ \boldsymbol{\mathcal{I}}^h &\subset \big\{\boldsymbol{v}\in[\mathcal{L}_2(\Omega)]^{\mathtt{n_{sd}}} \mid \boldsymbol{v}|_{\Omega_i}\in[\mathcal{P}^k(\Omega_i)]^{\mathtt{n_{sd}}},\ \boldsymbol{\nabla}\times\boldsymbol{v}|_{\Omega_i}=\boldsymbol{0} \text{ for } i=1,\ldots,\mathtt{n_{el}}\big\}. \end{aligned} \quad (2.6)$$

For instance, examples of solenoidal and irrotational basis in a 2D triangle for an approximation of degree $k=2$ are given in (1.4) and (1.5), and in Baker et al. (1990).

Under these circumstances, the IPM problem (2.3) can be split in two *uncoupled* problems. The first one solves for *divergence-free* velocities and the so-called *hybrid*

pressures: find $\boldsymbol{u}_h \in \boldsymbol{\mathcal{S}}^h$ and $\tilde{p}_h \in \boldsymbol{P}^h$ solution of

$$\begin{cases} a_{\mathtt{IP}}(\boldsymbol{u}_h, \boldsymbol{v}) + \left(\tilde{p}_h, [\![\boldsymbol{n}\cdot\boldsymbol{v}]\!]\right)_{\Gamma\cup\Gamma_D} = l_{\mathtt{IP}}(\boldsymbol{v}) & \forall \boldsymbol{v} \in \boldsymbol{\mathcal{S}}^h, \\ \left(\tilde{q}, [\![\boldsymbol{n}\cdot\boldsymbol{u}_h]\!]\right)_{\Gamma\cup\Gamma_D} = \left(\tilde{q}, \boldsymbol{n}\cdot\boldsymbol{u}_D\right)_{\Gamma_D} & \forall \tilde{q} \in \boldsymbol{P}^h, \end{cases} \tag{2.7a}$$

with the forms defined in (2.4).

The space of hybrid pressures (pressures along the sides in 2D, or faces in 3D) is simply:

$$\boldsymbol{P}^h := \left\{ \tilde{p} \mid \tilde{p} : \Gamma \cup \Gamma_D \longrightarrow \mathbb{R} \ \text{ and } \ \tilde{p} = [\![\boldsymbol{n}\cdot\boldsymbol{v}]\!] \ \text{ for some } \ \boldsymbol{v} \in \boldsymbol{\mathcal{S}}^h \right\}.$$

In fact, Cockburn and Gopalakrishnan (2005) demonstrate that $\boldsymbol{P}^h$ corresponds to piecewise polynomial pressures in the element sides in 2D or faces in 3D.

The second problem, which requires the solution of the previous one, evaluates the *interior pressures*: find $p_h \in \mathcal{Q}^h$ such that

$$b(\boldsymbol{v}, p_h) = l_{\mathtt{IP}}(\boldsymbol{v}) - a_{\mathtt{IP}}(\boldsymbol{u}_h, \boldsymbol{v}) - \left(\tilde{p}_h, [\![\boldsymbol{n}\cdot\boldsymbol{v}]\!]\right)_{\Gamma\cup\Gamma_D} \quad \forall \boldsymbol{v} \in \boldsymbol{\mathcal{J}}^h. \tag{2.7b}$$

It is important to note that equation (2.7b) is a post-process of the solution of (2.7a), with an element by element computation.

Note that the resulting method has many points in common with the LDG formulation stated by Carrero et al. (2005). Namely, both are formulated in terms of piecewise solenoidal velocities and hybrid pressures, the bilinear form is symmetric and positive definite and the pressure in the interior of the elements is computed as a post-process of the solution. Nevertheless, different rationales are followed for the LDG and IPM methods, leading to completely different formulations. For instance, one of the most remarkable differences is that the IPM formulation proposed here does not involve lifting operators, which induce an *approximate orthogonality* property in the LDG formulation (Carrero et al., 2005) and a lost of consistency. Moreover, the computation of the LDG liftings induces an extra computational cost and an increase

of the LDG stencil with respect to IPM.

2.1.3 Error bounds for IPM

This section presents the continuity and coercivity properties of the IPM bilinear form and the error bounds of the IPM Stokes formulation with solenoidal velocity (2.7).

For γ large enough, the IPM bilinear form $a_{\mathtt{IP}}$ defined in (2.4a) is continuous and coercive, that is: there exists a constant c such that

$$|a_{IP}(\boldsymbol{u},\boldsymbol{v})| \leq c \,|||\, \boldsymbol{u} \,|||\;\, |||\boldsymbol{v}\, ||| \quad \forall \boldsymbol{u},\boldsymbol{v} \in [\mathcal{H}^1(\hat{\Omega})]^{\mathtt{n_{sd}}} \tag{2.8}$$

and

$$m \,|||\, \boldsymbol{v}|||^2 \leq a_{IP}(\boldsymbol{v},\boldsymbol{v}) \quad \forall \boldsymbol{v} \in [\mathcal{H}^1(\hat{\Omega})]^{\mathtt{n_{sd}}} \tag{2.9}$$

for some constant $m > 0$ independent of the mesh size h, where the norm $|||\cdot|||$ is defined by

$$|||\, \boldsymbol{v}|||^2 = \|\boldsymbol{\nabla}^{\mathtt{S}}\boldsymbol{v}\|_\Omega^2 + \|h^{1/2}\{\boldsymbol{n}\cdot\boldsymbol{\nabla}^{\mathtt{S}}\boldsymbol{v}\}\|^2_{\Gamma\cup\Gamma_D} + \|h^{-1/2}[\![\boldsymbol{n}\otimes\boldsymbol{v}]\!]\|^2_{\Gamma\cup\Gamma_D} \quad \forall \boldsymbol{v} \in [\mathcal{H}^1(\hat{\Omega})]^{\mathtt{n_{sd}}} \tag{2.10}$$

with the usual $\mathcal{L}^2$-norms

$$\|\boldsymbol{f}\|_\Omega^2 = \sum_i \int_{\Omega_i} \boldsymbol{f}:\boldsymbol{f}\, d\Omega, \qquad \|f\|^2_{\Gamma\cup\Gamma_D} = \big(f,f\big)_{\Gamma\cup\Gamma_D}. \tag{2.11}$$

The continuity of $a_{\mathtt{IP}}$, that is equation (2.8), can be proven following standard arguments, see Hansbo and Larson (2002, 2008) for details, and the coercivity (2.9) is proven in Appendix A. The continuity and the coercivity of the bilinear form allow to prove the result of optimal error bound for velocity. Error bounds for pressure and hybrid pressure are also derived assuming that the following inf-sup condition holds.

Hypothesis 2.1.1 (inf-sup condition for hybrid pressure)**.** *The spaces of solenoidal*

velocities $\boldsymbol{\mathcal{S}}^h$ *and hybrid pressures* $\boldsymbol{P}^h$ *satisfy*

$$\sup_{\boldsymbol{v}\in\boldsymbol{\mathcal{S}}^h} \frac{\left(\tilde{q}, [\![\boldsymbol{n}\cdot\boldsymbol{v}]\!]\right)_{\Gamma\cup\Gamma_D}}{|||\boldsymbol{v}|||} \geq c_1 h \|\tilde{q}\|_{\Gamma\cup\Gamma_D} \quad \forall \tilde{q} \in \boldsymbol{P}^h, \tag{2.12}$$

for some constant c_1 *independent of the characteristic mesh size* h*.*

The satisfaction of this inf-sup condition is checked in Section 2.1.4 through a numerical inf-sup test. In all experiments, the numerical inf-sup test is passed for approximations of order k for velocity and $k-1$ for pressure. An analytical proof of the satisfaction of the inf-sup condition is considered as future work, outside the scope of this thesis.

Theorem 2.1.2 (Error bounds)**.** *Let* $\boldsymbol{u} \in [\mathcal{H}^{1+\alpha}(\Omega)]^{n_{sd}}$*,* $1 \leq \alpha \leq k$*, and* $p \in \mathcal{H}^{\alpha}(\Omega)$ *be the exact solution of the Stokes problem,* $\tilde{p} = \{p\}$ *on* $\Gamma\cup\partial\Omega$*, and* $(\boldsymbol{u}_h, \tilde{p}_h, p_h) \in \boldsymbol{\mathcal{S}}^h \times \boldsymbol{P}^h \times \mathcal{Q}^h$ *the numerical solution of the IPM system* (2.7)*, then, under the assumption of hypothesis 2.1.1*

$$|||\boldsymbol{u} - \boldsymbol{u}_h||| \leq K_1 h^{\alpha} |\boldsymbol{u}|_{[\mathcal{H}^{1+\alpha}(\Omega)]^{n_{sd}}} \tag{2.13a}$$

$$\|\tilde{p} - \tilde{p}_h\|_{\Gamma\cup\Gamma_D} \leq K_2 h^{\alpha-1} |\boldsymbol{u}|_{[\mathcal{H}^{1+\alpha}(\Omega)]^{n_{sd}}} \tag{2.13b}$$

$$\|p - p_h\|_{\Omega} \leq K_3 \left(h^{\alpha-\frac{1}{2}} |\boldsymbol{u}|_{[\mathcal{H}^{1+\alpha}(\Omega)]^{n_{sd}}} + h^{\alpha} \|p\|_{\mathcal{H}^{\alpha}(\Omega)} \right) \tag{2.13c}$$

where constants K_1*,* K_2*,* K_3 *are independent of the mesh size* h *and the exact solution.*

Elements of proof of the error bounds for hybrid and interior pressures can be found in Appendix A. The convergence rate of the velocity is optimal, that is $\boldsymbol{u}$ converges to $\boldsymbol{u}_h$ with order k for a $|||.|||$-like norm, see Montlaur et al. (2008) for details. Though these results prove that $\tilde{p}_h$ converges to $\tilde{p}$ with at least order $k-1$ and p_h converges to p with at least order $k-\frac{1}{2}$ in an $\mathcal{L}_2$-like norm, numerical experiments, as shown in Figure 2.1, actually indicate that $\tilde{p}_h$ and p_h respectively converge to $\tilde{p}$ and p with optimal order k. Similar results were obtained by Carrero et al. (2005).

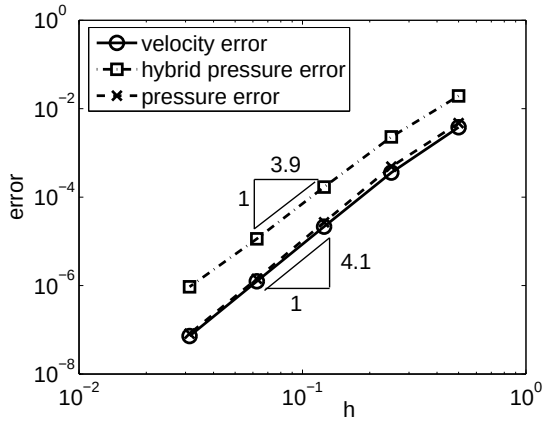

Figure 2.1: IPM convergence results with velocity approximation of degree $k = 4$ and pressure interpolation of degree 3, with $\gamma = 40$

Figure 2.1 shows the convergence under h-refinement for an order of approximation of 4 for velocity and 3 for pressure for a Stokes example with analytical solution, solved in a 2D square domain with Dirichlet and Neumann boundary conditions. Details of this example can be found in (Montlaur et al., 2008). As previously commented, optimal fourth order convergence is obtained for velocity error with $|||.|||$-norm and hybrid and interior pressure errors with $\mathcal{L}_2$-norms.

2.1.4 Numerical inf-sup test for IPM

This section presents a numerical inf-sup test for the IPM Stokes formulation with solenoidal velocity (2.7). Let us first recall how to perform a numerical inf-sup test on a general Stokes formulation.

Let us consider a weak form of a discretized incompressible Stokes problem: find $\boldsymbol{u}_h \in \boldsymbol{\mathcal{V}}^h$ and $p_h \in \mathcal{Q}^h$ such that

$$\begin{aligned} a\big(\boldsymbol{u}_h, \boldsymbol{v}\big) + b\big(\boldsymbol{v}, p_h\big) &= l\big(\boldsymbol{v}\big) \quad \forall\, \boldsymbol{v} \in \boldsymbol{\mathcal{V}}^h, \\ b\big(\boldsymbol{u}_h, q\big) &= 0 \qquad \forall\, q \in \mathcal{Q}^h. \end{aligned} \tag{2.14}$$

The inf-sup condition is passed if $\big(\boldsymbol{\mathcal{V}}^h, \mathcal{Q}^h\big)$ satisfy

$$\sup_{\boldsymbol{v}_h \in \boldsymbol{\mathcal{V}}^h} \frac{b\big(\boldsymbol{v}_h, q_h\big)}{|||\boldsymbol{v}_h||| \, \|q_h\|_\Omega} \geq k_h > 0 \quad \forall q_h \in \mathcal{Q}^h, \tag{2.15}$$

with the stability condition

$$\lim_{h \to 0} k_h \geq \beta > 0,$$

for some constant $\beta > 0$.

Giving an analytical proof of (2.15) for $\big(\boldsymbol{\mathcal{V}}^h, \mathcal{Q}^h\big)$ is usually not trivial. For this reason a numerical inf-sup test can be used in order to confirm the result of (2.15) with relatively little effort, following Chapelle and Bathe (1993), Huerta et al. (2004). For the inf-sup test (2.15), let $\mathbf{M}_{\boldsymbol{v}}$ and $\mathbf{M}_q$ be the mass matrices associated to the scalar products of $\boldsymbol{\mathcal{V}}^h$ and $\mathcal{Q}^h$ respectively, and let μ_{min} be the smallest non-zero eigenvalue defined by the following eigenvalue problem

$$\mathbf{B}^T \mathbf{M}_q \mathbf{B} \boldsymbol{v} = \mu^2 \mathbf{M}_{\boldsymbol{v}} \boldsymbol{v} \tag{2.16}$$

where $\mathbf{B}$ is the discretization of $b\big(\cdot, \cdot\big)$ in (2.14). Then the value of k_h is simply μ_{min}. The numerical test consists in testing a particular pair $\big(\boldsymbol{\mathcal{V}}^h, \mathcal{Q}^h\big)$ by calculating μ_{min} using meshes of increasing refinement. On the basis of three or four results it can be predicted whether the inf-sup value μ_{min} is probably bounded from underneath or, on the contrary, goes down to zero when the mesh is refined.

In order to come up with a numerical inf-sup test for hybrid pressure, see (2.12), $\mathbf{M}_{\boldsymbol{v}}$ and $\mathbf{M}_{\tilde{q}}$ are the mass matrices associated to the scalar products of $\boldsymbol{\mathcal{S}}^h$ and $\boldsymbol{P}^h$ respectively, that is

$$\begin{aligned}\big(\boldsymbol{u}, \boldsymbol{v}\big) = \big(\boldsymbol{\nabla}^{\mathtt{S}} \boldsymbol{u}, \boldsymbol{\nabla}^{\mathtt{S}} \boldsymbol{v}\big) + \big(h^{1/2}\{\boldsymbol{n} \cdot \boldsymbol{\nabla}^{\mathtt{S}} \boldsymbol{u}\}, h^{1/2}\{\boldsymbol{n} \cdot \boldsymbol{\nabla}^{\mathtt{S}} \boldsymbol{v}\}\big)_{\Gamma \cup \Gamma_D} \\ + \big(h^{-1/2}[\![\boldsymbol{n} \otimes \boldsymbol{u}]\!], h^{-1/2}[\![\boldsymbol{n} \otimes \boldsymbol{v}]\!]\big)_{\Gamma \cup \Gamma_D} \quad \forall \boldsymbol{u}, \boldsymbol{v} \in \boldsymbol{\mathcal{S}}^h,\end{aligned}$$

and

$$\big(p,q\big)_{\Gamma\cup\Gamma_D} \quad \forall p,q \in \boldsymbol{P}^h.$$

Then μ_{min} is the smallest non-zero eigenvalue defined by the following eigenvalue problem

$$\mathbf{B}^T\mathbf{M}_{\tilde{q}}\mathbf{B}\boldsymbol{v} = \mu^2\mathbf{M}_{\boldsymbol{v}}\boldsymbol{v} \tag{2.17}$$

where $\mathbf{B}$ is the discretization of $\big(\tilde{q},[\![\boldsymbol{n}\cdot\boldsymbol{v}]\!]\big)_{\Gamma\cup\Gamma_D}$ in (2.7a).

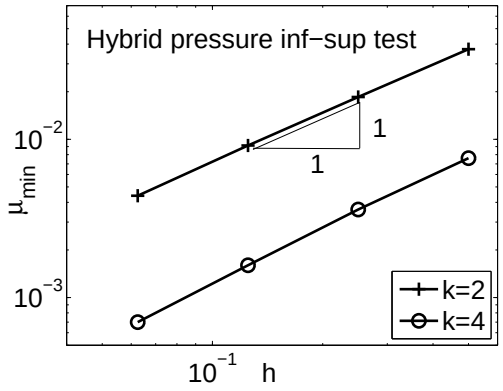

Figure 2.2: Numerical inf-sup test result for hybrid pressure.

In order to perform the numerical inf-sup test a sequence of four successive refined meshes is considered (uniform distribution of 8, 32, 128 and 512 elements). Approximations of order 4 and 2 for velocity and 3 and 1 for pressure are considered. Figure 2.2 shows that for the hybrid pressure a steady decrease in $log(\mu_{min})$ is observed, violating the classical inf-sup condition for $\big(\boldsymbol{S}^h,\boldsymbol{P}^h\big)$. Nevertheless a slope of 1 is observed, that is $\mu_{min} = \alpha h$, which fits the inf-sup condition (2.12).

2.1.5 Comparison with other DG methods

Other DG formulations, such as the Local Discontinuous Galerkin (LDG) or the Compact Discontinuous Galerkin (CDG) methods, can also be used to solve the incompressible Stokes equations with solenoidal velocities. Both formulations' weak forms can be written as the IPM weak form plus some extra terms, mainly involving lifting

operators. For example the uncoupled Stokes problem (2.7) can be solved using a CDG formulation, substituting $a_{\mathtt{IP}}$ and $l_{\mathtt{IP}}$ by

$$a_{\mathtt{CDG}}(\boldsymbol{u},\boldsymbol{v}) := a_{\mathtt{IP}}(\boldsymbol{u},\boldsymbol{v}) - \big(2\nu\boldsymbol{C}_{12}\otimes[\![\boldsymbol{n}\cdot\boldsymbol{\nabla}^{\mathtt{S}}\boldsymbol{v}]\!],[\![\boldsymbol{n}\otimes\boldsymbol{u}]\!]\big)_{\Gamma} - \big(2\nu\boldsymbol{C}_{12}\otimes[\![\boldsymbol{n}\cdot\boldsymbol{\nabla}^{\mathtt{S}}\boldsymbol{u}]\!],[\![\boldsymbol{n}\otimes\boldsymbol{v}]\!]\big)_{\Gamma} + \sum_{\Gamma_e\subset\Gamma\cup\Gamma_D}\Big(2\nu\big(r^e([\![\boldsymbol{n}\otimes\boldsymbol{u}]\!])+s^e(\boldsymbol{C}_{12}\cdot[\![\boldsymbol{n}\otimes\boldsymbol{u}]\!])\big),r^e([\![\boldsymbol{n}\otimes\boldsymbol{v}]\!])+s^e(\boldsymbol{C}_{12}\cdot[\![\boldsymbol{n}\otimes\boldsymbol{v}]\!])\Big) \tag{2.18a}$$

$$l_{\mathtt{CDG}}(\boldsymbol{v}) := l_{\mathtt{IP}}(\boldsymbol{v}) + \sum_{\Gamma_e\subset\Gamma_D}\Big(2\nu\, r^e(\boldsymbol{n}\otimes\boldsymbol{v}),r^e(\boldsymbol{n}\otimes\boldsymbol{u}_D)\Big) \tag{2.18b}$$

being $a_{\mathtt{IP}}$ and $l_{\mathtt{IP}}$ the IPM forms defined in (2.4), with $\gamma = hC_{11}$. The two local lifting operators r^e, s^e are defined in (B.16) and (B.17) in Appendix B, where the obtention of the CDG weak form for the incompressible Stokes equations is detailed, following the rationale proposed by Peraire and Persson (2008) for elliptic problems. The CDG formulation for Stokes and Navier-Stokes is proposed by Montlaur et al. (2009) and compared with IPM. The conclusions of the comparison are summarized here.

Remark : The implementation of CDG lifting operators, requires computing several elemental matrices, matrix inversions and products, for every side/face, see Montlaur et al. (2009). Thus, in addition to the implementation effort, lifting terms represent a clearly non-negligible increase in the computational cost relative to IPM. This is also the case for transient problems and it implies a non-negligible burden mostly for explicit time integrators. Auxiliary variables for the lifting operators have to be stored and computed (solving linear systems of equations in each element) at every time step.

Note that CDG, and it would also be the case for LDG, has two parameters, C_{11} and $\boldsymbol{C}_{12}$. The former, C_{11}, substitutes the consistent penalty parameter in $a_{\mathtt{IP}}$, that is $C_{11} = \gamma h^{-1}$, and it is thus a non-negative parameter of order $\mathcal{O}(h^{-1})$. The latter, is an additional vector, $\boldsymbol{C}_{12} \in \mathbb{R}^{\mathtt{n_{sd}}}$, defined for each interior side/face, see Peraire and Persson (2008) and (B.7) in Appendix B for details. Though both bilinear forms of CDG and LDG introduce more terms than IPM, because of the introduction of

lifting operators, CDG presents the major advantage, in front of LDG, that it is a compact formulation. That is, both IPM and CDG have the same compact stencil, where degrees of freedom of one element are only connected to those of immediate neighbors. This is why CDG has been preferred here in front of LDG.

While in an IPM formulation γ must be large enough to ensure coercivity of the bilinear form, in CDG, $C_{11} = 0$ may be considered on Γ, see Peraire and Persson (2008), giving more flexibility for the choice of this parameter. Nevertheless, note that on the Dirichlet boundary it must be positive, $C_{11} > 0$, to treat properly boundary conditions. The influence of the C_{11} parameter in CDG or γh^{-1} in IPM on the condition number of the diffusion matrix — the discretization of the bilinear form $a_{\texttt{CDG}}$ for CDG or $a_{\texttt{IP}}$ for IPM — is studied next. Figure 2.3 shows the evolution of the condition number of the diffusion matrix for a regular structured mesh with $h = 1/8$ and degree $k = 4$. For $C_{11} \geq 40h^{-1}$, i.e for $\gamma \geq 40$, large enough to ensure coercivity

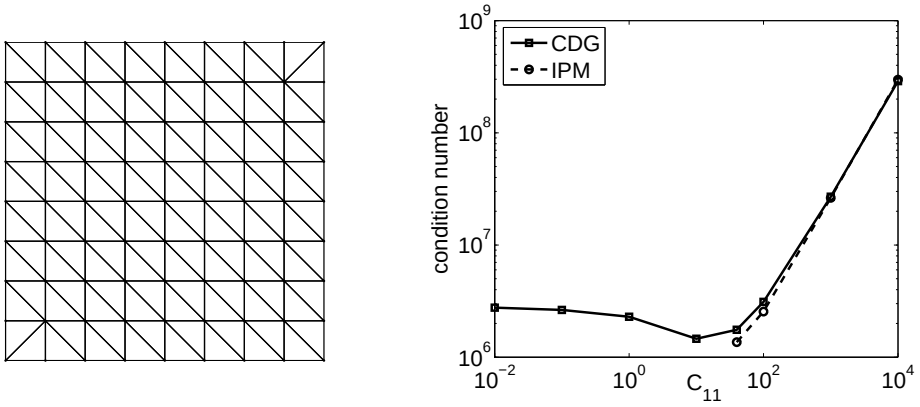

Figure 2.3: Structured mesh for $h = 1/8$ and dependency of the condition number of the diffusion matrix on the stabilization parameter $C_{11} = \gamma h^{-1}$, for CDG and IPM, with a fourth order approximation of the velocity ($k = 4$).

of the IPM bilinear form, similar condition numbers are obtained with both methods. Though CDG (and it would also be the case for LDG) allows to choose a value of C_{11} as small as wanted, Figure 2.3 shows that the condition number is rather constant for small values of C_{11}. Moreover the minimum value of the condition number is more or less the same for CDG and for IPM. Thus, the flexibility of CDG for the choice of

C_{11} does not imply any advantage in front of IPM for the conditioning of the matrix.

Numerical experiments, presented in Section 2.3 and Montlaur et al. (2009), also reveal that IPM and CDG present similar results for the accuracy of the numerical solution, both reaching optimal convergence rates for velocity and pressure.

Thus, the main differences between both methods are that CDG is less sensitive to the selection of the penalty parameter (tuning of C_{11} is almost eliminated), but it has the major disadvantage of the implementation and computation of the lifting operators. That is, IPM leads to a simpler and straight-forward implementation, avoiding the extra computational cost associated to CDG or LDG liftings.

2.1.6 Formulation with penalization of the discontinuity

The formulation with solenoidal spaces allows a computation of the velocity solution involving the pressure only in the boundary of the elements, i.e the hybrid pressure. The aim of this section is more ambitious: to obtain a completely decoupled formulation allowing the computation of the solenoidal velocity, with no presence of pressures at all. The introduction of a new penalty in the weak formulation achieves this purpose. For large engineering computations this second formulation represents an important save in the number of degrees of freedom in front of a formulation including hybrid pressure. However, the price of a totally decoupled velocity-pressure formulation is the lost of consistency, which provokes ill-conditioning, typical for non-consistent penalty formulations.

The IPM formulation with penalization proposed by Montlaur et al. (2008) exactly coincides with the DG method initially proposed and analyzed by Hansbo and Larson (2008). Nevertheless it is worth mentioning that in Montlaur et al. (2008) it is deduced from an alternative rationale, based on the IPM formulation (2.7a) and the introduction of a non-consistent penalty. The rationale is summarized next. The IPM formulation with solenoidal velocities (2.7a) can be rewritten as a saddle-point

problem, namely

$$(\boldsymbol{u}_h, \tilde{p}_h) = \arg \min_{\boldsymbol{v}\in\boldsymbol{\mathcal{S}}^h} \max_{\tilde{q}\in\boldsymbol{P}^h} \frac{1}{2} a_{\mathtt{IP}}(\boldsymbol{v},\boldsymbol{v}) - l_{\mathtt{IP}}(\boldsymbol{v}) + \big(\tilde{q}, [\![\boldsymbol{n}\cdot\boldsymbol{v}]\!]\big)_{\Gamma\cup\Gamma_D} - \big(\tilde{q}, \boldsymbol{n}\cdot\boldsymbol{u}_D\big)_{\Gamma_D}, \quad (2.19)$$

or, equivalently, as a minimization problem subject to normal continuity constraints,

$$\begin{aligned} \boldsymbol{u}_h = \arg \quad & \min_{\boldsymbol{v}\,\in\,\boldsymbol{\mathcal{S}}^h} && \frac{1}{2} a_{\mathtt{IP}}(\boldsymbol{v},\boldsymbol{v}) - l_{\mathtt{IP}}(\boldsymbol{v}). \\ & \text{s.t. } [\![\boldsymbol{n}\cdot\boldsymbol{v}]\!] = 0 \text{ in } \Gamma \\ & \boldsymbol{n}\cdot\boldsymbol{v} = \boldsymbol{n}\cdot\boldsymbol{u}_D \text{ in } \Gamma_D \end{aligned} \quad (2.20)$$

Note that the terms with pressures are cancelled thanks to the imposed continuity constraints. As usual in constrained minimization problems, (2.20) can be solved using a *non-consistent penalty*, see for instance Babuska (1973). The corresponding minimization problem with penalty is

$$\boldsymbol{u}_h = \arg \min_{\boldsymbol{v}\in\boldsymbol{\mathcal{S}}^h} \frac{1}{2} a_{\mathtt{IP}}(\boldsymbol{v},\boldsymbol{v}) - l_{\mathtt{IP}}(\boldsymbol{v}) + \beta \left[\big([\![\boldsymbol{n}\cdot\boldsymbol{v}]\!], [\![\boldsymbol{n}\cdot\boldsymbol{v}]\!]\big)_{\Gamma} - \big(\boldsymbol{n}\cdot(\boldsymbol{u}_D - \boldsymbol{v}), \boldsymbol{n}\cdot(\boldsymbol{u}_D - \boldsymbol{v})\big)_{\Gamma_D} \right]$$

where β is a scalar penalty to be chosen. The solution of this optimization problem is the solution of the following IPM weak formulation with penalty: find $\boldsymbol{u}_h^\beta \in \boldsymbol{\mathcal{S}}^h$ such that

$$a_{\mathtt{IP}}(\boldsymbol{u}_h^\beta, \boldsymbol{v}) + \beta\big([\![\boldsymbol{n}\cdot\boldsymbol{u}_h^\beta]\!], [\![\boldsymbol{n}\cdot\boldsymbol{v}]\!]\big)_{\Gamma\cup\Gamma_D} = l_{\mathtt{IP}}(\boldsymbol{v}) + \beta\big(\boldsymbol{n}\cdot\boldsymbol{v}, \boldsymbol{n}\cdot\boldsymbol{u}_D\big)_{\Gamma_D} \quad (2.21)$$

for all $\boldsymbol{v} \in \boldsymbol{\mathcal{S}}^h$. In the following, we refer to this weak formulation as *Interior Penalty Method with Penalty* (IPMP) in front of the IPM formulation described in (2.7a).

Once the velocity is obtained, pressure can be computed as a postprocess in two steps. First an approximation of the hybrid pressure can be obtained introducing the

solution of (2.21) in (2.7a), namely

$$\tilde{p}_h^\beta = \begin{cases} \beta \, [\![\boldsymbol{n} \cdot \boldsymbol{u}_h^\beta]\!] & \text{on } \Gamma, \\ \beta \, \boldsymbol{n} \cdot [\boldsymbol{u}_h^\beta - \boldsymbol{u}_D] & \text{on } \Gamma_D. \end{cases}$$

Then, with $\boldsymbol{u}_h^\beta$ and $\tilde{p}_h^\beta$ the interior pressure can be determined as the solution of (2.7b).

As previously commented, a major advantage of solenoidal spaces is the reduction in the number of degrees of freedom (dof) for the DG solution, and an additional reduction in the number of dof is achieved with the introduction of the non-consistent penalty parameter. Figure 2.4 shows the number of dof for a typical finite element mesh corresponding to a continuous Galerkin (CG) discretization, a DG nodal interpolation (DG), a IPM-DG solenoidal approximation (IPM-DGS), and a IPMP-DG solenoidal approximation (IPMP-DGS). The hypothesis made to count dof in function of the order of approximation k are detailed by Montlaur et al. (2009). Note that for CG and DG, the number of dof for velocities and interior pressures is contemplated, whereas for the IPM-DGS approximation the number of dof for velocities and hybrid pressures is considered, see problem (2.7a). For the IPMP-DGS approximation only the number of dof for velocities is taken into account, see equation (2.21).

Figure 2.4 shows the important reduction in dof when using solenoidal approximations with hybrid pressures (IPM) and without pressure (IPMP) in a DG formulation. Compared with CG, the IPM-DGS and IPMP-DGS lead to much less dof in 2D, and to a competitive number of dof in 3D. Moreover, note that CG and standard DG behave similarly when increasing k, whereas the growth of the number of dof for the IPM-DGS and IPMP-DGS methods is much slower. Here the penalization is introduced to eliminate the pressure in the IPM formulation, but the same strategy could be used with solenoidal CDG or LDG formulations. Equation (2.21) can be applied using a CDG or LDG formulation instead of IPM and the save in dof is exactly the same as the one exposed in Figure 2.1.6.

It is important to remark that the IPMP formulation (2.21) involves two penalties with important differences. The first one is inherited from the IPM formulation, i.e.

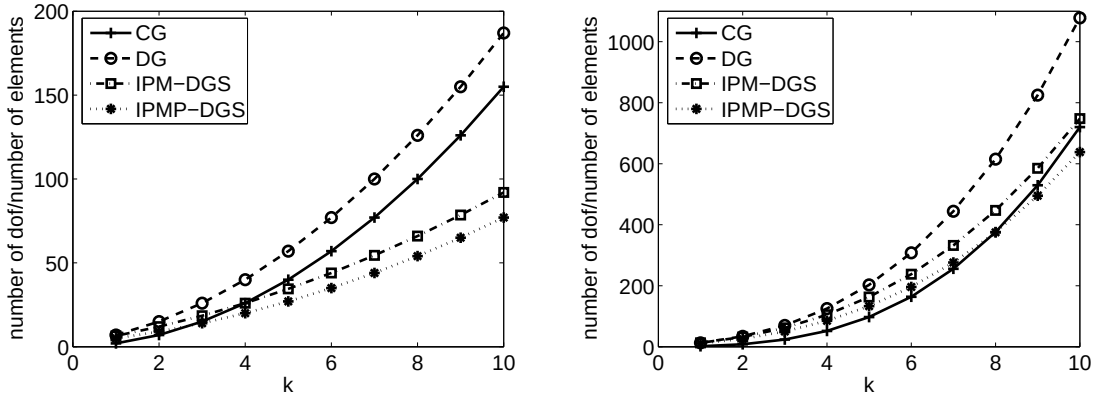

(a) $2D$ (b) $3D$

Figure 2.4: Comparison of the total number of dof, divided by the number of elements, for a typical finite element mesh corresponding to a continuous Galerkin (CG) discretization, a discontinuous Galerkin nodal interpolation (DG), a IPM-DG solenoidal approximation (IPM-DGS), and a IPMP-DG solenoidal approximation (IPMP-DGS), in $2D$ (a) and $3D$ (b), with order k for velocity and $k-1$ for pressure.

γh^{-1} in the bilinear form $a_{\mathtt{IP}}(\cdot,\cdot)$ defined in (2.4a). It is a consistent penalty in the sense that the solution of the original problem (2.1) is solution of the IPM formulation (2.7a) and therefore, as usual in IPM formulations, in practice, moderate values of the constant parameter γ provide accurate and optimally convergent results. This is not the case for the second penalty. The penalty β in the IPMP formulation (2.21) is a non-consistent penalty: the solution of the IPMP formulation verifies the continuity of the normal component of the velocity and the Dirichlet boundary conditions only in the limit, for β going to infinity. This lack of consistency is the origin of the usual drawbacks of penalty techniques: the tuning of the penalty parameter affects the accuracy of the solution and, in practice, too large values of β are needed, leading to ill-conditioned systems of equations.

2.2 DG formulation for the Navier-Stokes equations

The strong form for the momentum conservation equation and the incompressibility condition of the steady Navier-Stokes problem can be written as

$$-2\boldsymbol{\nabla}\cdot(\nu\boldsymbol{\nabla}^{\mathtt{S}}\boldsymbol{u})+\boldsymbol{\nabla}p+(\boldsymbol{u}\cdot\boldsymbol{\nabla})\boldsymbol{u}=\boldsymbol{f} \qquad \text{in } \widehat{\Omega}, \tag{2.22}$$

$$\boldsymbol{\nabla}\cdot\boldsymbol{u}=0 \qquad \text{in } \widehat{\Omega}, \tag{2.23}$$

with boundary and interface conditions (2.1c)-(2.1f).

A standard upwind numerical flux, see for instance Kanschat and Schötzau (2008), is used for the definition of the trilinear form associated to the convective term

$$\begin{aligned} &c\big(\boldsymbol{w};\boldsymbol{u},\boldsymbol{v}\big):=-\big((\boldsymbol{w}\cdot\boldsymbol{\nabla})\boldsymbol{v},\boldsymbol{u}\big)\\ &+\sum_{i=1}^{\mathtt{n_{el}}}\int_{\partial\Omega_i\setminus\Gamma_N}\frac{1}{2}\big[(\boldsymbol{w}\cdot\boldsymbol{n}_i)(\boldsymbol{u}^{ext}+\boldsymbol{u})-|\boldsymbol{w}\cdot\boldsymbol{n}_i|\,(\boldsymbol{u}^{ext}-\boldsymbol{u})\big]\cdot\boldsymbol{v}d\Gamma+\int_{\Gamma_N}(\boldsymbol{w}\cdot\boldsymbol{n})\boldsymbol{u}\cdot\boldsymbol{v}d\Gamma. \end{aligned} \tag{2.24}$$

where $\boldsymbol{u}^{ext}$ denotes the exterior trace of $\boldsymbol{u}$ taken over the side/face under consideration, that is

$$\boldsymbol{u}^{ext}(\boldsymbol{x})=\lim_{\varepsilon\to0^+}\boldsymbol{u}(\boldsymbol{x}+\varepsilon\boldsymbol{n}_i)\qquad\text{for } \boldsymbol{x}\in\partial\Omega_i.$$

As for the Stokes problem, the velocity space is split in a solenoidal part and an irrotational one, and the IPM formulation for Navier-Stokes equations is split in two uncoupled problems. The first one solves for divergence-free velocities and hybrid pressures: find $\boldsymbol{u}_h\in\boldsymbol{\mathcal{S}}^h$ and $\tilde{p}_h\in\boldsymbol{P}^h$ solution of

$$\begin{cases} a_{\mathtt{IP}}\big(\boldsymbol{u}_h,\boldsymbol{v}\big)+c\big(\boldsymbol{u}_h;\boldsymbol{u}_h,\boldsymbol{v}\big)+\big(\tilde{p}_h,[\![\boldsymbol{n}\cdot\boldsymbol{v}]\!]\big)_{\Gamma\cup\Gamma_D}=l_{\mathtt{IP}}\big(\boldsymbol{v}\big) & \forall\boldsymbol{v}\in\boldsymbol{\mathcal{S}}^h,\\ \big(\tilde{q},[\![\boldsymbol{n}\cdot\boldsymbol{u}_h]\!]\big)_{\Gamma\cup\Gamma_D}=\big(\tilde{q},\boldsymbol{n}\cdot\boldsymbol{u}_D\big)_{\Gamma_D} & \forall\tilde{q}\in\boldsymbol{P}^h, \end{cases} \tag{2.25a}$$

with the forms defined in (2.4) and (2.24), and the second problem is: find $p_h \in \mathcal{Q}^h$ such that

$$b\big(\boldsymbol{v}, p_h\big) = l_{\mathtt{IP}}\big(\boldsymbol{v}\big) - a_{\mathtt{IP}}\big(\boldsymbol{u}_h, \boldsymbol{v}\big) - \big(\tilde{p}_h, [\![\boldsymbol{n}\cdot\boldsymbol{v}]\!]\big)_{\Gamma\cup\Gamma_D} - c\big(\boldsymbol{u}_h; \boldsymbol{u}_h, \boldsymbol{v}\big) \quad \forall \boldsymbol{v} \in \boldsymbol{\mathcal{J}}^h. \tag{2.25b}$$

When solving the unsteady incompressible Navier-Stokes equations, the original convective term of the strong form, $(\boldsymbol{u}\cdot\boldsymbol{\nabla})\boldsymbol{u}$ is replaced by $(\boldsymbol{u}\cdot\boldsymbol{\nabla})\boldsymbol{u} - \frac{1}{2}(\boldsymbol{\nabla}\cdot\boldsymbol{u})\boldsymbol{u}$, which is a legitimate modification for a divergence-free velocity field, see Temam (2001). This guarantees unconditional stability, in the case of an implicit or semi-implicit time integration, see Donea and Huerta (2003). The skew-symmetric trilinear convective term becomes

$$\begin{aligned}\tilde{c}\big(\boldsymbol{w}; \boldsymbol{u}, \boldsymbol{v}\big) := \frac{1}{2}\Big[&- \big((\boldsymbol{w}\cdot\boldsymbol{\nabla})\boldsymbol{v}, \boldsymbol{u}\big) + \big((\boldsymbol{w}\cdot\boldsymbol{\nabla})\boldsymbol{u}, \boldsymbol{v}\big) \\ + \sum_{i=1}^{\mathtt{n_{el}}} \int_{\partial\Omega_i\setminus\Gamma_N} \frac{1}{2}\big[(\boldsymbol{w}\cdot\boldsymbol{n}_i)(\boldsymbol{u}^{ext}+\boldsymbol{u}) - |\boldsymbol{w}\cdot\boldsymbol{n}_i|\,(\boldsymbol{u}^{ext}-\boldsymbol{u})\big]\cdot\boldsymbol{v}\,d\Gamma &+ \int_{\Gamma_N}(\boldsymbol{w}\cdot\boldsymbol{n})\boldsymbol{u}\cdot\boldsymbol{v}\,d\Gamma\Big]\end{aligned}$$

Under these circumstances, the unsteady IPM problem becomes: first find $\boldsymbol{u}_h \in \boldsymbol{\mathcal{S}}^h$ and $\tilde{p}_h \in \boldsymbol{P}^h$ solution of

$$\begin{cases} \big(\boldsymbol{u}_h^t, \boldsymbol{v}\big) + a_{\mathtt{IP}}\big(\boldsymbol{u}_h, \boldsymbol{v}\big) + \tilde{c}\big(\boldsymbol{u}_h; \boldsymbol{u}_h, \boldsymbol{v}\big) + \big(\tilde{p}_h, [\![\boldsymbol{n}\cdot\boldsymbol{v}]\!]\big)_{\Gamma\cup\Gamma_D} = l_{\mathtt{IP}}\big(\boldsymbol{v}\big) & \forall \boldsymbol{v} \in \boldsymbol{\mathcal{S}}^h, \\ \big(\tilde{q}, [\![\boldsymbol{n}\cdot\boldsymbol{u}_h]\!]\big)_{\Gamma\cup\Gamma_D} = \big(\tilde{q}, \boldsymbol{n}\cdot\boldsymbol{u}_D\big)_{\Gamma_D} & \forall \tilde{q} \in \boldsymbol{P}^h, \end{cases} \tag{2.26}$$

and then: find $p_h \in \mathcal{Q}^h$ such that

$$b\big(\boldsymbol{v}, p_h\big) = l_{\mathtt{IP}}\big(\boldsymbol{v}\big) - \big(\boldsymbol{u}_h^t, \boldsymbol{v}\big) - a_{\mathtt{IP}}\big(\boldsymbol{u}_h, \boldsymbol{v}\big) - \big(\tilde{p}_h, [\![\boldsymbol{n}\cdot\boldsymbol{v}]\!]\big)_{\Gamma\cup\Gamma_D} - \tilde{c}\big(\boldsymbol{u}_h; \boldsymbol{u}_h, \boldsymbol{v}\big) \quad \forall \boldsymbol{v} \in \boldsymbol{\mathcal{J}}^h. \tag{2.27}$$

The second problem (2.27) is a postprocess that allows to compute pressure in the elements' interior, usually at the end of the computation, or after the iterations in each time step. For example, if interior pressure p_h needs to be calculated at time t^n,

(2.27) is solved at t^n, where $\boldsymbol{u}_h^t$ can be approximated using

$$\boldsymbol{u}_h^t\big|^n = \frac{\boldsymbol{u}_h^{t^n} - \boldsymbol{u}_h^{t^{n-1}}}{\Delta t}, \text{ for first order accuracy in time,} \tag{2.28a}$$

$$\boldsymbol{u}_h^t\big|^n = \frac{\boldsymbol{u}_h^{t^{n+1}} - \boldsymbol{u}_h^{t^{n-1}}}{2\Delta t}, \text{ for second order accuracy in time,} \tag{2.28b}$$

$$\boldsymbol{u}_h^t\big|^n = \frac{-\boldsymbol{u}_h^{t^{n+2}} + 8\boldsymbol{u}_h^{t^{n+1}} - 8\boldsymbol{u}_h^{t^{n-1}} + \boldsymbol{u}_h^{t^{n-2}}}{12\Delta t}, \text{ for fourth order accuracy in time.} \tag{2.28c}$$

2.3 Numerical examples

In this section, numerical examples show the applicability and accuracy of the proposed methods. An example with analytical solution is first used to study the behavior of IPMP for Stokes and then to compare IPM and CDG from an accuracy point of view for Navier-Stokes. The applicability of IPM to the Navier-Stokes equations is then demonstrated through the classical benchmark test of the driven cavity example. Finally an example of a flow in an idealized porous medium, that is following Darcy's law, used to describe oil, water, and gas flows through petroleum reservoirs, is shown. Other examples are also presented by Montlaur et al. (2008, 2009). These examples show the diversity of the possibilities of application of the methodology developed in this thesis.

2.3.1 IPMP analysis

An example with analytical solution is considered to study the behavior of IPMP, that is, the influence of the extra non-consistent penalty in front of the IPM method. The steady incompressible Stokes equations are solved in a 2D square domain $\Omega =]0,1[\times]0,1[$ with Dirichlet boundary conditions on three sides, and Neumann boundary condition on the fourth side $\{x = 0\}$. A body force is imposed in order to have the

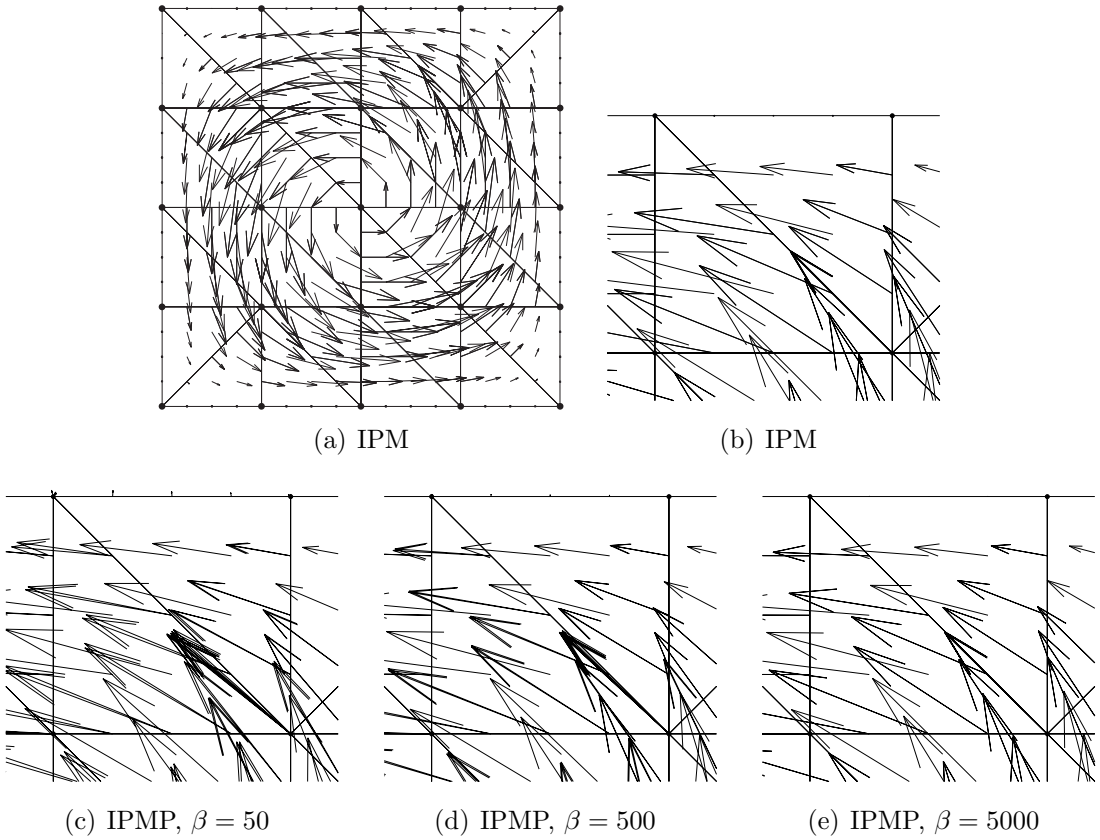

(a) IPM (b) IPM

(c) IPMP, $\beta = 50$ (d) IPMP, $\beta = 500$ (e) IPMP, $\beta = 5000$

Figure 2.5: IPM velocity solution (a) and detail (b) and IPMP velocity solution for $\beta = 50$ (c), $\beta = 500$ (d) and $\beta = 5000$ (e), with $k = 4$, $\gamma = 40$.

polynomial exact solution

$$\boldsymbol{u} = \begin{pmatrix} x^2(1-x)^2(2y - 6y^2 + 4y^3) \\ -y^2(1-y)^2(2x - 6x^2 + 4x^3) \end{pmatrix},$$

$$p = x(1-x). \tag{2.29}$$

see Montlaur et al. (2008).

Fourth order approximation for velocity and cubic approximation for pressure (i.e. $k = 4$) are considered. Figure 2.5 shows the solution of velocity obtained with IPM and with IPMP for different values of β. IPM only needs moderate values of γ to

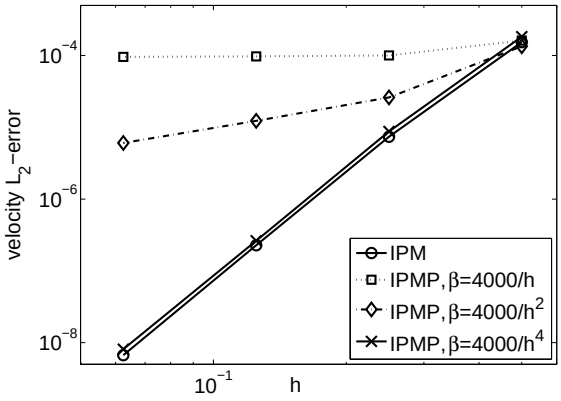

Figure 2.6: Stokes analytical example. Influence on the non-consistent penalty parameter β on the $\mathcal{L}_2$-error convergence, with $k = 4$, $\gamma = 40$

ensure coercity of the diffusion bilinear form and good properties of continuity of velocity. However when using IPMP, large values of the non-consistent parameter β are necessary to ensure moderate discontinuities of normal velocity. Note that for instance, for a mesh of 72 elements, for $k = 4$ and $\beta = 5000$, value ensuring good continuity of the solution for IPMP, the condition number of the diffusion matrix is around 3×10^7, whereas with IPM it is around 2×10^6. But the problem to solve is reduced from a dimension of 848^2 (with velocity and hybrid pressure) to 640^2 (with velocity only).

Figure 2.6 now presents the evolution of the velocity $\mathcal{L}_2$-error under h-refinement for IPM and for IPMP for differents values of β. Note that as usual when using non-consistent penalty formulations, see Babuska (1973), optimal convergence rates are obtained by taking a penalty β of order h^{-k}. For this choice of β, the accuracy obtained is similar to the one obtained with IPM, see Montlaur et al. (2008) for further comparison between IPM and IPMP. As previously commented, the main difference between IPM and IPMP is that while moderate values of the consistent penalty γ of order h^{-1} provide optimal orders of convergence with IPM, large values of the non-consistent penalty β of order h^{-k} are needed for IPMP. That is, though IPM presents the advantage of a further reduction of the number of dof, its drawbacks are that the tuning of β affects the accuracy of the solution and large values of β lead to

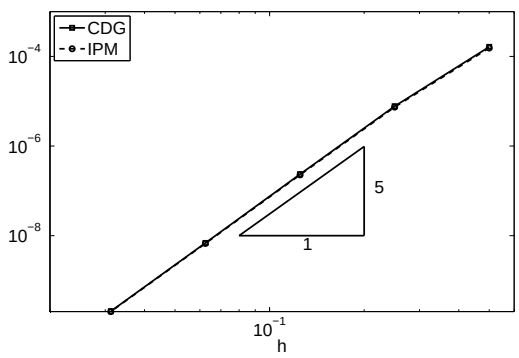

(a) Velocity $\mathcal{L}_2$-error

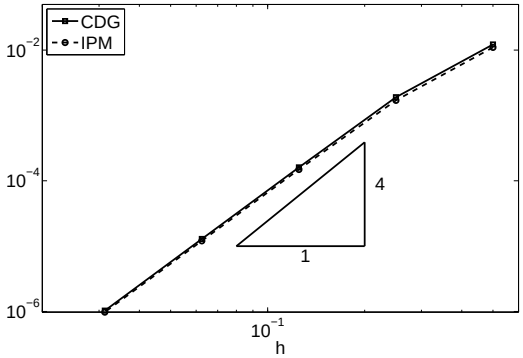

(b) Hybrid pressure $\mathcal{L}_2$-error

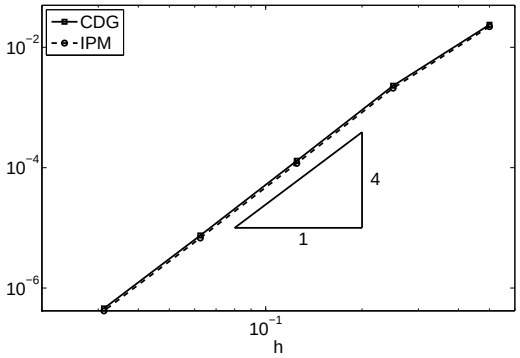

(c) Interior pressure $\mathcal{L}_2$-error

Figure 2.7: Comparison of $\mathcal{L}_2$-errors obtained with CDG and IPM, for a fourth order approximation of the velocity and a cubic interpolation of hybrid and interior pressures, with $C_{11} = 40h^{-1}$ and $\gamma = 40$ respectively.

ill-conditioned diffusion matrices.

2.3.2 IPM and CDG accuracy comparison

The same example with analytical solution described in 2.3.1 is now considered to compare CDG or IPM from an accuracy point of view. This example is adapted to solve the Navier-Stokes equations. That is, the body force term is changed so that the solution (2.29) is solution of the Navier-Stokes equations, see Montlaur et al. (2009). Once again fourth order approximation for velocity and cubic approximation for pressure (i.e. $k = 4$) are considered. A value of $C_{11} = 40h^{-1}$, corresponding to

penalty parameter $\gamma = 40$, is considered, which is close to the minimum value that ensures coercivity of the IPM bilinear form. With these selections of C_{11} and γ, similar results are obtained as seen in Figure 2.7: both methods reach optimal convergence rates for velocity and hybrid pressure, with similar accuracy.

The influence of C_{11} on the accuracy of CDG is analyzed by Montlaur et al. (2009) and it is shown that for any value of C_{11}, optimal convergence is obtained, with similar accuracy.

2.3.3 Driven cavity example

A standard benchmark test for the Navier-Stokes equations is now considered to show the applicability of IPM. A plane flow of an isothermal fluid in a lid-driven cavity is modelled in a 2D square domain $\Omega =]0,1[\times]0,1[$, with zero body force and one moving wall. A continuous velocity

$$\boldsymbol{u} = \begin{cases} (10x, 0)^T & \text{for } 0 \leq x \leq 0.1 \\ (1, 0)^T & \text{for } 0.1 \leq x \leq 0.9 \\ (10 - 10x, 0)^T & \text{for } 0.9 \leq x \leq 1 \end{cases}$$

is imposed on the exterior upper boundary $\{y = 1\}$, and a zero velocity $\boldsymbol{u} = (0, 0)^T$ is enforced on the three other sides.

Figure 2.8 shows the velocity streamlines, which are conformed to the expected solution. The main vortex moves toward the center of the cavity for increasing Reynolds number. Velocity profiles at the vertical centerline are shown in Figure 2.9 for $Re = 1,400$. It can be noticed that as the Reynolds number increases, the boundary layers are more obvious and the variations in the velocity are sharper.

2.3.4 Flow in an idealized porous medium

This last example shows another kind of application of incompressible flows. A fluid in an idealized porous medium is subject to a friction force proportional to the fluid

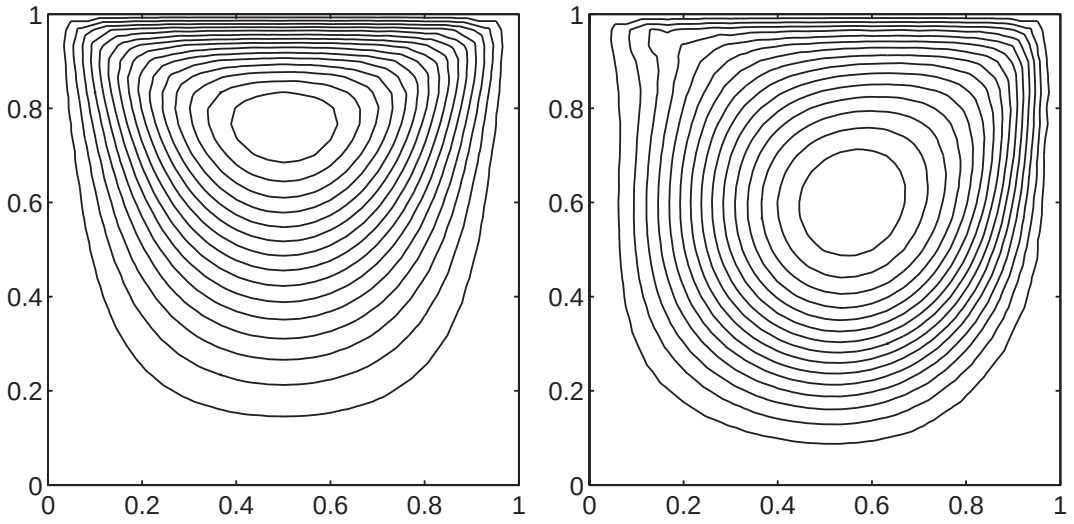

(a) $Re = 1$ (b) $Re = 400$

Figure 2.8: Driven cavity: velocity streamlines for $Re = 1$ (a) and $Re = 400$ (b), $k = 2$, $h = 0.0667$, $\gamma = 10$.

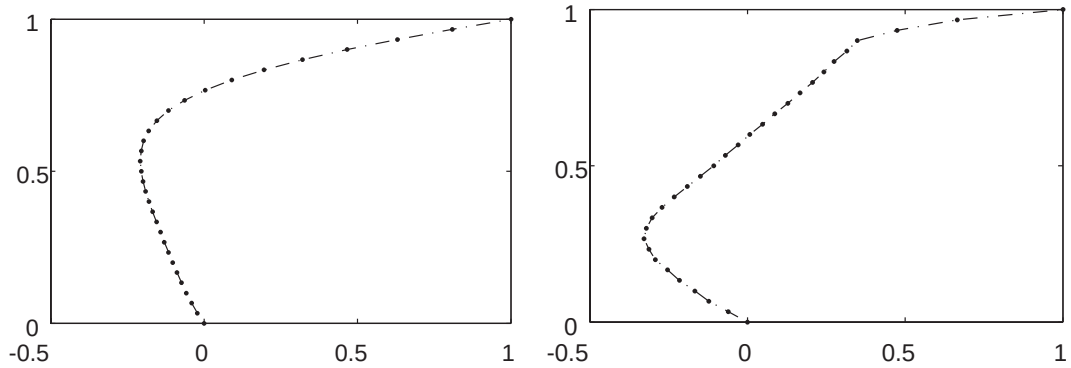

(a) $Re = 1$ (b) $Re = 400$

Figure 2.9: Driven cavity: velocity profiles at the vertical centerline, for $Re = 1$ (a) and $Re = 400$ (b), $k = 2$, $h = 0.0667$, $\gamma = 10$.

velocity $\boldsymbol{u}$. This kind of problem is derived from the Stokes equations and it follows Darcy's law. It is valid for slow, viscous flow, such as groundwater flows. Darcy's law is also used to describe oil, water, and gas flows through petroleum reservoirs. The

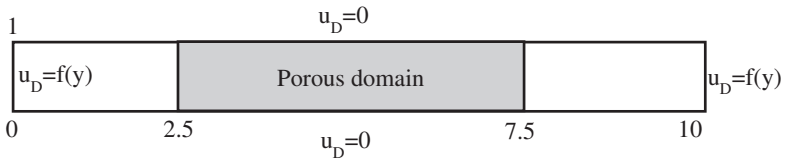

Figure 2.10: Computational domain. The porous domain is limited to the central part, of length $5l$ and height l.

problem to be solved is

$$-\boldsymbol{\nabla}\cdot\boldsymbol{\sigma} = -\alpha\boldsymbol{u} \qquad \text{in } \widehat{\Omega},$$

$$\boldsymbol{\nabla}\cdot\boldsymbol{u} = 0 \qquad \text{in } \widehat{\Omega},$$

with boundary and interface conditions (2.1c)-(2.1f), and where α is the inverse of the local permeability of the medium ($\alpha = 0$ for an empty medium and $\alpha = +\infty$ for a solid wall), see Okkels et al. (2005).

These equations are solved in the computational domain shown in Figure 2.10, consisting of a long straight channel of height l and length $L = 10l$. The porous domain is limited to the central part of length $5l$. The porous domain is filled with porous material of arbitrary value $\alpha = 100$ for $2.5 < x < 7.5$ except for two regions verifying

$$x \in]3.5, 6.5[\quad \text{and} \quad y \in]0, \frac{1}{3}[\cup]\frac{2}{3}, 1[,$$

where empty medium is assumed, see white region in Figure 2.11. Dirichlet boundary conditions prescribe a parabolic velocity profile at the inlet and at the outlet, and a no-slip condition for the fluid on the channel sides.

A detail of the IPM velocity result in the porous domain is shown in Figure 2.11, demonstrating the capability of IPM for the solution of Darcy's problems. As expected, the two empty regions divert the flow away from the center of the channel: the flow tends to go into the empty domains, with higher velocities than in the porous region.

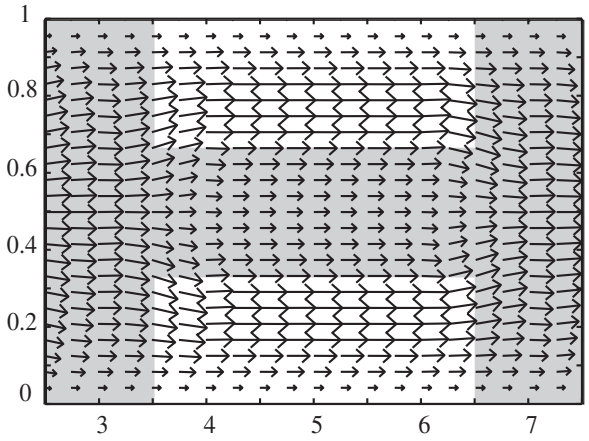

Figure 2.11: Velocity vectors within the porous domain of length $5l$. The grey part represents a porous material, the white ones an empty domain.

2.4 Summary

Discontinuous Galerkin (DG) formulations with solenoidal approximations for the simulation of incompressible flow are proposed, with applications to the Stokes and Navier-Stokes equations. First, the methodology of Interior Penalty Method (IPM) is followed to develop an IPM-DG formulation for Stokes and Navier-Stokes problems. The resulting bilinear form for the diffusion term is symmetric and coercive. Then the interpolation space is decomposed in every element into a solenoidal part and an irrotational part. This allows to split the IPM weak form in two uncoupled problems. The first one solves for velocity and hybrid pressure, and the second one allows the evaluation of pressures in the interior of the elements as a post-process. An alternative to IPM is the Compact Discontinuous Galerkin (CDG) formulation with solenoidal velocities that presents the advantage of eliminating the tuning of the penalty parameter, but has the major disadvantage of the implementation and computation of local lifting operators. Both IPM and CDG lead to efficient, compact and high-order formulations, which show similar results for the condition number of the diffusion matrix and for the accuracy of the numerical solution.

The formulation with solenoidal velocities and hybrid pressures presents an important save in the number of degrees of freedom (dof) compared to continuous Galerkin

or classical Discontinuous Galerkin techniques. A formulation introducing a penalty parameter for the weak enforcement of continuity of the normal velocity along element sides is also proposed in order to further reduce the number of dof. It leads to another DG formulation where the computation of velocities and pressures is completely decoupled, representing an important computational save, but where the non-consistent penalty term leads to ill-conditioned systems of equations.

Chapter 3

High-order Implicit Runge-Kutta methods for unsteady incompressible flows

Chapter 2 shows how Discontinuous Galerkin (DG) methods are used to discretize the incompressible Navier-Stokes equations, taking advantage of the possibility to easily define high-order divergence-free approximations. The resulting DG schemes are efficient and have high-order properties in space. The objective of this chapter is to obtain an implicit and high-order time integration method, so that the resulting scheme proposed in this thesis has high-order properties both in time and space.

An implicit scheme is preferred in order to be able to solve multiple spatial scales occurring in high Reynolds number flow or in boundary layers, without having to decrease drastically the time step size. This choice leads to nonlinear algebraic systems of equations, which need to be solved at each time step. The time algorithms discussed in this chapter are applied using the solenoidal IPM-DG formulation previously proposed, since it is an efficient scheme, allowing an important save in degrees of freedom. Nevertheless, the time algorithms proposed here would be equally applicable to other types of spatial discretization schemes, for example using classical Discontinuous Galerkin or continuous Galerkin methods.

Section 3.1 proposes several high-order implicit Runge-Kutta (IRK) methods for incompressible flows. IRK methods are chosen to solve such problems because they reach high orders of accuracy and are unconditionally stable. Section 3.1.1 shows

how the incompressible Navier-Stokes equations are considered as Differential Algebraic Equations (DAE), that is a system of Ordinary Differential Equations (ODE) corresponding to the conservation of momentum equation, plus algebraic constraints corresponding to the incompressibility condition. Section 3.1.2 emphasizes the main advantages and disadvantages of fully implicit Runge-Kutta methods (IRK) and semi-implicit Runge-Kutta methods (SDIRK), describing the systems of equations obtained in each case, as well as the orders of convergence achieved. Section 3.1.3 discusses the asymptotic stability of the proposed methods for the Oseen equations. Eventually numerical examples, presented in Section 3.2, show the applicability of the methods and compare their accuracy and cost with a classical Crank-Nicolson scheme.

3.1 DAE Runge-Kutta methods for unsteady incompressible flows

3.1.1 DAE for incompressible flows

The strong form of the unsteady incompressible Navier-Stokes problem can be written as

$$\frac{\partial \boldsymbol{u}}{\partial t} - 2\boldsymbol{\nabla}\cdot(\nu\boldsymbol{\nabla}^{\mathbf{S}}\boldsymbol{u}) + \boldsymbol{\nabla}p + (\boldsymbol{u}\cdot\boldsymbol{\nabla})\boldsymbol{u} = \boldsymbol{f} \qquad \text{in } \hat{\Omega}, \tag{3.1a}$$

$$\boldsymbol{\nabla}\cdot\boldsymbol{u} = 0 \qquad \text{in } \hat{\Omega}, \tag{3.1b}$$

with boundary and interface conditions (2.1c)-(2.1f), and initial condition being $\boldsymbol{u}(\boldsymbol{x},0) = \boldsymbol{u}_0$ in $\hat{\Omega}$.

Here the space discretization of the incompressible Navier-Stokes equations is carried out using the IPM-DG scheme with solenoidal approximations that has been detailed in Chapter 2. Nevertheless, the algorithms discussed in this chapter would be equally applicable to other types of discretization schemes, such as classical Discontinuous Galerkin or continuous Galerkin. In any case, the space discretization of

the unsteady incompressible Navier-Stokes problem (3.1) can be written as

$$\begin{cases} \mathbf{M}\dot{\mathbf{u}} + \mathbf{K}\mathbf{u} + \mathbf{C}(\mathbf{u})\mathbf{u} + \mathbf{G}\mathbf{p} = \mathbf{f_1} \\ \mathbf{G}^T\mathbf{u} = \mathbf{f_2} \end{cases} \tag{3.2}$$

where $\mathbf{M}$ is the mass matrix, $\mathbf{K}$ the diffusion matrix, $\mathbf{C}$ the convection matrix, $\mathbf{G}$ the pressure matrix, $\mathbf{u}$ and $\mathbf{p}$ the vectors of nodal values, or approximation coefficients of velocity and pressure respectively, and $\mathbf{f_1}$ and $\mathbf{f_2}$ vectors taking into account force term and boundary conditions. This system, of $\mathtt{n_{dof}}$ degrees of freedom, can also be written as

$$\begin{cases} \dot{\mathbf{u}} = \mathcal{F}(t, \mathbf{u}, \mathbf{p}) \\ 0 = \mathcal{G}(t, \mathbf{u}) \end{cases} \tag{3.3}$$

where

$$\begin{aligned} \mathcal{F}(t, \mathbf{u}, \mathbf{p}) &= \mathbf{M}^{-1}\left(\mathbf{K}\mathbf{u} + \mathbf{C}(\mathbf{u})\mathbf{u} + \mathbf{G}\mathbf{p} - \mathbf{f_1}\right), \\ \mathcal{G}(t, \mathbf{u}) &= \mathbf{G}^T\mathbf{u} - \mathbf{f_2}. \end{aligned} \tag{3.4}$$

Note that $\frac{\partial \mathcal{G}}{\partial \mathbf{u}}\frac{\partial \mathcal{F}}{\partial \mathbf{p}} = \mathbf{G}^T\mathbf{M}^{-1}\mathbf{G}$ is invertible, therefore (3.3) is a Hessenberg index-2 DAE system (Hairer et al., 1989).

DAEs originate in the modelisation of various physical or chemical phenomena and have been deeply studied during the last years (Hairer et al., 1989; Brenan et al., 1996). They are classified by their differential index, that is, the minimum number of times that the DAE system must be differentiated to obtain an ODE. As previously commented, the discrete incompressible Stokes or Navier-Stokes equations are index-2 DAE systems. Instead of reformulating DAEs as ODEs, many numerical methods defined for ODEs have been adapted to DAEs, as for example multistep Backward Differentiation Formulae (BDFs) (Brenan and Engquist, 1988) or Runge-Kutta methods (Brenan et al., 1996). Runge-Kutta methods have been first regarded as poor competitors to multistep methods, mainly because the order of convergence obtained was less than the order obtained for ODEs, and the higher the index, the higher the reduction, for most DAEs. Ulterior results from Hairer and Wanner (1991) have however shown that good Runge-Kutta methods can form the basis of a competitive

code, because they are unconditionally stable and can reach orders of convergence as high as when applied to ODE.

In this work, Runge-Kutta methods for index-2 DAE are considered (Hairer and Wanner, 1991). An s-stage Runge-Kutta method for (3.3) reads

$$\begin{aligned} \mathbf{u}^{n+1} &= \mathbf{u}^n + \Delta t \sum_{i=1}^{s} b_i \mathbf{l}_i \\ \mathbf{p}^{n+1} &= \mathbf{p}^n + \Delta t \sum_{i=1}^{s} b_i \mathbf{k}_i \end{aligned} \tag{3.5}$$

where $\mathbf{l}_i$ and $\mathbf{k}_i$ are defined by

$$\mathbf{l}_i = \mathcal{F}(t^n + c_i \Delta t, \mathbf{u}^n + \Delta t \sum_{j=1}^{s} a_{ij} \mathbf{l}_j, \mathbf{p}^n + \Delta t \sum_{j=1}^{s} a_{ij} \mathbf{k}_j) \tag{3.6a}$$

$$0 = \mathcal{G}(t^n + c_i \Delta t, \mathbf{u}^n + \Delta t \sum_{j=1}^{s} a_{i,j} \mathbf{l}_j) \tag{3.6b}$$

for $i = 1, ..., s$. Coefficients a_{ij}, b_i, c_i come from the Butcher array, whose general form is seen in Table 3.1. Depending on the specific form of the Butcher array, implicit,

c_1	a_{11}	a_{12}	$\cdots$	a_{1s}
c_2	a_{21}	a_{22}	$\cdots$	a_{2s}
$\vdots$	$\vdots$	$\vdots$		$\vdots$
c_s	a_{s1}	a_{s2}	$\cdots$	a_{ss}
	b_1	b_2	$\cdots$	b_s

Table 3.1: Butcher array

semi-implicit or explicit Runge-Kutta methods are obtained. A Runge-Kutta method is said to be explicit if its Butcher array is strictly lower triangular, that is $a_{ij} = 0$ for $j > i$. Otherwise the method is implicit (IRK). In particular, an implicit method is said to be semi-implicit, or singly diagonally implicit (SDIRK), if $a_{ij} = 0$ for $j > i$ and $a_{ii} \neq 0$ for some i. This work focuses on fully implicit and semi-implicit methods because of their stability properties. In fact, explicit Runge-Kutta methods can not

even be used in the form of (3.5)-(3.6) for Hessenberg index-2 DAEs, because the resulting system (3.6) is under-determined to solve for $\mathbf{l}_i$ and $\mathbf{k}_i$. Nevertheless Pereira et al. (2001) proved that explicit Runge-Kutta methods can be applied to DAE, using a different formulation than (3.5)-(3.6). This formulation can be found in Appendix C, where it is also shown that the order of convergence of explicit Runge-Kutta methods applied to DAE is less than the one reached for a regular ODE.

3.1.2 IRK and SDIRK methods

Table 3.2 shows Butcher diagrams for 2- and 3-stage Radau IIA-IRK methods. Radau IIA-IRK methods are a special case of IRK methods satisfying the additional property: $b_j = a_{sj}$ for $j = 1, \cdots, s$. These methods are called IRK(DAE) and they stand out from all IRK methods in view of their applicability to DAE since at the last stage, $\mathbf{u}^{n+1}$ directly satisfies $\mathcal{G}\left(t^{n+1}, \mathbf{u}^{n+1}\right) = 0$.

$\frac{1}{3}$	$\frac{5}{12}$	$-\frac{1}{12}$
1	$\frac{3}{4}$	$\frac{1}{4}$
	$\frac{3}{4}$	$\frac{1}{4}$

$\frac{4-\sqrt{6}}{10}$	$\frac{88-7\sqrt{6}}{360}$	$\frac{296-169\sqrt{6}}{1800}$	$\frac{-2+3\sqrt{6}}{225}$
$\frac{4+\sqrt{6}}{10}$	$\frac{296+169\sqrt{6}}{1800}$	$\frac{88+7\sqrt{6}}{360}$	$\frac{-2-3\sqrt{6}}{225}$
1	$\frac{16-\sqrt{6}}{36}$	$\frac{16+\sqrt{6}}{36}$	$\frac{1}{9}$
	$\frac{16-\sqrt{6}}{36}$	$\frac{16+\sqrt{6}}{36}$	$\frac{1}{9}$

Table 3.2: Butcher array for 2-stage (left) and 3-stage (right) Radau IIA-IRK methods

Table 3.3 shows the order of convergence for index-2 DAE (such as the discrete incompressible Navier-Stokes problem), and for ODE, for s-stage Radau IA, IIA and Lobatto IIIC methods. Other methods, such as Gauss or Lobatto IIIA, exist but when applied to DAE they present higher order reduction with respect to ODE, so they have not been chosen here. It can be seen that for index-2 DAE, the best orders of convergence for velocity and pressure are obtained for a Radau IIA-IRK method and the order of convergence for velocity is the same as the one obtained for an ODE. This is thus the scheme selected here. 2- and 3-stage Radau IIA-IRK are compared from accuracy and cost points of view in Section 3.2.2.

Note that the solution of an index-2 DAE system, such as (3.3), with an s-stage

Method	DAE: $\boldsymbol{u}$ error	DAE: p error	ODE error
Radau IA	h^s	h^{s-1}	h^{2s-1}
Radau IIA	h^{2s-1}	h^s	h^{2s-1}
Lobatto IIIC	h^{2s-2}	h^{s-1}	h^{2s-2}

Table 3.3: Orders of convergence for s-stage IRK methods for index-2 DAEs and for ODEs (Butcher, 1987; Hairer and Wanner, 1991).

implicit Runge-Kutta method requires solving a non-linear system of equations of dimension $s\mathtt{n}_{\mathtt{dof}}$ at each time step, where $\mathtt{n}_{\mathtt{dof}}$ is the number of degrees of freedom in (3.3): find $\mathbf{l}_i$ and $\mathbf{k}_i$, such that

$$\begin{aligned}
&\left(\mathbf{K}+\mathbf{C}_{(\mathbf{u}^n+\Delta t\sum a_{ij}\mathbf{l}_j)}\right)\left(\mathbf{u}^n+\Delta t\sum_{j=1}^{s}a_{ij}\mathbf{l}_j\right)\\
&+\mathbf{G}\left(\mathbf{p}^n+\Delta t\sum_{j=1}^{s}a_{ij}\mathbf{k}_j\right)+\mathbf{M}\mathbf{l}_i-\mathbf{f_1}\left(t^n+c_i\Delta t\right)=\mathbf{0}\\
&\mathbf{G}^T\left(\mathbf{u}^n+\Delta t\sum_{j=1}^{s}a_{ij}\mathbf{l}_j\right)-\mathbf{f_2}\left(t^n+c_i\Delta t\right)=\mathbf{0}
\end{aligned}$$

for $i=1\ldots s$.

Table 3.4 now shows the Butcher diagram for a 2-stage SDIRK method. The

$\frac{3\pm\sqrt{3}}{6}$	$\frac{3\pm\sqrt{3}}{6}$	0
$\frac{3\mp\sqrt{3}}{6}$	$\frac{\mp\sqrt{3}}{3}$	$\frac{3\pm\sqrt{3}}{6}$
	$\frac{1}{2}$	$\frac{1}{2}$

Table 3.4: Butcher array for 2-stage SDIRK methods

computational effort in implementing semi-implicit methods is substantially less than for a fully implicit method, indeed s systems of dimension $\mathtt{n}_{\mathtt{dof}}$ are to be solved, instead of a problem of dimension $s\mathtt{n}_{\mathtt{dof}}$ in the fully implicit scheme. Also for a linear problem, as for example the Stokes problem, one may hope to use repeatedly the stored LU-factorization of the iterative matrix. Nevertheless this method does not allow to reach high orders of convergence, as seen in Table 3.5. Unlike for ODE problems, increasing

Number of stages	DAE: $\boldsymbol{u}$ error	DAE: p error	ODE error
2	2	1	3
3	2	1	4
5	2	1	6

Table 3.5: Orders of convergence for SDIRK methods for index-2 DAEs and for ODEs (Butcher, 1987; Hairer and Wanner, 1991).

the number of stages of SDIRK methods does not improve the order of convergence for index-2 DAE systems: the order of convergence obtained for an index-2 DAE system is always 2 for velocity and 1 for pressure, for 2, 3 and 5 stages. Furthermore Norsett (1974) conjectured and presented some evidence for the belief that for any s even number greater than two, no SDIRK method exists. That is why no 4-stage method appears in Table 3.5. The 2-stage SDIRK is thus the most efficient SDIRK method and is chosen here.

The solution of an index-2 DAE system, such as (3.3), with a 2-stage SDIRK method requires solving two non-linear systems of equations of dimension $\mathtt{n_{dof}}$ at each time step: first, find $\mathbf{l}_1$ and $\mathbf{k}_1$ such that

$$\begin{aligned}\left(\mathbf{K}+\mathbf{C}_{(\mathbf{u}^n+\Delta t a_{11}\mathbf{l}_1)}\right)\left(\mathbf{u}^n+\Delta t a_{11}\mathbf{l}_1\right)+\mathbf{G}\left(\mathbf{p}^n+\Delta t a_{11}\mathbf{k}_1\right)+\mathbf{M}\mathbf{l}_1-\mathbf{f_1}(t^n+c_1\Delta t)&=\mathbf{0}\\ \mathbf{G}^T\left(\mathbf{u}^n+\Delta t a_{11}\right)-\mathbf{f_2}(t^n+c_1\Delta t)&=\mathbf{0}\end{aligned}$$

then, given $\mathbf{l}_1$ and $\mathbf{k}_1$, find $\mathbf{l}_2$ and $\mathbf{k}_2$ such that

$$\begin{aligned}&\left(\mathbf{K}+\mathbf{C}_{(\mathbf{u}^n+\Delta t(a_{21}\mathbf{l}_1+a_{22}))}\right)\left(\mathbf{u}^n+\Delta t(a_{21}\mathbf{l}_1+a_{22}\mathbf{l}_2)\right)\\ &\quad+\mathbf{G}\left(\mathbf{p}^n+\Delta t(a_{21}\mathbf{k}_1+a_{22}\mathbf{k}_2)\right)+\mathbf{M}\mathbf{l_2}-\mathbf{f_1}(t^n+c_2\Delta t)=\mathbf{0}\\ &\qquad\mathbf{G}^T\left(\mathbf{u}^n+\Delta t(a_{21}\mathbf{l}_1+a_{22}\mathbf{l}_2)\right)-\mathbf{f_2}(t^n+c_2\Delta t)=\mathbf{0}.\end{aligned}$$

The cost of solving DAE systems with SDIRK is thus substantially less than the cost of solving DAE with IRK methods, but the numerical example of Section 3.2.2 shows that the improved accuracy obtained using IRK is worth the extra cost needed for

the solution of larger systems of equations.

3.1.3 Asymptotic stability

As a step towards the study of the asymptotic properties of the solution of the incompressible Navier-Stokes equations, the linear homogeneous Oseen equations are now considered. The results of asymptotic stability for this scheme can then be extended to the non-linear Navier-Stokes equations. The strong form of the unsteady incompressible homogeneous Oseen problem is

$$\frac{\partial \boldsymbol{u}}{\partial t} - 2\boldsymbol{\nabla}\cdot(\nu\boldsymbol{\nabla}^{\mathtt{S}}\boldsymbol{u}) + \boldsymbol{\nabla}p + (\boldsymbol{w}\cdot\boldsymbol{\nabla})\boldsymbol{u} = \mathbf{0} \qquad \text{in } \hat{\Omega}, \tag{3.8a}$$

$$\boldsymbol{\nabla}\cdot\boldsymbol{u} = 0 \qquad \text{in } \hat{\Omega}, \tag{3.8b}$$

where $\boldsymbol{w}$ is a given velocity field, with boundary and interface conditions (2.1c)-(2.1f), and initial condition being $\boldsymbol{u}(\boldsymbol{x},0) = \boldsymbol{u}_0$ in $\hat{\Omega}$. Its discretized form is

$$\dot{\mathbf{u}} + \mathbf{M}^{-1}(\mathbf{K}+\mathbf{C})\,\mathbf{u} + \mathbf{M}^{-1}\mathbf{G}\mathbf{p} = \mathbf{0}, \tag{3.9a}$$

$$\mathbf{G}^T\mathbf{u} = \mathbf{0}. \tag{3.9b}$$

Following the discussion of asymptotic properties of solutions of general linear DAEs, and in particular the cases of index-2 DAEs by Hanke and März (1996) and Hanke et al. (1998), let $\mathbf{A} = \mathbf{M}^{-1}(\mathbf{K}+\mathbf{C})$ and $\mathbf{H} = \mathbf{M}^{-1}\mathbf{G}\left(\mathbf{G}^T\mathbf{M}^{-1}\mathbf{G}\right)^{-1}\mathbf{G}^T$. From (3.9b) we get

$$\mathbf{H}\mathbf{u} = \mathbf{0}. \tag{3.10}$$

Then multiplying (3.9a) by $\mathbf{G}^T$

$$\mathbf{p} = -\left(\mathbf{G}^T\mathbf{M}^{-1}\mathbf{G}\right)^{-1}\mathbf{G}^T\left[\dot{\mathbf{u}} + \mathbf{A}\mathbf{u}\right]. \tag{3.11}$$

Substituting again $\mathbf{p}$ in (3.9a)

$$\dot{\mathbf{u}} + \mathbf{A}\mathbf{u} - \mathbf{M}^{-1}\mathbf{G}\left(\mathbf{G}^T\mathbf{M}^{-1}\mathbf{G}\right)^{-1}\mathbf{G}^T\left[\dot{\mathbf{u}} + \mathbf{A}\mathbf{u}\right] = \mathbf{0},$$

which can be written as

$$\left(\mathbf{I} - \mathbf{H}\right)\dot{\mathbf{u}} + \left(\mathbf{I} - \mathbf{H}\right)\mathbf{A}\mathbf{u} = \mathbf{0}$$

or, using (3.10) as

$$\left[\left(\mathbf{I} - \mathbf{H}\right)\dot{\mathbf{u}}\right] = -\left(\mathbf{I} - \mathbf{H}\right)\mathbf{A}\left[\left(\mathbf{I} - \mathbf{H}\right)\mathbf{u}\right] \tag{3.12}$$

Thus, the solution of (3.9) consists of three parts: one ODE (3.12) for the variable $\left(\mathbf{I} - \mathbf{H}\right)\mathbf{u}$ – note that $\mathbf{H}$ is constant in time – and two algebraic equations (3.10) and (3.11), for $\left(\mathbf{I} - \mathbf{H}\right)\mathbf{u}$, $\mathbf{H}\mathbf{u}$ and $\mathbf{p}$. Studying the eigenvalues of $\left(\mathbf{I} - \mathbf{H}\right)\mathbf{A}$ and using stability functions for Runge-Kutta schemes give necessary conditions for the asymptotic stability of the solution, as it will be seen in Section 3.2.1.

3.2 Numerical examples

Numerical examples are now considered to show the applicability of the proposed methods. First, the asymptotic stability of SDIRK and IRK methods is checked. Then, an example with analytical solution is used to compare RK methods with a classical Crank Nicolson method from accuracy and cost points of view. The flow past a circle example is finally used to show the good behavior of the proposed methods and to demonstrate that the resulting method proposed in this thesis allows to obtain high accuracy in the description of incompressible flows and in particular in critical regions of the flow in which important flow pattern changes occur.

3.2.1 Asymptotic stability

The purpose of this section is to check the unconditional stability of SDIRK and Radau IIA-IRK methods for the Oseen equations. For each method, stability functions $R(\lambda\Delta t) = R(z)$ are recalled for eigenvalues λ and time step Δt. For a DAE system, as the Oseen problem, λ represents the eigenvalues of $(\mathbf{I} - \mathbf{H})\,\mathbf{A}$, see (3.12). For SDIRK and Radau IIA-IRK methods, the stability functions are defined as follows, see Hairer and Wanner (1991), with $z = \lambda\Delta t$

$$
\begin{aligned}
R(z) &= \frac{1 + (1-2\gamma)\,z + \left(\frac{1}{2} - 2\gamma + \gamma^2\right) z^2}{(1-\gamma z)^2} && \text{for 2-stage SDIRK with } \gamma = \frac{3 \pm \sqrt{3}}{6},\\
R(z) &= \frac{6 + 2z}{6 - 4z + z^2} && \text{for 2-stage Radau IIA-IRK,}\\
R(z) &= \frac{60 + 24z + 3z^2}{60 - 36z + 9z^2 - z^3} && \text{for 3-stage Radau IIA-IRK.}
\end{aligned}
$$

Figure 3.1 shows the stability regions (part of the complex plane shown in white), that is, verifying $|R(\lambda\Delta t)| \leq 1$, for 2-stage SDIRK, 2- and 3-stage Radau IIA-IRK schemes. Note that the whole left-hand side of the complex plane belongs to the stability regions of Radau IIA-IRK and SDIRK with $\gamma = \frac{3+\sqrt{3}}{6}$, making these schemes unconditionally stable for the incompressible Oseen problem. Figure 3.2 shows the positions of the product $\lambda\Delta t$, where λ are the eigenvalues of $(\mathbf{I} - \mathbf{H})\,\mathbf{A}$. Two Reynolds numbers are considered $Re = 100, 10000$, a fifth order approximation for velocities, that is $k = 5$, and space and time discretization of respectively $h = 0.1$ and $\Delta t = 1$. It can be seen that even for high Reynolds number the products $\lambda\Delta t$ remain in the left-hand side of the complex plane, that is eigenvalues with negative real part. Thus the solution of the incompressible Oseen equations is unconditionally stable for 2-stage SDIRK, with $\gamma = \frac{3+\sqrt{3}}{6}$, and also for 2- and 3-stage Radau IIA-IRK schemes. However, note that for 2-stage SDIRK with $\gamma = \frac{3-\sqrt{3}}{6}$, it is only conditionally stable, that is, Δt has to be taken small enough so that all $\lambda\Delta t$ stand within the stable region. Though this analysis only gives a necessary condition for the asymptotic stability of the solution of the incompressible Oseen equations, numerical experiments show that

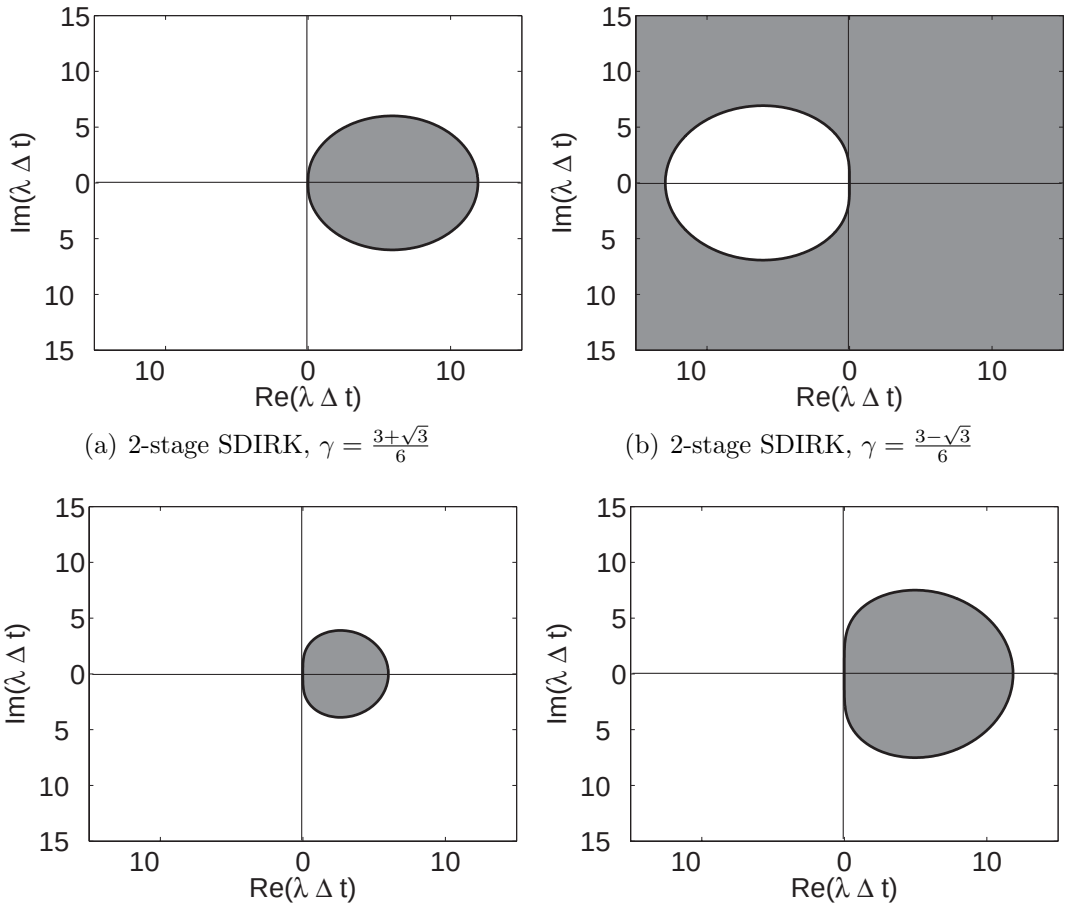

(a) 2-stage SDIRK, $\gamma = \frac{3+\sqrt{3}}{6}$

(b) 2-stage SDIRK, $\gamma = \frac{3-\sqrt{3}}{6}$

(c) 2-stage Radau IIA-IRK

(d) 3-stage Radau IIA-IRK

Figure 3.1: Stability regions in the complex plane for SDIRK and IRK methods. The stable region corresponds to the white part.

this is actually also a sufficient condition and that the same results stand when applied to the incompressible Navier-Stokes equations.

3.2.2 Runge-Kutta and Crank-Nicolson accuracy and cost comparison

An unsteady example with analytical solution proposed by Guermond et al. (2006) is now used to compare the accuracy and cost of 2- and 3- stage Radau IIA-IRK,

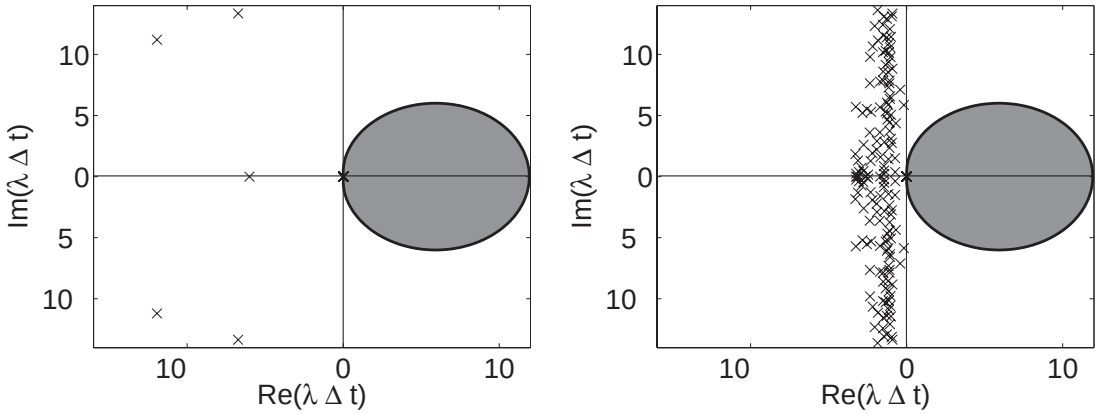

(a) $Re = 100$ (b) $Re = 1000$

Figure 3.2: Position of $\lambda\Delta t$ marked with $\times$, where λ represents the eigenvalues of $(\mathbf{I} - \mathbf{H})\,\mathbf{A}$ for $Re = 100$, 10000, for $k = 5$, $\Delta t = 1$ and $h = 0.1$, for an Oseen problem and stability region for 2-stage SDIRK scheme with $\gamma = \frac{3+\sqrt{3}}{6}$.

2-stage SDIRK with $\gamma = \frac{3+\sqrt{3}}{6}$, and Crank-Nicolson (CN) methods, which all are unconditionally stable methods for incompressible Navier-Stokes problems. The incompressible Navier-Stokes equations are solved in a 2D square domain $\Omega =]0, \frac{1}{2}[\times]0, \frac{1}{2}[$ with Dirichlet boundary conditions on three sides and Neumann boundary condition on the fourth side $\{x = 0\}$. A body force

$$\boldsymbol{f} = \begin{pmatrix} 2\nu sin(x+t)sin(y+t) + cos(x-y+t) + sin(x+y+2t) + sin(x+t)cos(x+t) \\ 2\nu cos(x+t)cos(y+t) - cos(x-y+t) - sin(x+y+2t) - sin(y+t)cos(y+t) \end{pmatrix}$$

is imposed in order to have the exact solution

$$\boldsymbol{u} = \begin{pmatrix} sin(x+t)sin(y+t) \\ cos(x+t)cos(y+t) \end{pmatrix},$$

$$p = sin(x-y+t).$$

Polynomial interpolation of degree $k = 4$ for velocity and 3 for pressure is chosen and an unstructured mesh of 128 elements is used, see Figure 3.3, in order to show that the implicit time integration methods presented here can deal perfectly with important variations of mesh size. Here the size of the elements is $0.01 \leq h \leq 0.1$. The calculation is made until a final time $t = 40$. The initial condition prescribes the exact solution on the whole domain.

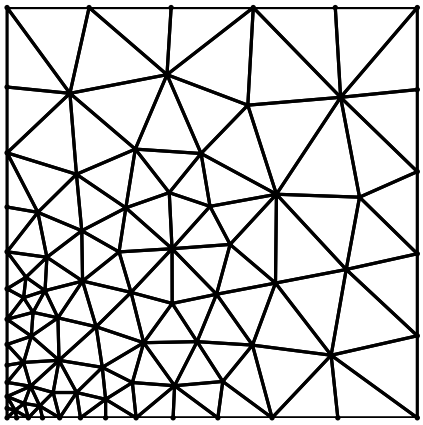

Figure 3.3: Unsteady analytical example: unstructured mesh of 128 elements, size of the elements is such that $0.01 \leq h \leq 0.1$.

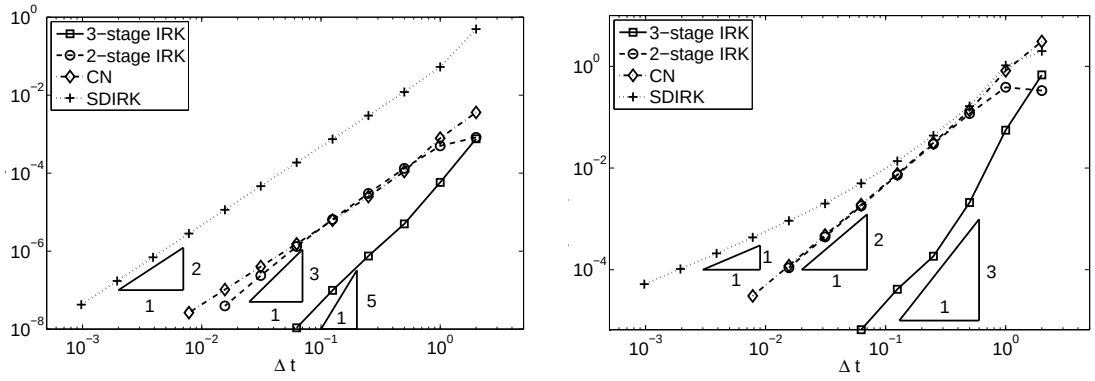

(a) Velocity error

(b) Hybrid pressure error

Figure 3.4: Unsteady analytical example: velocity and hybrid pressure $\mathcal{L}_2$-errors for 3-stage and 2-stage IRK, SDIRK and CN methods, $k = 4$, $0.01 \leq h \leq 0.1$.

Figure 3.4 shows the convergence of error under Δt-refinement obtained when solving (2.26) for velocity and hybrid pressure. The highest orders of convergence, almost fourth order for velocity and third order for hybrid pressure, are obtained when using the 3-stage Radau IIA-IRK method. Note that sub-optimal orders of convergence of the velocity error are obtained for Radau IIA-IRK methods for this example, but using a finer mesh would allow to reach optimal theoretical orders of convergence. This has been checked through scalar examples. An order of convergence of almost 4 is obtained instead of an optimal order of 5 for 3-stage IRK, and of around 2.6 instead of 3 for 2-stage IRK. SDIRK and CN show the expected second order in time for velocity but SDIRK has a much worse accuracy than the other methods. As for hybrid pressure, optimal orders are obtained for all methods, third order for 3-stage IRK, second order for 2-stage IRK and CN, and first order for SDIRK. Figure 3.5 shows the accuracy of the numerical solution of the interior pressure

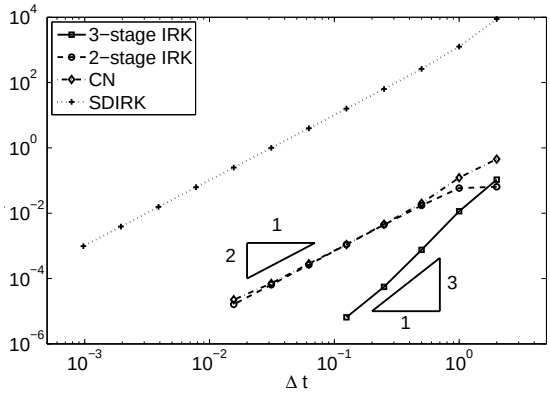

Figure 3.5: Unsteady analytical example: interior pressure $\mathcal{L}_2$-errors for 3-stage and 2-stage IRK, SDIRK and CN methods, $k = 4$, $0.01 \leq h \leq 0.1$.

obtained as a post-process by solving (2.27) using a fourth order approximation for the derivative of $\boldsymbol{u}_h$, see (2.28c). It can be seen that using this fourth order time derivative approximation, interior pressure reaches the same optimal orders of convergence as the ones obtained for hybrid pressure error.

Figures 3.4 and 3.5 demonstrate that 3-stage Radau IIA-IRK is the most accurate method when compared to other methods such as CN, 2-stage Radau IIA-IRK, or

SDIRK. Nevertheless it is also the most expensive, since for example compared to CN, it requires three times more evaluations of the convective residue at each iteration and it also leads to a larger non-linear system to solve. It is thus necessary to balance the higher precision obtained with the higher cost per iteration needed.

Let us recall that a high-order time integration scheme is desired to obtain the same level of accuracy in time as in space. The global error, for velocity for example, is

$$e = c_1 h^k + c_2 \Delta t^r$$

where k is the order of the space velocity interpolation and r the order of the time integration. Assuming that a characteristic mesh size is $h = 0.1$. For $k = 4$, the order of magnitude of precision obtained in space is around 10^{-4}. If a scheme like 3-stage Radau IIA-IRK, reaching fourth or fifth order in time, is used, a time step of $\Delta t = 0.1$ can be considered to reach equivalent accuracy in time and in space. Whereas if a second order method as for example CN, is used, a time step of $\Delta t = 0.01$ has to be taken. This means that ten times more time steps are needed with CN than with 3-stage Radau IIA-IRK to reach the same time accuracy. Note that Figure 3.4(a) confirms this fact, the velocity error obtained with 3-stage Radau IIA-IRK for a time step of $\Delta t = 0.1$ is equivalent to the one obtained with a CN scheme for $\Delta t \approx 0.01$.

Now let us compare the cost of both methods. As previously commented, 3-stage Radau IIA-IRK requires three evaluations of the convective residue when only one evaluation is needed for CN. At each iteration, it has been checked for 3-stage Radau IIA-IRK that almost 90% of the CPU time is spent in evaluating the convective residue and only 10% in other operations such as the solution of the non-linear system. Note that in order to decrease this cost, future work plans to use a mixed implementation using Matlab and C++ in order to optimize the calculation of the convective residue, which is where most CPU time is spent in the whole code, see Section 4.1.1. Thus, roughly speaking, 3-stage Radau IIA-IRK is three times more expensive than CN at each iteration. In both cases a Broyden method is used to solve the non-linear system and the same number of iterations is needed to solve the non-linear system at each time step. Since 3-stage Radau IIA-IRK needs ten times less time steps than CN to

reach equivalent precision for velocity, globally and for high levels of precision, 3-stage Radau IIA-IRK is three times more efficient than CN. The same comparison can be made with hybrid pressure. Though the differences are not that obvious because levels of precision for pressure are more similar, 3-stage IRK is again more efficient than CN. The following study confirms these numbers.

Figure 3.6 compares the $\mathcal{L}_2$-errors of velocity and hybrid pressures obtained with 2- and 3- stage Radau IIA-IRK, 2-stage SDIRK and Crank-Nicolson methods as a function of the CPU cost needed. For low accuracy, both for velocity and hybrid

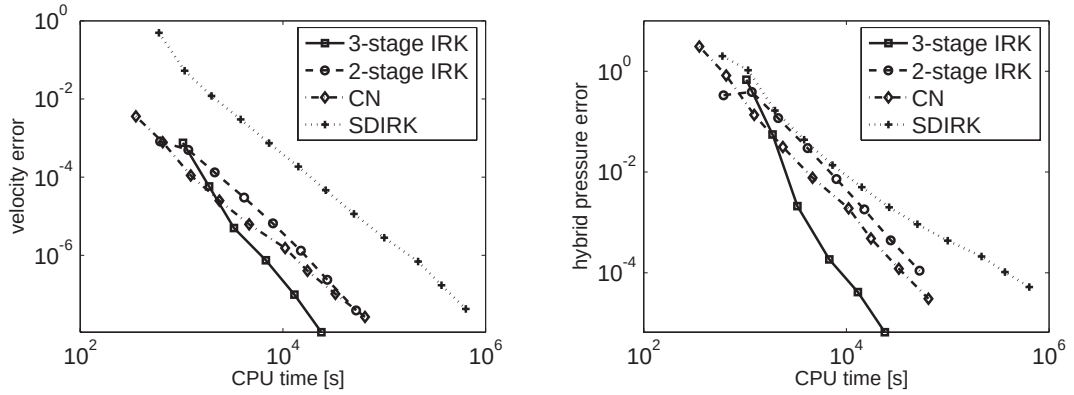

(a) Velocity error (b) Hybrid pressure error

Figure 3.6: Unsteady analytical example: velocity and hybrid pressure $\mathcal{L}_2$-errors, as a function of the CPU cost for 3-stage and 2-stage IRK, SDIRK and CN methods, $k = 4$, $0.01 \leq h \leq 0.1$.

pressures, all methods, except SDIRK, have an equivalent precision-to-cost ratio. But when higher accuracy is wanted, that is for example for an error less than 10^{-4} for velocity and less than 10^{-2} for hybrid pressure, the higher order of convergence of 3-stage Radau IIA-IRK balances its higher cost per iteration, and it becomes the most efficient method. Figure 3.7 shows the $\mathcal{L}_2$-error of the interior pressure, obtained from (2.27) using a fourth order approximation for the time derivative, as a function of the CPU cost. Similar results to those previously commented for velocity and hybrid pressures are obtained for interior pressure demonstrating that 3-stage Radau IIA-IRK is the most efficient scheme when high accuracy is required.

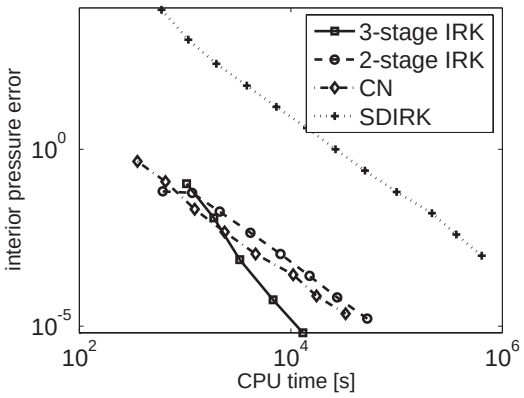

Figure 3.7: Unsteady analytical example: interior pressure $\mathcal{L}_2$-error, as a function of the CPU cost for 3-stage and 2-stage IRK, SDIRK and CN methods, $k = 4$, $0.01 \leq h \leq 0.1$.

3.2.3 Flow past a circle

In the present section we consider a mixed Dirichlet/Neumann problem simulating the flow past a circle in a uniform stream. The flow past a two-dimensional cylinder is one of the most studied problems of aerodynamics. It is a classical benchmark test and it is relevant to many engineering applications. The flow pattern depends on the Reynolds number defined here as $Re = \frac{u_\infty D}{\nu}$, where u_∞ is the mean fluid velocity and D the circle's diameter. Here $u_\infty = 1$ and $D = 1$ are considered.

In this example, a high-order mesh generator *EZ4U* is used, see Roca (2009) and Roca et al. (2007). Indeed, the environment *EZ4U* has a high-order export feature, which generates middle edge nodes over curves of the domain, and inner face nodes that follow curved edges of the elements. This allows to obtain high-order elements, which is especially interesting in a DG formulation, and to describe properly the flow around curved objects of study, see Figure 3.8(b). An unstructured mesh of 472 fourth order elements is used for the geometry description, as seen in Figure 3.8. These fourth order elements are used for numerical integration and in the post-process. Fourth order of solenoidal approximation for the velocity is also used ($k = 4$) and third order for pressure.

Dirichlet boundary condition is imposed on the inlet, $\boldsymbol{u}_D = (1, 0)$, and no-slip

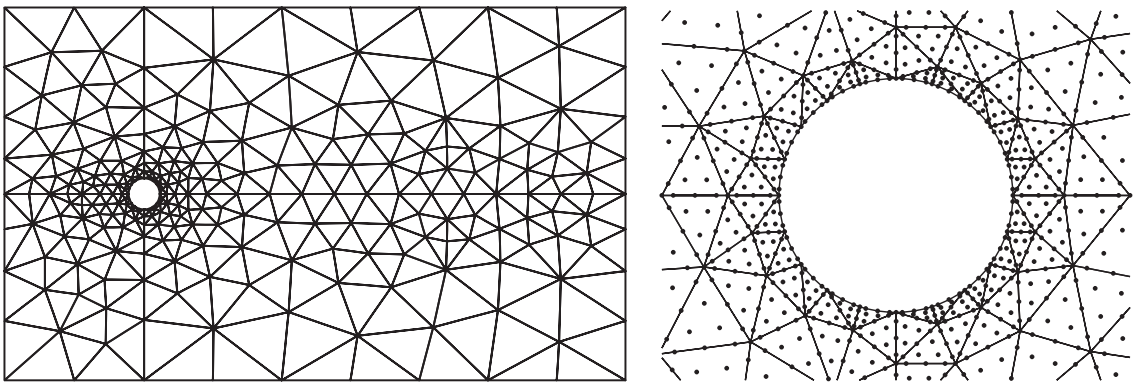

(a) Mesh of the total domain (b) Zoom in the vicinity of the circle

Figure 3.8: Flow past a circle: unstructured mesh of 472 fourth order elements

condition, $\boldsymbol{u}_D = (0,0)$, on the circle. Null Neumann conditions are imposed on the three other sides. The initial conditions prescribe a unitary velocity field $\boldsymbol{u}_0 = (1,0)$ on the whole domain, except on the circle boundary where $\boldsymbol{u}_0 = (0,0)$. Since it has proven to be the most efficient method, see Section 3.2.2, 3-stage Radau IIA IRK is used for time integration.

The flow patterns caused by the flow past a circle are studied for various values of the Reynolds number, within the range of $Re = 1 - 100$, where the flow stays laminar.

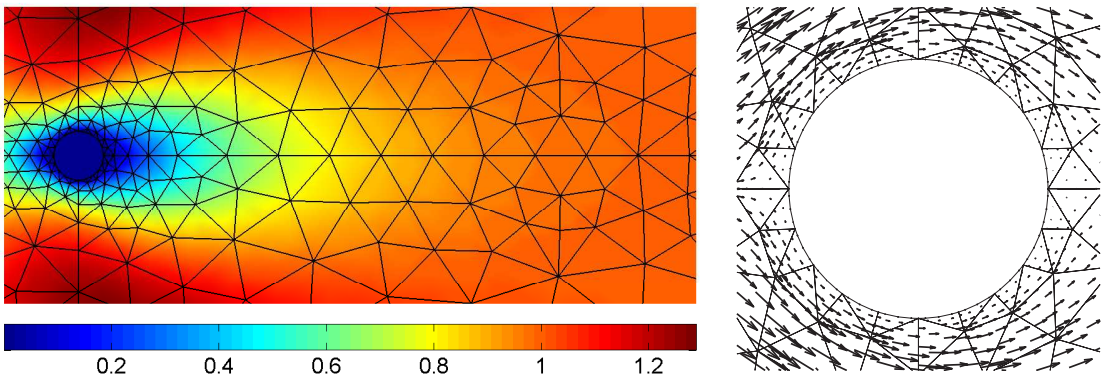

(a) Velocity module (b) Velocity vectors in the vicinity of the circle

Figure 3.9: Flow past a circle: velocity of the flow for $Re = 1$

For small Reynolds number, $Re = 1$, the flow is smooth, it passes the circle and

reform on the other side with no distorsion, as seen in Figure 3.9. Note that a zoom around the circle in Figure 3.9(b) allows to check that high-order elements coupled with high orders of approximation allow to obtain an accurate description of the boundary layer.

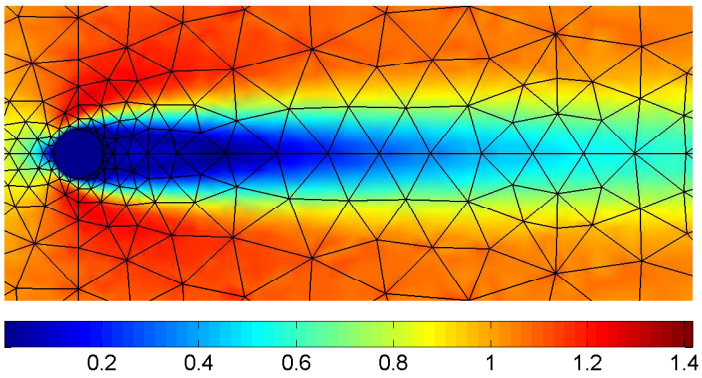

Figure 3.10: Flow past a circle: velocity of the flow for $Re = 40$

For higher Reynolds numbers, $Re = 40$, inertia begins to play a more important role and two stationary vortices are present behind the circle. Figure 3.10 shows velocity magnitude and velocity vectors for $Re = 40$. For these two examples at low Reynolds number, the solution reaches a stationary state.

For higher Reynolds number, for example here $Re = 100$, an unsteady solution is obtained. A time step $\Delta t = 0.03$ is used on the time interval $[0, 100]$, and $\Delta t = 0.01$ on $[100, 120]$, to better capture the period of the periodic flow pattern. A sequence of velocity vectors and modules are depicted in Figures 3.11 and 3.12. Figure 3.11 describes the transient solution developed until more or less $t = 60$, whereas Figure 3.12 shows two shots of the periodic solution.

At the beginning of the simulation, the flow is symmetrical and looks like a potential flow, as for very low Reynolds number. With progress in time, flow separation occurs, see Figure 3.11(a) at $t = 6$, and two small stationary eddies are formed in the downstream wake region. These eddies are fed by circulation from the shear layers and grow in size, with time. For $t = 15$, the two attached, symmetrical eddies of opposite circulation can be noticed in Figure 3.11(b). They grow further in size, along and

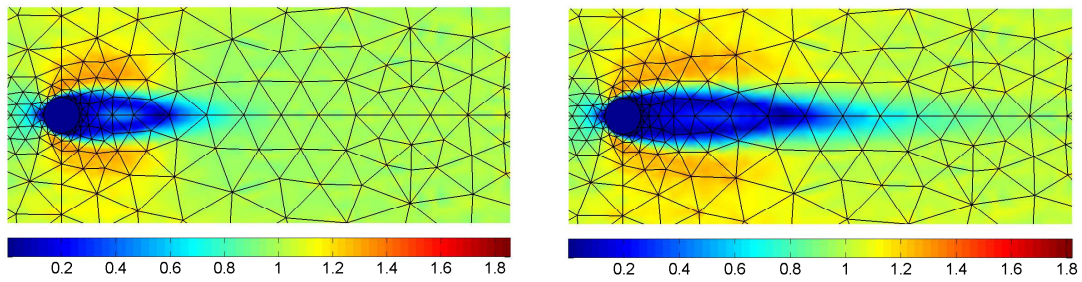

(a) t=6 (b) t=15

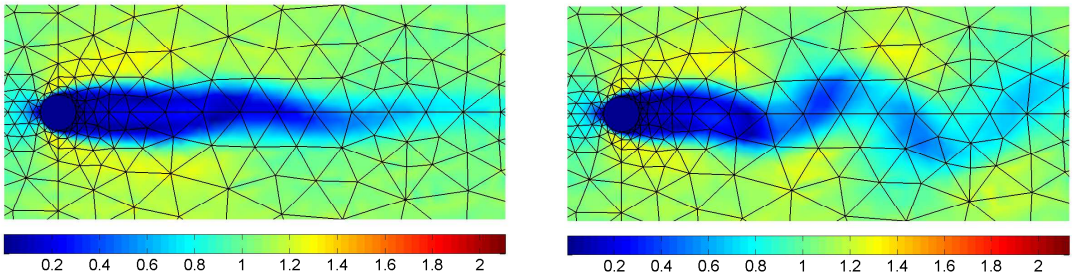

(c) t=24 (d) t=33

Figure 3.11: Flow past a circle: velocity module and vectors of the flow for $Re = 100$, transient phase.

across the stream, and result in a wake, which is much wider and longer and starts to show some non-symmetric pattern in Figure 3.11(c) at $t = 24$. At further time, vortex shedding starts, as first seen in Figure 3.11(d). The vortices are not stationary anymore but detach from the top and bottom of the cylinder. This happens in an alternating fashion and this non-symmetric flow pattern is known as the Von Karman vortex. Figure 3.12, shows the flow pattern once it has reached the periodic solution. Figure 3.13 shows more precisely how the flow detaches successively from the top and from the bottom of the sphere creating a vortex behind the circle.

These phases of the solution are also captured by the evolution of the lift coefficient C_L, which is defined by

$$C_L = \int_0^{2\pi} \boldsymbol{\sigma}_y d\boldsymbol{x}$$

where $\boldsymbol{\sigma}_y$ is the y-component of the Cauchy stress $\boldsymbol{\sigma}$. Studying the evolution of the lift coefficient allows to confirm the periodic nature of the flow pattern. Figure 3.14

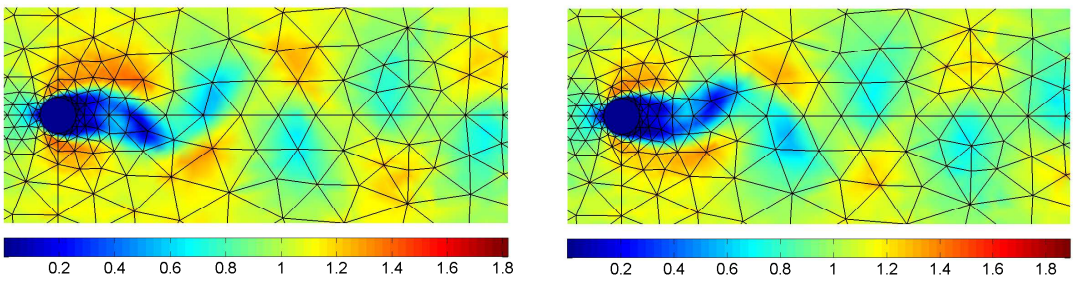

(a) t=96 (b) t=105

Figure 3.12: Flow past a circle: velocity module and vectors of the flow for $Re = 100$, periodic phase.

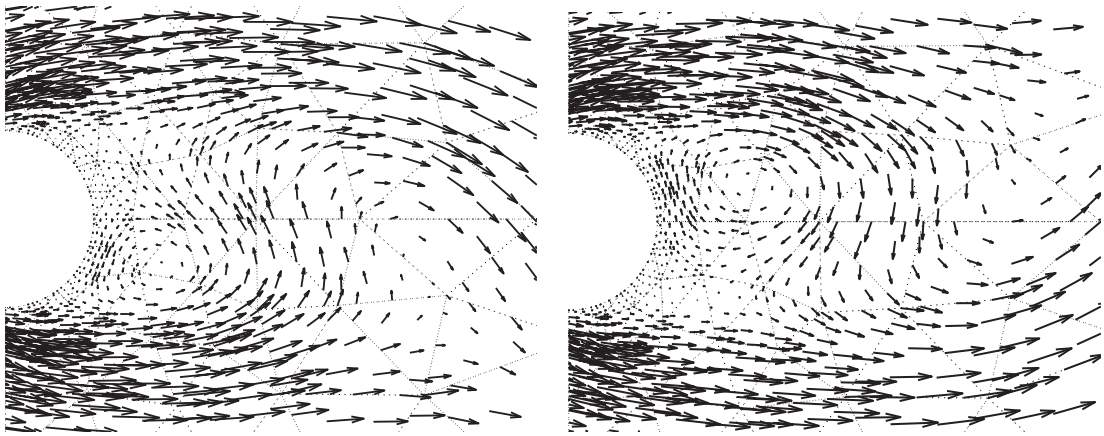

(a) t=96 (b) t=105

Figure 3.13: Flow past a circle: velocity vectors in the vicinity of the circle for $Re = 100$, periodic phase.

shows C_L as a function of time and confirms that from a time of around $t = 60$ the flow pattern reaches the periodic solution. It also allows to study the frequency of the Von Karman vortex. Roshko (1954) experimentally established the relation between the Strouhal number and the Reynolds number, for flows past a circle and for Reynolds numbers between 90 and 150 as

$$S = 0.212 \left(1 - \frac{21.2}{Re}\right), \tag{3.13}$$

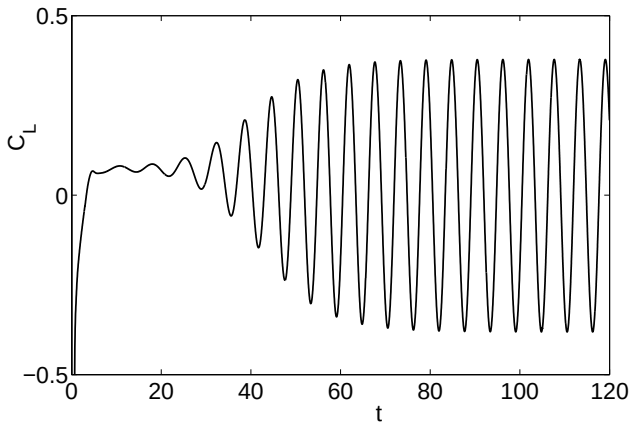

Figure 3.14: Flow past a circle: evolution of the lift coefficient with time

where S is the Strouhal number, dimensionless number describing oscillating flow mechanisms, defined from the frequency of vortex shedding f_S as

$$S = \frac{f_S D}{u_\infty},$$

with D and u_∞ characteristic lengths and velocity of the problem previously defined. In Figure 3.14, the period of the periodic movement is measured and is found equal to $T = 5.96$, which corresponds to $S = 0.1678$, which is in good agreement with experimental results and reported numerical simulations from Roshko (1954) and Simo and Armero (1994), as seen in Table 3.6. Note that in order to obtain a better

	3-stage IRK	2-stage IRK	Roshko (3.13)	Simo and Armero (1994)
S	0.1678	0.170	0.1671	0.167

Table 3.6: Flow past a circle: Strouhal number results for $Re = 100$

measure of the period T, the time step Δt has been set up to a value of 0.01 on a few periods, once the periodic solution is reached. A similar value of Strouhal number is obtained when using a 2-stage IRK method, confirming the general good behavior of the Radau IIA-IRK methods, for the solution of the incompressible Navier-Stokes problem.

3.3 Summary

The space discretization, using DG formulation with solenoidal approximations, presented in the previous chapter for incompressible steady flow equations is now considered for unsteady flows. The incompressible Navier-Stokes equations are interpreted as a system of Differential Algebraic Equations (DAE), that is a system of ODEs corresponding to the conservation of momentum equation, plus algebraic constraints corresponding to the incompressibility condition. High-order implicit Runge-Kutta (IRK) methods are considered to solve this DAE system. In particular Radau IIA-IRK methods are chosen since they reach the same orders of convergence as the ones obtained for an ODE problem. Unconditionally stable schemes are obtained, allowing maximum flexibility for the choice of the time step, which can be taken constant or can vary with time, depending on the problem considered. High orders of accuracy in time are reached. A numerical example with analytical solution shows that the resulting IRK time integration scheme is very competitive, compared to classical Crank Nicolson methods, and is more efficient when high accuracy is required. That is, even though the cost per iteration is bigger for IRK, the higher order of accuracy makes that a bigger Δt can be used, reaching a steady state faster. Also, at equal cost or at equal Δt the precision of 3-stage Radau IIA-IRK is better than the one obtained with Crank Nicolson, except for low precision results. The classical benchmark example of the flow past a circle confirms the good behavior of the proposed Radau IIA-IRK high-order methods.

Chapter 4

Conclusions and future developments

The main conclusions of the presented work have been drawn at the end of each chapter. The most salient results are summarized below.

The first contribution has been to derive a new Interior Penalty Discontinuous Galerkin (IPM-DG) formulation with divergence-free approximations for incompressible flows. First, the methodology of IPM is followed, leading to a symmetric and coercive bilinear form for the diffusion term. Then, the interpolation space is decomposed into a solenoidal part and an irrotational part. It allows to reduce the total number of degrees of freedom for both velocity and pressure by splitting the IPM weak form in two uncoupled problems. The first one solves for velocity and hybrid pressure, and the second one allows the evaluation of pressures in the interior of the elements as a post-process. The total number of degrees of freedom (dof) is highly reduced, compared to classical DG and even to continuous Galerkin methods.

Second, an alternative to IPM has been developed for the incompressible Navier-Stokes equations: the Compact Discontinuous Galerkin (CDG) formulation, also using solenoidal velocities. It presents the major advantage of eliminating the tuning of the penalty parameter, but it requires implementation and computation of local lifting operators. Both IPM and CDG with solenoidal interpolation lead to efficient, compact and high-order formulations, with similar accuracy of the numerical solution.

Third, another formulation with a penalty parameter for the weak enforcement

of continuity of the normal velocity along element sides has been proposed in order to further reduce the number of dof. It leads to another DG formulation where the computation of velocity and pressure is completely decoupled, representing an important computational save, but where the non-consistent penalty term leads to ill-conditioned systems of equations.

Finally, Implicit Runge-Kutta (IRK) methods have been used to solve unsteady incompressible flows. Unconditionally stable time integration methods are obtained, allowing maximum flexibility in the choice of the time step. Higher order of accuracy in time are obtained than the ones usually reached with classical methods for incompressible flows. IRK are used at a very competitive cost when compared to more classical methods such as a Crank-Nicolson method, that is, the extra cost needed to compute high-order IRK is more than balanced by the extra accuracy obtained. Thus the DG methods with solenoidal interpolation proposed in this thesis present the appealing advantages of high orders in space as well as in time.

Classical 2D examples, solved with the Matlab code developed along this thesis, have been used to show the applicability and the accuracy, both in space and in time, of the proposed methods. As further commented in 4.1.1, future work will focus on optimizing the code developed for the methods proposed in this thesis, in order to reduce the CPU cost needed for more complex examples, to adapt the code to 3D problems and to expand its scope of applications.

4.1 Future developments

4.1.1 Code further development

This thesis has focused on developing several Discontinuous Galerkin methods with solenoidal velocities and on exploring the various possibilities of time integration schemes that best fit the proposed spatial discretization scheme. All numerical methods have then been coded using Matlab, which has proven to be efficient when dealing with multidimensional arrays. Nevertheless for transitory examples, where not only

iterations in time are needed but also inner iterations in order to solve non-linear systems, the code has not yet been optimized to its maximum. Actually when several nested loops are needed, as it is the case for transitory simulations, calculations made in the inner loops are the ones with the biggest computational cost. For example, the computation of the convection residue requires a loop in time, a loop in iterations for the resolution of the non-linear system, a loop in elements and sides/faces and finally the most inner loop is the loop in Gauss points, where the basis functions eventually have to be evaluated. This calculation, within four nested loops, represents the biggest part of the total computational cost at each iteration and could be improved. A C++/Matlab library is being coded within the LaCàn (Laboratori de Càlcul Numèric) research group in order to take advantage of the best features of both coding languages. For example, in our case, programming with C++ the inner loops, where basis functions are computed, would decrease the total computational cost. Future work will focus on adapting the code developed for the DG formulations proposed in this thesis to a mixed code in C++ and Matlab in order to decrease the total computational cost.

Optimizing the 2D code of the high-order DG methods presented in this thesis is actually a necessary step towards the 3D implementation, which is the next task to be fulfilled. This will allow to simulate incompressible flows in more complex physical situations, as would be for example complete Formula One aileron, wind tunnels or micro-aerial vehicles, which are some possible 3D examples of application of the incompressible Navier-Stokes equations.

In this thesis, classical isoparametric transformation has been used when dealing with curved elements, for instance in the flow past a circle example. Another possibility is to use NURBS-Enhanced Finite Element Method (NEFEM), with an exact geometry description, which has proven very efficient for computing accurate solution in presence of curved boundaries, see Sevilla et al. (2008) and Sevilla (2009) for applications to Euler equations. NEFEM advantages for incompressible flows could then also be explored.

Finally, and once again to widen the scopes of application, the code will be adapted

to problems with free surfaces, in order to be able to simulate flows with moving free surfaces.

4.1.2 Raviart and Thomas - MAC approach

The MAC (Marker And Cell) method, see Harlow and Welch (1965), is one of the best methods for Navier-Stokes equations due to its high stability and efficiency. Unfortunately, it is difficult to generalize the MAC scheme to high-order elements and to irregular mesh. Kanschat (2008) shows that the lowest order Raviart-Thomas (RT) element (RT_0) on rectangular meshes is algebraically equivalent to MAC scheme. Developing an efficient method, with solenoidal approximation for velocity, and where RT elements would generalize the MAC scheme to high-order elements, would be an interesting future research line. Rectangular RT elements could be used for regular meshes, triangular RT elements for irregular meshes, and then connection between both would be needed.

RT elements were introduced on 2D triangle or quadrilateral meshes by Raviart and Thomas (1977). Optimal-order approximations in H(div) of smooth vector fields were obtained on 2D shape-regular rectangular meshes. The generalization to 3D tetrahedra or cube meshes was done by Nédélec (1980). A good review of existing RT elements is also presented by Brezzi and Fortin (1991). Fluid solid systems, linear elasticity or second order elliptic problems are some examples of applications of RT elements. For example, fluid displacements are discretized in fluid-structure vibroacoustic interaction problems by Bermúdez et al. (1995) or numerical approximations of the displacement form of the acoustic wave equation are solved using RT elements, see Jenkins (2007).

For a divergence-free approach as the one proposed in this thesis, the resolution of the Stokes problem could be done very efficiently using a mixed mesh of rectangular and triangle elements, for a 2D problem (or of tetrahedra and hexahedra for 3D). Figure 4.1 shows the nodes of velocity and pressure for the rectangular RT_1 element. For this element, x-component of the velocity is cellwise linear and discontinuous in

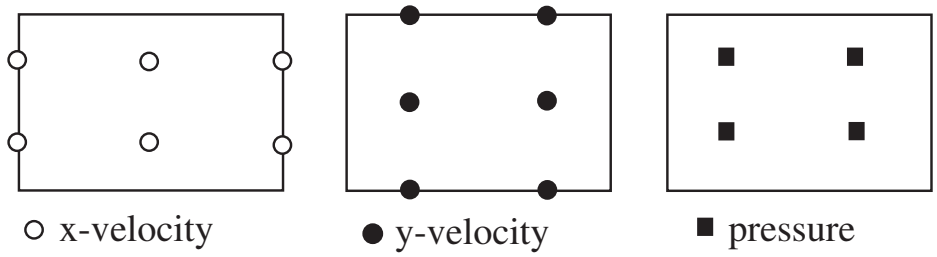

Figure 4.1: RT_1 rectangular element

y-direction, and cellwise quadratic and continuous in x-direction; y-component of the velocity is vice-versa and p is bilinear. As illustrated in Figure 4.1 for the particular example of RT_1 element, in a general rectangular RT formulation x-component of the velocity is continuous in x-direction and discontinuous in the y-direction and vice-versa for the y-component of the velocity. This property, added to the solenoidal property of the basis functions, would allow to cancel some terms of the weak form and to solve separately for the x- and y-components of the velocity, reducing the size of the system to solve. Then for irregular mesh, triangular RT elements would be used, the challenge consisting in computing (x, y) basis functions for high-order triangular RT elements, which is far from trivial.

Bibliography

Arnold, D. N. (1982). An interior penalty finite element method with discontinuous elements. *SIAM J. Numer. Anal. 19*(4), 742–760.

Babuska, I. (1973). The finite element method with penalty. *Math. Comp. 27*, 221–228.

Baker, G. A., W. N. Jureidini, and O. A. Karakashian (1990). Piecewise solenoidal vector fields and the Stokes problem. *SIAM J. Numer. Anal. 27*(6), 1466–1485.

Bassi, F. and S. Rebay (1997). A high-order accurate discontinuous finite element method for the numerical solution of the compressible Navier-Stokes equations. *J. Comput. Phys. 131*(2), 267–279.

Bassi, F. and S. Rebay (2001). Numerical evaluation of two Discontinuous Galerkin Methods for the compressible Navier-Stokes equations. *Int. J. Numer. Methods Eng. 40*(10), 197–207.

Bermúdez, A., R. Durán, M. Muschietti, R. Rodríguez, and J. Solomin (1995). Finite element vibration analysis of fluid-solid systems without spurious modes. *SIAM J. Numer. Anal. 32*, 1280–1295.

Brenan, K., S. Campbell, and L. Petzold (1996). *Numerical Solution of Initial-Value Problems in Differential-Algebraic Equations*. SIAM.

Brenan, K. E. and B. E. Engquist (1988). Backward differentiation approximations of nonlinear differential/algebraic systems. *Math. Comp. 51*(184), 659–676.

Brezzi, F. and M. Fortin (1991). *Mixed and hybrid finite element methods*, Volume 15 of *Springer Series in Computational Mathematics*. New York: Springer-Verlag.

Butcher, J. (1987). *The numerical analysis of ordinary differential equations*. Wiley.

Carrero, J., B. Cockburn, and D. Schötzau (2005). Hybridized globally divergence-free LDG methods. Part I: The Stokes problem. *Math. Comp. 75*(254), 533–563.

Chapelle, D. and K.-J. Bathe (1993). The inf-sup test. *Comput. Struct. 4-5*(47), 537–545.

Chorin, A. (1968). Numerical solution of the Navier-Stokes equations. *Math. Comp. 22*(104), 745–762.

Cockburn, B. (2004). *Discontinuous Galerkin methods for Computational Fluid Dynamics*, Volume 3 Fluids. Chichester: John Wiley & Sons.

Cockburn, B. and J. Gopalakrishnan (2005). Incompressible finite elements via hybridization. Part I: the Stokes system in two space dimensions. *SIAM J. Numer. Anal. 43*(4), 1627–1650.

Cockburn, B., G. Kanschat, I. Perugia, and D. Schötzau (2001). Superconvergence of the Local Discontinuous Galerkin method for elliptic problems on cartesian grids. *SIAM J. Numer. Anal. 39*(1), 264–285.

Cockburn, B., G. Kanschat, and D. Schötzau (2005a). The local discontinuous Galerkin method for linearized incompressible fluid flow: a review. *Computers and Fluids 34*, 491–506.

Cockburn, B., G. Kanschat, and D. Schötzau (2005b). A locally conservative LDG method for the incompressible Navier-Stokes equations. *Math. Comp. 74*(251), 1067–1095.

Cockburn, B., G. Kanschat, and D. Schötzau (2007). A note on Discontinuous Galerkin divergence-free solutions of the Navier-Stokes equations. *J. Sci. Comput. 31*(1-2), 61–73.

Cockburn, B., F. Li, and C. Shu (2004). Locally divergence-free Discontinuous Galerkin methods for the Maxwell equations. *J. Comput. Phys. 194*, 588–610.

Cockburn, B. and C.-W. Shu (1998). The Local Discontinuous Galerkin method for time-dependent convection-diffusion systems. *SIAM J. Numer. Anal. 35*(6), 2440–2463.

Crouzeix, M. and P.-A. Raviart (1973). Conforming and nonconforming finite element methods for solving the stationary Stokes equations. I. *Rev. Française Automat. Informat. Recherche Opérationnelle Sér. Rouge 7*(R-3), 33–75.

Donea, J., S. Giuliani, H. Laval, and L. Quartapelle (1981). Finite element solution of the unsteady Navier-Stokes equations by a fractional step method. *Comput. Meth. Appl. Mech. Eng. 30*, 53–73.

Donea, J. and A. Huerta (2003). *Finite element methods for flow problems*. Chichester: John Wiley & Sons.

Griffiths, D. F. (1981). An approximately divergence-free 9-node velocity element (with variations) for incompressible flows. *Int. J. Numer. Methods Fluids 1*(4), 323–346.

Grote, M. J., A. Schneebeli, and D. Schötzau (2008). Interior penalty discontinuous Galerkin method for Maxwell's equations: optimal L_2-norm error estimates. *IMA Journal of Numerical Analysis 28*(3), 440–468.

Guermond, J., P. Minev, and J. Shen (2006). An overview of projection methods for incompressible flows. *Comput. Meth. Appl. Mech. Eng. 195*, 6011–6045.

Gunzburger, M. D. (1989). *Finite element methods for viscous incompressible flows. A guide to theory, practice, and algorithms*. Boston, MA: Academic Press.

Hairer, E., C. Lubich, and M. Roche (1989). *The Numerical Solution of Differential-Algebraic Systems by Runge-Kutta Methods*. Springer-Verlag.

Hairer, E. and G. Wanner (1991). *Solving Ordinary Differential Equations II- Stiff and Differential-Algebraic Problems*. Springer-Verlag.

Hanke, M., E. Izquierdo, and R. März (1998). On asymptotics in case of linear index-2 Differential-Algebraic Equations. *SIAM J. Numer. Anal. 35*(4), 1326–1346.

Hanke, M. and R. März (1996). On asymptotics in case of DAE's. *ZAMM 76 Suppl.1*, 99–102.

Hansbo, A. and P. Hansbo (2004). A finite element method for the simulation of strong and weak discontinuities in solid mechanics. *Comput. Meth. Appl. Mech. Eng. 193*(33-35), 3523–3540.

Hansbo, P. and M. Larson (2003). Discontinuous Galerkin and the Crouziex-Raviart element: application to elasticity. *ESAIM-Mathematical Modelling and Numerical Analysis 37*(1), 63–72.

Hansbo, P. and M. G. Larson (2002). Discontinuous Galerkin methods for incompressible and nearly incompressible elasticity by Nitsche's method. *Comput. Meth. Appl. Mech. Eng. 191*(17-18), 1895–1908.

Hansbo, P. and M. G. Larson (2008). Piecewise divergence-free Discontinuous Galerkin methods for Stokes flow. *Commun. Numer. Meth. Eng. 24*(5), 355–366.

Harlow, F. H. and J. E. Welch (1965). Numerical calculation of time-dependent viscous incompressible flow of fluid with free surface. *Phys. Fluids 8*(12), 2182–2189.

Houzeaux, M., M. Vázquez, and A. R. (2009). A massively parallel fractional step solver for incompressible flows. *J. Comput. Phys.* (Accepted for publication).

Huerta, A., Y. Vidal, and P. Villon (2004). Pseudo-divergence-free element free Galerkin method for incompressible fluid flow. *Comput. Meth. Appl. Mech. Eng. 193*(12-14), 1119–1136.

Jansen, K., C. Whiting, and G. Hulbert (2000). A generalized-α method for integrating the filtered Navier-Stokes equations with a stabilized finite element method. *Comput. Meth. Appl. Mech. Eng. 190*(3), 305–319.

Jenkins, E. W. (2007). Numerical solution of the acoustic wave equation using Raviart-Thomas elements. *Journal of Computational and Applied Mathematics 206*(1), 420–431.

Kanschat, G. (2008). Divergence-free discontinuous Galerkin schemes for the Stokes equations and the MAC scheme. *Int. J. Numer. Methods Fluids 56*(7), 941–950.

Kanschat, G. and D. Schötzau (2008). Energy norm a posteriori error estimation for divergence-free discontinuous Galerkin approximations of the Navier-Stokes equations. *Int. J. Numer. Methods Fluids 57*(9), 1093 – 1113.

Karakashian, O. A. and W. N. Jureidini (1998). A nonconforming finite element method for the stationary Navier-Stokes equations. *SIAM J. Numer. Anal. 35*(1), 93–120 (electronic).

Kim, J. and P. Moin (1985). Application of a fractional-step method to incompressible Navier-Stokes equations. *J. Comput. Phys. 59*, 308–323.

Kim, K., S.-J. Baek, and H. Jin Sung (2002). An implicit velocity decoupling procedure for the incompressible Navier-Stokes equations. *Int. J. Numer. Methods Fluids 38*(2), 125–138.

Linnick, M. N. and H. F. Fasel (2005). A high-order immersed interface method for simulating unsteady incompressible flows on irregular domains. *J. Comput. Phys. 204*, 157–192.

Liu, J.-G. and C.-W. Shu (2000). A high-order Discontinuous Galerkin method for 2D incompressible flows. *J. Comput. Phys. 160*, 577–596.

Montlaur, A., S. Fernandez-Mendez, and A. Huerta (2008). A discontinuous Galerkin method with divergence-free interpolation for the incompressible Stokes equations. *Int. J. Numer. Methods Fluids 57*(9), 1071–1092.

Montlaur, A., S. Fernandez-Mendez, J. Peraire, and A. Huerta (2009). Discontinuous Galerkin methods for the Navier-Stokes equations using solenoidal approximations. *Int. J. Numer. Methods Fluids* (Accepted for publication).

Mozolevsky, I., E. Süri, and P. Bösing (2007). Discontinuous Galerkin finite element approximations of the two-dimensional Navier-Stokes equations in stream-function formulation. *Commun. Numer. Meth. Eng. 23*(6), 447–459.

Nédélec, J. (1980). Mixed finite elements in R^3. *Numer. Math. 35*, 315–341.

Nitsche, J. (1971). Uber ein Variations zur Lösung von Dirichlet-Problemen bei Verwendung von Teilräumen die keinen Randbedingungen unterworfen sind. *Abh. Math. Se. Univ. 36*, 9–15.

Norsett, S. (1974). One-step methods of hermite type for numerical integration of stiff systems. *BIT 14*, 63–77.

Okkels, F., L. Olesen, and H. Bruus (2005). Applications of topology optimization in the design of micro- and nanofluidic systems. In *Technical Proceedings of the 2005 NSTI Nanotechnology Conference and Trade Show*, Volume 1, Anaheim, CA, pp. 575 – 578.

Peraire, J. and P.-O. Persson (2008). The Compact Discontinuous Galerkin (CDG) method for elliptic problems. *SIAM J. Sci. Stat. Comput. 30*(4), 1806–1824.

Pereira, J., M. Kobayashi, and J. Pereira (2001). A fourth-order-accurate finite volume compact method for the incompressible Navier-Stokes solutions. *J. Comput. Phys. 167*(1), 217–243.

Persson, P.-O. and J. Peraire (2008). Newton-GMRES preconditioning for discontinuous Galerkin discretizations of the Navier-Stokes equations. *SIAM J. Sci. Comput. 30*(6), 2709–2733.

Raviart, P. and J. Thomas (1977). Primal hybrid finite element methods for 2nd order elliptic equations. *Math. Comp. 31*(138), 391–413.

Reed, W. and T. Hill (1973). Triangular mesh methods for the neutron transport equation. In *Tech. Report LA-UR-73-479*, Los Alamos Scientific Laboratory.

Roca, X. (2009). *Paving the path towards automatic hexahedral mesh generation*. Ph. D. thesis, Universitat Politènica de Catalunya.

Roca, X., J. Sarrate, and E. Ruiz-Gironès (2007). A graphical modeling and mesh generation environment for simulations based on boundary representation data. In *Congresso de Métodos Numéricos em Engenharia, Porto, Portugal, 2007*.

Roshko, A. (1954). On the development of turbulent wakes from vortex streets. *NACA Report* (1191).

Sevilla, R. (2009). *NURBS-Enhanced Finite Element Method (NEFEM).* Ph. D. thesis, Universitat Politènica de Catalunya.

Sevilla, R., S. Fernández-Méndez, and A. Huerta (2008). NURBS-enhanced finite element method (NEFEM) for Euler equations. *Int. J. Numer. Methods Fluids 57*(9), 1051–1069.

Simo, J. and F. Armero (1994). Unconditional stability and long-term behaviour of transient algorithms for the incompressible Navier Stokes and Euler equations. *Comput. Meth. Appl. Mech. Eng. 111*, 111–154.

Temam, R. (2001). *Navier-Stokes equations - Theory and numerical analysis.* AMS Chelsea Publishing.

Toselli, A. (2002). *hp* discontinuous Galerkin approximations for the Stokes problem. *Math. Models Meth. Appl. Sci. 12*(11), 1565–1597.

Wang, L. and D. J. Mavriplis (2007). Implicit solution of the unsteady Euler equations for high-order accurate discontinuous Galerkin discretizations. *J. Comput. Phys. 225*(2), 1994–2015.

Appendix A

Error bounds of IPM with solenoidal approximations

This appendix gives elements of demonstration of the continuity and coercivity properties of the IPM bilinear form and of the error bounds of the IPM Stokes formulation with solenoidal velocity (2.7). Norm $|||\cdot|||$ and $\mathcal{L}^2$-norms used here are respectively defined in (2.10) and (2.11). Full Dirichlet conditions are considered and the mesh considered is composed of elements of straight edges.

Lemma A.0.1 (Continuity of $a_{\mathtt{IP}}$)**.** *The IPM bilinear form a_{IP} defined in* (2.4a) *is continuous, that is: there exists a constant c such that*

$$|a_{IP}(\boldsymbol{u},\boldsymbol{v})| \leq c\,|||\,\boldsymbol{u}\,|||\;\;|||\boldsymbol{v}\,||| \quad \forall \boldsymbol{u},\boldsymbol{v} \in [\mathcal{H}^1(\hat{\Omega})]^{n_{sd}}. \tag{A.1}$$

Proof. The continuity of $a_{\mathtt{IP}}$ in equation (A.1) can be proven following IPM standard arguments, see Hansbo and Larson (2002, 2008) for details.

Lemma A.0.2. *For $f \in \boldsymbol{\mathcal{V}}^h$, and h the mesh parameter defined in* (2.5)*, the following inverse inequality holds: there exists a constant c such that*

$$\|h^{1/2}\{f\}\|^2_{\Gamma\cup\Gamma_D} \leq c\|f\|^2_{\Omega} \tag{A.2}$$

Proof. Following finite element dimensionality and scaling from a unit reference element, see Hansbo and Larson (2002), we have

$$\|h^{1/2} f\|^2_{\partial\Omega_i} \leq c_1 \|f\|^2_{\Omega_i}. \tag{A.3}$$

Summing (A.3) for all elements we get

$$\sum_{i=1}^{\mathtt{n_{el}}} \|h^{1/2} f\|^2_{\partial\Omega_i} = \|h^{1/2} 2\{f\}\|^2_{\Gamma} + \|h^{1/2} f\|^2_{\Gamma_D} \leq c_1 \|f\|^2_{\Omega},$$

which proves (A.2). □

This lemma is used in the demonstration of the coercivity of $a_{\mathtt{IP}}$ coming next.

Lemma A.0.3 (Coercivity of $a_{\mathtt{IP}}$)**.** *For γ large enough, the IPM bilinear form a_{IP} defined in* (2.4a) *is coercive. For any constant $m > 0$*

$$m \,|||\, \boldsymbol{v} |||^2 \leq a_{IP}\big(\boldsymbol{v}, \boldsymbol{v}\big) \quad \forall \boldsymbol{v} \in [\mathcal{H}^1(\hat{\Omega})]^{n_{sd}} \tag{A.4}$$

for some $\gamma > 0$.

Proof. Given some constant $m > 0$ independent of the mesh size h

$$\begin{aligned} a_{\mathtt{IP}}\big(\boldsymbol{v}, \boldsymbol{v}\big) - m|||\boldsymbol{v}|||^2 = a\big(\boldsymbol{v}, \boldsymbol{v}\big) - 2\big(2\nu\{\boldsymbol{\nabla}^{\mathtt{S}}\boldsymbol{v}\}, [\![\boldsymbol{n}\otimes\boldsymbol{v}]\!]\big)_{\Gamma\cup\Gamma_D} + \gamma\big(h^{-1}[\![\boldsymbol{n}\otimes\boldsymbol{v}]\!], [\![\boldsymbol{n}\otimes\boldsymbol{v}]\!]\big)_{\Gamma\cup\Gamma_D} \\ - m\big(\|\boldsymbol{\nabla}^{\mathtt{S}}\boldsymbol{v}\|^2_{\Omega} + \|h^{1/2}\{\boldsymbol{n}\cdot\boldsymbol{\nabla}^{\mathtt{S}}\boldsymbol{v}\}\|^2_{\Gamma\cup\Gamma_D} + \|h^{-1/2}[\![\boldsymbol{n}\otimes\boldsymbol{v}]\!]\|^2_{\Gamma\cup\Gamma_D}\big). \end{aligned}$$

That is

$$\begin{aligned} a_{\mathtt{IP}}\big(\boldsymbol{v}, \boldsymbol{v}\big) - m\,|||\,\boldsymbol{v}|||^2 = (2\nu - m)\|\boldsymbol{\nabla}^{\mathtt{S}}\boldsymbol{v}\|^2_{\Omega} + (\gamma - m)\|h^{-1/2}[\![\boldsymbol{n}\otimes\boldsymbol{v}]\!]\|^2_{\Gamma\cup\Gamma_D} \\ - m\|h^{1/2}\{\boldsymbol{n}\cdot\boldsymbol{\nabla}^{\mathtt{S}}\boldsymbol{v}\}\|^2_{\Gamma\cup\Gamma_D} - 2\big(2\nu\{\boldsymbol{\nabla}^{\mathtt{S}}\boldsymbol{v}\}, [\![\boldsymbol{n}\otimes\boldsymbol{v}]\!]\big)_{\Gamma\cup\Gamma_D}. \end{aligned} \tag{A.5}$$

Using the Cauchy-Schwarz inequality

$$\big(2\nu\{\boldsymbol{\nabla}^{\mathtt{S}}\boldsymbol{v}\},[\![\boldsymbol{n}\otimes\boldsymbol{v}]\!]\big)_{\Gamma\cup\Gamma_D}\leq 2\nu\|h^{1/2}\{\boldsymbol{\nabla}^{\mathtt{S}}\boldsymbol{v}\}\|_{\Gamma\cup\Gamma_D}\|h^{-1/2}[\![\boldsymbol{n}\otimes\boldsymbol{v}]\!]\|_{\Gamma\cup\Gamma_D},$$

then using Lemma A.0.2 there exists a constant C such that

$$\big(2\nu\{\boldsymbol{\nabla}^{\mathtt{S}}\boldsymbol{v}\},[\![\boldsymbol{n}\otimes\boldsymbol{v}]\!]\big)_{\Gamma\cup\Gamma_D}\leq 2\nu C\|\boldsymbol{\nabla}^{\mathtt{S}}\boldsymbol{v}\|_{\Omega}\|h^{-1/2}[\![\boldsymbol{n}\otimes\boldsymbol{v}]\!]\|_{\Omega},$$

and using that $2ab<\frac{a^2}{\epsilon}+b^2\epsilon$ for an arbitrary constant ϵ

$$\big(2\nu\{\boldsymbol{\nabla}^{\mathtt{S}}\boldsymbol{v}\},[\![\boldsymbol{n}\otimes\boldsymbol{v}]\!]\big)_{\Gamma\cup\Gamma_D}\leq\frac{\nu C}{\epsilon}\|\boldsymbol{\nabla}^{\mathtt{S}}\boldsymbol{v}\|_{\Omega}^2+\nu C\epsilon\|h^{-1/2}[\![\boldsymbol{n}\otimes\boldsymbol{v}]\!]\|_{\Gamma\cup\Gamma_D}^2. \tag{A.6}$$

Now using the Lemma 4 of Hansbo and Larson (2002), there exists a constant D such that

$$\|h^{1/2}\{\boldsymbol{n}\cdot\boldsymbol{\nabla}^{\mathtt{S}}\boldsymbol{v}\}\|_{\Gamma\cup\Gamma_D}^2\leq D\|\boldsymbol{\nabla}^{\mathtt{S}}\boldsymbol{v}\|_{\Omega}^2. \tag{A.7}$$

Eventually substituting (A.6) and (A.7) in (A.5)

$$a_{\mathtt{IP}}\big(\boldsymbol{v},\boldsymbol{v}\big)-m|||\boldsymbol{v}|||^2\geq(2\nu-m-\frac{2\nu C}{\epsilon}-mD)\|\boldsymbol{\nabla}^{\mathtt{S}}\boldsymbol{v}\|_{\Omega}^2+(\gamma-m-2\nu C\epsilon)\|h^{-1/2}[\![\boldsymbol{n}\otimes\boldsymbol{v}]\!]\|_{\Gamma\cup\Gamma_D}^2.$$

Thus, the coercivity is ensured if $2\nu-m-\frac{2\nu C}{\epsilon}-mD\geq 0$ and $\gamma-m-2\nu C\epsilon\geq 0$. The first condition is satisfied if the arbitrary constant ϵ is taken $\epsilon\geq\frac{2\nu C}{2\nu-m(1+D)}$. The second condition is verified when $\gamma\geq m+2\nu C\epsilon$, that is for γ big enough, which ends up the proof of the coercivity. □

These properties of continuity and coercivity of the bilinear form $a_{\mathtt{IP}}$ are used in the derivation of the error bounds for velocity, hybrid pressure and pressure.

Theorem A.0.4 (Velocity error bound)**.** *Let* $\boldsymbol{u}\in[\mathcal{H}^{1+\alpha}(\Omega)]^{n_{sd}}$, $1\leq\alpha\leq k$, *be the exact velocity of the Stokes problem, and* $\boldsymbol{u}_h\in\boldsymbol{\mathcal{S}}^h$ *the numerical velocity of the IPM*

system (2.7)*, then*

$$|||\, \boldsymbol{u} - \boldsymbol{u}_h |||_{} \leq K_1 h^{\alpha} |\boldsymbol{u}|_{[\mathcal{H}^{1+\alpha}(\Omega)]^{n_{sd}}} \tag{A.8}$$

where K_1 *is independent of the mesh size and the exact solution.*

Proof. See Montlaur et al. (2008).

Theorem A.0.5 (Hybrid pressure error bound)**.** *Let* $\boldsymbol{u} \in [\mathcal{H}^{1+\alpha}(\Omega)]^{n_{sd}}$*,* $1 \leq \alpha \leq k$*, and* $p \in \mathcal{L}_2(\Omega)$ *be the exact solution of the Stokes problem,* $\tilde{p} = \{p\}$ *on* $\Gamma \cup \partial\Omega$*, and* $(\boldsymbol{u}_h, \tilde{p}_h) \in \boldsymbol{\mathcal{S}}^h \times \boldsymbol{P}^h$ *numerical solution of the IPM system* (2.7)*, then, under the assumptions of hypothesis 2.1.1*

$$\|\tilde{p} - \tilde{p}_h\|_{\Gamma \cup \Gamma_D} \leq K_2 h^{\alpha - 1} |\boldsymbol{u}|_{[\mathcal{H}^{1+\alpha}(\Omega)]^{n_{sd}}} \tag{A.9}$$

where K_2 *is independent of the mesh size and the exact solution.*

Proof. IPM is a consistent formulation, thus $(\boldsymbol{u}, \tilde{p}) \in [\mathcal{H}^{1+\alpha}(\Omega)]^{\mathtt{n_{sd}}} \times \mathcal{L}_2(\Omega)$ exact solution of the Stokes problem is also solution of the IPM weak form (2.7a), that is

$$\big(\tilde{p}, [\![\boldsymbol{n} \cdot \boldsymbol{v}]\!]\big)_{\Gamma \cup \Gamma_D} = l_{\mathtt{IP}}\big(\boldsymbol{v}\big) - a_{\mathtt{IP}}\big(\boldsymbol{u}, \boldsymbol{v}\big), \quad \forall \boldsymbol{v} \in \boldsymbol{\mathcal{S}}^h.$$

The numerical solution $(\boldsymbol{u}_h, \tilde{p}_h) \in \boldsymbol{\mathcal{S}}^h \times \boldsymbol{P}^h$ also verifies

$$\big(\tilde{p}_h, [\![\boldsymbol{n} \cdot \boldsymbol{v}]\!]\big)_{\Gamma \cup \Gamma_D} = l_{\mathtt{IP}}\big(\boldsymbol{v}\big) - a_{\mathtt{IP}}\big(\boldsymbol{u}_h, \boldsymbol{v}\big) \quad \forall \boldsymbol{v} \in \boldsymbol{\mathcal{S}}^h,$$

thus, substracting the last equations

$$\Big|\big(\tilde{p} - \tilde{p}_h, [\![\boldsymbol{n} \cdot \boldsymbol{v}]\!]\big)_{\Gamma \cup \Gamma_D}\Big| = \big|a_{\mathtt{IP}}\big(\boldsymbol{u} - \boldsymbol{u}_h, \boldsymbol{v}\big)\big| \quad \forall \boldsymbol{v} \in \boldsymbol{\mathcal{S}}^h. \tag{A.10}$$

Using the inf-sup condition (2.12) and equation (A.10), we get

$$\|\tilde{p} - \tilde{p}_h\|_{\Gamma \cup \Gamma_D} \leq \alpha h^{-1} \frac{\left| a_{\mathtt{IP}}\big(\boldsymbol{u} - \boldsymbol{u}_h, \boldsymbol{v}\big) \right|}{|||\boldsymbol{v}|||} \quad \forall \boldsymbol{v} \in \boldsymbol{\mathcal{S}}^h. \tag{A.11}$$

Then, using the continuity property of $a_{\mathtt{IP}}$ seen in (A.1)

$$\|\tilde{p} - \tilde{p}_h\|_{\Gamma \cup \Gamma_D} \leq c h^{-1} \, ||| \, \boldsymbol{u} - \boldsymbol{u}_h ||| \tag{A.12}$$

and finally using the velocity error bound (A.8), we obtain the hybrid pressure error bound (A.9). □

Lemma A.0.6 (inf-sup condition for pressure)**.** *The spaces of velocities $\boldsymbol{\mathcal{V}}^h$ and pressures $\mathcal{Q}^h$ satisfy*

$$\sup_{\boldsymbol{v} \in \boldsymbol{\mathcal{V}}^h} \frac{b\big(\boldsymbol{v}, q\big)}{|||\boldsymbol{v}|||} \geq c_2 \|P_{\mathcal{Q}^h} q\|_\Omega \quad \forall q \in \mathcal{Q}^h, \tag{A.13}$$

for some constant c_2 independent of the characteristic mesh size h and where $P_{\mathcal{Q}^h}$ is the $\mathcal{L}_2$-projection onto $\mathcal{Q}^h$.

This lemma is proved by Carrero et al. (2005), and is used in the proof of the error bound for interior pressure.

Theorem A.0.7 (Interior pressure error estimate)**.** *Let $\boldsymbol{u} \in [\mathcal{H}^{1+\alpha}(\Omega)]^{\mathtt{n_{sd}}}$, $1 \leq \alpha \leq k$, and $p \in \mathcal{H}^\alpha(\Omega)$ be the exact solution of the Stokes problem, $\tilde{p} = \{p\}$ on $\Gamma \cup \partial\Omega$, and $(\boldsymbol{u}_h, \tilde{p}_h, p_h) \in \boldsymbol{\mathcal{S}}^h \times \boldsymbol{P}^h \times \mathcal{Q}^h$ the numerical solution of the IPM system* (2.7)*, then*

$$\|p - p_h\|_\Omega \leq K_3 \left(h^{\alpha - \frac{1}{2}} |\boldsymbol{u}|_{[\mathcal{H}^{1+\alpha}(\Omega)]^{\mathtt{n_{sd}}}} + h^\alpha \|p\|_{\mathcal{H}^\alpha(\Omega)} \right) \tag{A.14}$$

where K_3 is independent of the mesh size and the exact solution.

Proof. The exact velocity and interior pressure $(\boldsymbol{u}, p) \in [\mathcal{H}^{1+\alpha}(\Omega)]^{\mathtt{n_{sd}}} \times \mathcal{H}^\alpha(\Omega)$

solution of the Stokes problem verifies (2.3), that is

$$b\big(\boldsymbol{v},p\big) = l_{\mathtt{IP}}\big(\boldsymbol{v}\big) - a_{\mathtt{IP}}\big(\boldsymbol{u},\boldsymbol{v}\big) - \big(\tilde{p},[\![\boldsymbol{n}\cdot\boldsymbol{v}]\!]\big)_{\Gamma\cup\Gamma_D} \quad \forall \boldsymbol{v}\in\boldsymbol{\mathcal{V}}^h,$$

and the numerical solution $(\boldsymbol{u}_h,p_h)\in\boldsymbol{\mathcal{S}}^h\times\mathcal{Q}^h$ also verifies

$$b\big(\boldsymbol{v},p_h\big) = l_{\mathtt{IP}}\big(\boldsymbol{v}\big) - a_{\mathtt{IP}}\big(\boldsymbol{u}_h,\boldsymbol{v}\big) - \big(\tilde{p}_h,[\![\boldsymbol{n}\cdot\boldsymbol{v}]\!]\big)_{\Gamma\cup\Gamma_D} \quad \forall \boldsymbol{v}\in\boldsymbol{\mathcal{V}}^h.$$

Thus, substracting these equations, we have

$$b\big(\boldsymbol{v},p-p_h\big) = -a_{\mathtt{IP}}\big(\boldsymbol{u}-\boldsymbol{u}_h,\boldsymbol{v}\big) - \big(\tilde{p}-\tilde{p}_h,[\![\boldsymbol{n}\cdot\boldsymbol{v}]\!]\big)_{\Gamma\cup\Gamma_D} \quad \forall \boldsymbol{v}\in\boldsymbol{\mathcal{V}}^h,$$

and therefore

$$\big|b\big(\boldsymbol{v},p-p_h\big)\big| \le \big|a_{\mathtt{IP}}\big(\boldsymbol{u}-\boldsymbol{u}_h,\boldsymbol{v}\big)\big| + \Big|\big(\tilde{p}-\tilde{p}_h,[\![\boldsymbol{n}\cdot\boldsymbol{v}]\!]\big)_{\Gamma\cup\Gamma_D}\Big| \quad \forall \boldsymbol{v}\in\boldsymbol{\mathcal{V}}^h. \tag{A.15}$$

Using the inf-sup condition (A.13) and equation (A.15), we get

$$\|P_{\mathcal{Q}^h}p-p_h\|_\Omega \le \frac{\alpha}{|||\boldsymbol{v}|||}\left(\big|a_{\mathtt{IP}}\big(\boldsymbol{u}-\boldsymbol{u}_h,\boldsymbol{v}\big)\big| + \Big|\big(\tilde{p}-\tilde{p}_h,[\![\boldsymbol{n}\cdot\boldsymbol{v}]\!]\big)_{\Gamma\cup\Gamma_D}\Big|\right) \quad \text{for some } \boldsymbol{v}\in\boldsymbol{\mathcal{V}}^h. \tag{A.16}$$

Then, using the Cauchy-Schwartz inequality and the definition of the $|||.|||$-norm

$$\begin{aligned}\Big|\big(\tilde{p}-\tilde{p}_h,[\![\boldsymbol{n}\cdot\boldsymbol{v}]\!]\big)_{\Gamma\cup\Gamma_D}\Big| &\le \|\tilde{p}-\tilde{p}_h\|_{\Gamma\cup\Gamma_D}\,|[\![\boldsymbol{n}\cdot\boldsymbol{v}]\!]|_{\Gamma\cup\Gamma_D}\\ &\le \|\tilde{p}-\tilde{p}_h\|_{\Gamma\cup\Gamma_D}\|[\![\boldsymbol{n}\otimes\boldsymbol{v}]\!]\|_{\Gamma\cup\Gamma_D}\\ &\le \|\tilde{p}-\tilde{p}_h\|_{\Gamma\cup\Gamma_D}h^{\frac{1}{2}}\;|||\boldsymbol{v}|||,\end{aligned}$$

using the continuity property of $a_{\mathtt{IP}}$ (A.1)

$$\|P_{\mathcal{Q}^h}p-p_h\|_\Omega \le c\left(|||\boldsymbol{u}-\boldsymbol{u}_h\;||| + h^{\frac{1}{2}}\|\tilde{p}-\tilde{p}_h\|_{\Gamma\cup\Gamma_D}\right), \tag{A.17}$$

and using velocity and hybrid pressure error bounds previously obtained

$$\|P_{\mathcal{Q}^h} p - p_h\|_\Omega \leq c h^{\alpha - \frac{1}{2}} |\boldsymbol{u}|_{[\mathcal{H}^{1+\alpha}(\Omega)]^{\mathtt{n_{sd}}}}. \tag{A.18}$$

Eventually,

$$\|p - p_h\|_\Omega \leq \|p - P_{\mathcal{Q}^h} p\|_\Omega + \|P_{\mathcal{Q}^h} p - p_h\|_\Omega \tag{A.19}$$

then, (A.18) and the well-known approximation result lead to the interior pressure error bound (A.14) $\square$.

Appendix B

LDG and CDG methods for the incompressible Stokes equations

Following the development of Peraire and Persson (2008) for an elliptic problem, the weak form of a compact discontinuous Galerkin (CDG) formulation for the incompressible Stokes problem is derived next. The main differences with the Local Discontinuous Galerkin, see for example Cockburn et al. (2001, 2005b), are emphasized.

Introducing the velocity gradient $\boldsymbol{\sigma} = 2\nu\boldsymbol{\nabla}^{\mathtt{S}}\boldsymbol{u}$, the incompressible Stokes equations can be rewritten as the following system of first order equations

$$\boldsymbol{\sigma} = 2\nu\boldsymbol{\nabla}^{\mathtt{S}}\boldsymbol{u} \qquad \text{in } \hat{\Omega}, \tag{B.1a}$$

$$-\boldsymbol{\nabla}\cdot\boldsymbol{\sigma} + \boldsymbol{\nabla}p = \boldsymbol{f} \qquad \text{in } \hat{\Omega}, \tag{B.1b}$$

$$\boldsymbol{\nabla}\cdot\boldsymbol{u} = 0 \qquad \text{in } \hat{\Omega}, \tag{B.1c}$$

with boundary and interface conditions (2.1c)-(2.1f).

B.1 The weak form of the Stokes problem

Multiplying equations (B.1a), (B.1b) and (B.1c) by smooth test functions $\boldsymbol{\tau} \in \boldsymbol{\Sigma}$, $\boldsymbol{v} \in \boldsymbol{\mathcal{V}}$ and $q \in \mathcal{Q}$ respectively, and integrating by parts over an arbitrary subset

$\Omega_i \subset \Omega$ with outward normal unit vector $\boldsymbol{n}$, the weak problem becomes

$$\int_{\Omega_i} \boldsymbol{\sigma} : \boldsymbol{\tau} d\Omega = -\int_{\Omega_i} 2\nu \boldsymbol{u} \cdot \boldsymbol{\nabla} \cdot \boldsymbol{\tau} d\Omega + \int_{\partial\Omega_i} 2\nu \boldsymbol{u} \cdot \boldsymbol{\tau} \cdot \boldsymbol{n} d\Gamma, \tag{B.2a}$$

$$\int_{\Omega_i} \left[\boldsymbol{\sigma} : \boldsymbol{\nabla}^{\mathtt{S}} \boldsymbol{v} - p\boldsymbol{\nabla} \cdot \boldsymbol{v}\right] d\Omega - \int_{\partial\Omega_i} \left[\boldsymbol{\sigma} : (\boldsymbol{v} \otimes \boldsymbol{n}) - p\boldsymbol{v} \cdot \boldsymbol{n}\right] d\Gamma = \int_{\Omega_i} \boldsymbol{f} \cdot \boldsymbol{v} d\Omega, \tag{B.2b}$$

$$-\int_{\Omega_i} \boldsymbol{u} \cdot \boldsymbol{\nabla} q d\Omega + \int_{\partial\Omega_i} \boldsymbol{u} \cdot \boldsymbol{n} q d\Gamma = 0. \tag{B.2c}$$

Note that the above equations are well defined for functions $(\boldsymbol{\sigma}, \boldsymbol{u}, p)$ and $(\boldsymbol{\tau}, \boldsymbol{v}, q)$ in $\boldsymbol{\Sigma} \times \boldsymbol{\mathcal{V}} \times \mathcal{Q}$ where the spaces

$$\begin{aligned}
\boldsymbol{\Sigma} &= \{\boldsymbol{\tau} \in [\mathcal{L}_2(\Omega)]^{\mathtt{n_{sd}^2}} | \boldsymbol{\tau} = \boldsymbol{\tau}^{\boldsymbol{T}}\}, \\
\boldsymbol{\mathcal{V}} &= \{\boldsymbol{v} \in [\mathcal{L}_2(\Omega)]^{\mathtt{n_{sd}}} \ ; \ \boldsymbol{v}|_{\Omega_i} \in [\mathcal{H}^1(\Omega_i)]^{\mathtt{n_{sd}}} \quad \forall \Omega_i\} \\
\mathcal{Q} &= \{q \in [\mathcal{L}_2(\Omega)]\}
\end{aligned}$$

are associated to the partition of the domain $\widehat{\Omega} := \bigcup_{i=1}^{\mathtt{n_{el}}} \Omega_i$.

In order to rewrite all $\mathtt{n_{el}}$ weak problems defined in (B.2) as one weak problem, finite element subspaces are used. $\boldsymbol{\mathcal{V}}^h \subset \boldsymbol{\mathcal{V}}$ and $\mathcal{Q}^h \subset \mathcal{Q}$ have been defined in (1.1) and $\boldsymbol{\Sigma}^h \subset \boldsymbol{\Sigma}$ is such that $\boldsymbol{\Sigma}^h = \boldsymbol{\nabla}^{\mathtt{S}} \boldsymbol{\mathcal{V}}^h$. Moreover, using the definition of jumps and means, we have the following property

$$\sum_i \int_{\partial\Omega_i} p\boldsymbol{v} \cdot \boldsymbol{n} d\Gamma = \int_\Gamma \left(\llbracket p\boldsymbol{n} \rrbracket \{\boldsymbol{u}\} + \{p\} \llbracket \boldsymbol{v} \cdot \boldsymbol{n} \rrbracket\right) d\Gamma + \int p\boldsymbol{u} \cdot \boldsymbol{n} d\Gamma,$$

for vectors and scalars and an equivalent one for vectors and tensors. Now, using this property and boundary condition (2.1f), and adding equations (B.2) for $i = 1, \ldots \mathtt{n_{el}}$, the unique weak problem becomes: find $\boldsymbol{\sigma}_h \in \boldsymbol{\Sigma}^h$, $u_h \in \boldsymbol{\mathcal{V}}^h$, $p_h \in \mathcal{Q}^h$ such that

$$\int_\Omega \boldsymbol{\sigma}_h : \boldsymbol{\tau} d\Omega = -\int_\Omega 2\nu \boldsymbol{u}_h \cdot \boldsymbol{\nabla} \cdot \boldsymbol{\tau} d\Omega + \int_{\Gamma \cup \Gamma_D \cup \Gamma_N} 2\nu \hat{\boldsymbol{u}}_h^\sigma \cdot \llbracket \boldsymbol{\tau} \cdot \boldsymbol{n} \rrbracket d\Gamma, \quad \forall \boldsymbol{\tau} \in \boldsymbol{\Sigma}^h \tag{B.3a}$$

$$\int_\Omega [\boldsymbol{\sigma}_h : \boldsymbol{\nabla}^{\mathtt{S}} \boldsymbol{v} - p_h \boldsymbol{\nabla}\cdot\boldsymbol{v}] d\Omega - \int_{\Gamma\cup\Gamma_D} [\hat{\boldsymbol{\sigma}}_h : [\![\boldsymbol{v}\otimes\boldsymbol{n}]\!] - \hat{p}_h [\![\boldsymbol{v}\cdot\boldsymbol{n}]\!]] d\Gamma - \int_{\Gamma_N} \boldsymbol{t}\cdot\boldsymbol{v} d\Gamma = \int_\Omega \boldsymbol{f}\cdot\boldsymbol{v} d\Omega, \quad \forall \boldsymbol{v}\in\boldsymbol{\mathcal{V}}^h \quad \text{(B.3b)}$$

$$-\int_\Omega \boldsymbol{u}_h\cdot\boldsymbol{\nabla} q d\Omega + \int_{\Gamma\cup\Gamma_D} \hat{\boldsymbol{u}}_h^p \cdot [\![\boldsymbol{n} q]\!] d\Gamma = 0 \quad \forall q\in\mathcal{Q}^h. \quad \text{(B.3c)}$$

where $\hat{\boldsymbol{u}}_h^\sigma$, $\hat{\boldsymbol{\sigma}}_h$, $\hat{p}_h$ and $\hat{\boldsymbol{u}}_h^p$ are numerical fluxes defined in the following sections.

Note that if we use the integration by parts formula

$$-\int_\Omega \boldsymbol{v}\cdot\boldsymbol{\nabla}\cdot\boldsymbol{\tau} d\Omega = \int_\Omega \boldsymbol{\tau}\cdot\boldsymbol{\nabla}\boldsymbol{v} d\Omega - \int_\Gamma ([\![\boldsymbol{n}\otimes\boldsymbol{v}]\!] : \{\boldsymbol{\tau}\} + \{\boldsymbol{v}\}\cdot[\![\boldsymbol{n}\cdot\boldsymbol{\tau}]\!]) d\Gamma - \int_{\partial\Omega} \boldsymbol{v}\cdot\boldsymbol{\tau}\cdot\boldsymbol{n} d\Gamma$$

valid for all $\boldsymbol{\tau}\in\boldsymbol{\Sigma}^h$ and $\boldsymbol{u}\in\boldsymbol{\mathcal{V}}^h$, equation (B.3a) can also be written as

$$\int_\Omega \boldsymbol{\sigma}_h : \boldsymbol{\tau} d\Omega = \int_\Omega 2\nu\boldsymbol{\tau}\cdot\boldsymbol{\nabla}^{\mathtt{S}}\boldsymbol{u}_h d\Omega - \int_\Gamma 2\nu \left([\![\boldsymbol{n}\otimes\boldsymbol{u}_h]\!] : \{\boldsymbol{\tau}\} - \{\hat{\boldsymbol{u}}_h^\sigma - \boldsymbol{u}_h\}\cdot[\![\boldsymbol{n}\cdot\boldsymbol{\tau}]\!]\right) d\Gamma + \int_{\Gamma_D\cup\Gamma_N} 2\nu(\hat{\boldsymbol{u}}_h^\sigma - \boldsymbol{u}_h)\cdot\boldsymbol{\tau}\cdot\boldsymbol{n} d\Gamma \quad \text{(B.4)}$$

Since the CDG formulation proposed here for Stokes is closely related to the LDG method proposed by Cockburn et al. (2005b), a description of the LDG approach is given next.

B.1.1 Numerical fluxes

Following the definition of the diffusive fluxes by Cockburn et al. (2001) for LDG

$$\hat{\boldsymbol{\sigma}}_h = \{\boldsymbol{\sigma}_h\} - C_{11}[\![\boldsymbol{n}\otimes\boldsymbol{u}_h]\!] + \boldsymbol{C}_{12}\otimes[\![\boldsymbol{n}\cdot\boldsymbol{\sigma}_h]\!] \quad \text{and} \quad \hat{\boldsymbol{u}}_h^\sigma = \{\boldsymbol{u}_h\} - \boldsymbol{C}_{12}\cdot[\![\boldsymbol{n}\otimes\boldsymbol{u}_h]\!], \quad \text{(B.5)}$$

on interior sides/faces Γ and

$$\hat{\boldsymbol{\sigma}}_h = \boldsymbol{\sigma}_h - C_{11}(\boldsymbol{u}_h - \boldsymbol{u}_D)\otimes\boldsymbol{n} \text{ and } \hat{\boldsymbol{u}}_h^\sigma = \boldsymbol{u}_D \text{ on } \Gamma_D, \quad \text{and } \hat{\boldsymbol{u}}_h^\sigma = \boldsymbol{u}_h \text{ on } \Gamma_N. \quad \text{(B.6)}$$

C_{11} is a positive constant, defined in Section 2.1.5, and $\boldsymbol{C}_{12}$ is a vector that has to be determined for each interior edge of the domain according to

$$\boldsymbol{C}_{12} = \frac{1}{2}(S_{ij}\boldsymbol{n}_i + S_{ji}\boldsymbol{n}_j) \tag{B.7}$$

where $S_{ij} \in \{0, 1\}$ denotes the switch associated with element Ω_i on the face that element Ω_i shares with element Ω_j. There are several possible choices of the switches, always satisfying $S_{ij} + S_{ji} = 1$, see Peraire and Persson (2008); Cockburn et al. (2001) for details. One possibility is the *natural switch*, which takes into account the element numbering to set S_{ij}. Another alternative is to use a *consistent* switch that satisfies

$$0 < \sum_{e \in \partial\Omega_i} S_{ij} < \mathtt{n_{sd}} + 1.$$

Considering the numbering of the nodes for each element Ω_i is one possible option for a consistent switch.

Numerical fluxes related to incompressibility constraint are now defined. If a face lies inside the domain Ω (i.e. on interior sides/faces Γ)

$$\hat{\boldsymbol{u}}_h^p = \{\boldsymbol{u}_h\} \quad \text{and} \quad \hat{p}_h = \{p_h\}, \tag{B.8}$$

whereas on the Dirichlet boundary Γ_D

$$\hat{\boldsymbol{u}}_h^p = \boldsymbol{u}_D \quad \text{and} \quad \hat{p}_h = p_h. \tag{B.9}$$

B.1.2 LDG formulation

Using the expression of the fluxes previously defined, equation (B.4) can now be written as

$$\int_\Omega \boldsymbol{\sigma}_h : \boldsymbol{\tau} d\Omega = \int_\Omega 2\nu\boldsymbol{\tau} \cdot \boldsymbol{\nabla}^{\mathbf{S}} \boldsymbol{u}_h d\Omega - \int_\Gamma 2\nu([\![\boldsymbol{n} \otimes \boldsymbol{u}_h]\!] : \{\boldsymbol{\tau}\} + \boldsymbol{C}_{12} \cdot [\![\boldsymbol{n} \otimes \boldsymbol{u}_h]\!] \cdot [\![\boldsymbol{n} \cdot \boldsymbol{\tau}]\!]) d\Gamma + \int_{\Gamma_D} 2\nu(\boldsymbol{u}_D - \boldsymbol{u}_h) \cdot \boldsymbol{\tau} \cdot \boldsymbol{n} d\Gamma \quad \text{(B.10)}$$

As usual in LDG (Cockburn et al., 2005a), two local lifting operators are defined in order to obtain an expression for $\boldsymbol{\sigma}_h$ as a function of $\boldsymbol{u}_h$, the lifting operators are introduced: $r : [\mathcal{L}_2(\Gamma \cup \Gamma_D)]^{\mathtt{n}_{\mathtt{sd}}^2} \to \boldsymbol{\Sigma}^h$ is defined by

$$\int_\Omega r(\boldsymbol{\sigma}) : \boldsymbol{\tau}\, d\Omega = \int_{\Gamma \cup \Gamma_D} \boldsymbol{\sigma} : \{\boldsymbol{\tau}\} d\Gamma \quad \forall \boldsymbol{\tau} \in \boldsymbol{\Sigma}^h, \quad \text{(B.11)}$$

The second lifting, $s : [\mathcal{L}_2(\Gamma)]^{\mathtt{n}_{\mathtt{sd}}} \to \boldsymbol{\Sigma}^h$ is defined by

$$\int_\Omega s(\boldsymbol{v}) : \boldsymbol{\tau}\, d\Omega = \int_\Gamma \boldsymbol{v} \cdot [\![\boldsymbol{n} \cdot \boldsymbol{\tau}]\!] d\Gamma \quad \forall \boldsymbol{\tau} \in \boldsymbol{\Sigma}^h. \quad \text{(B.12)}$$

Thus equation (B.10) defining $\boldsymbol{\sigma}_h$ in terms of $\boldsymbol{u}_h$ can be rewritten as

$$\boldsymbol{\sigma}_h = 2\nu \boldsymbol{\nabla}^{\mathbf{S}} \boldsymbol{u}_h - \bar{\boldsymbol{\sigma}}_h,$$

where $\bar{\boldsymbol{\sigma}}_h$ is

$$\bar{\boldsymbol{\sigma}}_h = 2\nu \left(r([\![\boldsymbol{n} \otimes \boldsymbol{u}_h]\!]) + s(\boldsymbol{C}_{12} \cdot [\![\boldsymbol{n} \otimes \boldsymbol{u}_h]\!]) \right) \quad \text{on } \Gamma,$$

and

$$\bar{\boldsymbol{\sigma}}_h = -2\nu r\big(\boldsymbol{n} \otimes (\boldsymbol{u}_D - \boldsymbol{u}_h)\big) \quad \text{on } \Gamma_D.$$

Setting $\boldsymbol{\tau} = \boldsymbol{\nabla}^{\mathbf{S}} \boldsymbol{v}$ in equation (B.10) allows to substitute the term implying $\boldsymbol{\sigma}$ in

equation (B.3b), which can be rewritten as

$$\begin{aligned}\int_\Omega 2\nu\boldsymbol{\nabla}^{\mathtt{S}}\boldsymbol{v}:\boldsymbol{\nabla}^{\mathtt{S}}\boldsymbol{u}_h d\Omega - \int_\Gamma 2\nu\left(\llbracket\boldsymbol{n}\otimes\boldsymbol{u}_h\rrbracket:\{\boldsymbol{\nabla}^{\mathtt{S}}\boldsymbol{v}\} + \boldsymbol{C}_{12}\cdot\llbracket\boldsymbol{n}\otimes\boldsymbol{u}_h\rrbracket\cdot\llbracket\boldsymbol{n}\cdot\boldsymbol{\nabla}^{\mathtt{S}}\boldsymbol{v}\rrbracket\right)d\Gamma \\ + \int_{\Gamma_D} 2\nu(\boldsymbol{u}_D-\boldsymbol{u}_h)\cdot\boldsymbol{\nabla}^{\mathtt{S}}\boldsymbol{v}\cdot\boldsymbol{n}d\Gamma \\ = \int_\Gamma \hat{\boldsymbol{\sigma}}_h:\llbracket\boldsymbol{n}\otimes\boldsymbol{v}\rrbracket d\Gamma + \int_{\Gamma_D}\hat{\boldsymbol{\sigma}}_h:(\boldsymbol{v}\otimes\boldsymbol{n})d\Gamma + \int_{\Gamma_N}\boldsymbol{v}\cdot\boldsymbol{t}d\Gamma \\ + \int_\Omega p_h\boldsymbol{\nabla}\cdot\boldsymbol{v}d\Omega - \int_\Gamma \hat{p}_h\llbracket\boldsymbol{v}\cdot\boldsymbol{n}\rrbracket d\Gamma - \int_{\Gamma_D}\hat{p}_h\boldsymbol{v}\cdot\boldsymbol{n}d\Gamma + \int_\Omega\boldsymbol{f}\cdot\boldsymbol{v}d\Omega \quad \text{(B.13)}\end{aligned}$$

Further calculation consists in susbtituting the expression of the fluxes in (B.13) and leads to a formulation where only velocity and pressure terms appear, that is $\boldsymbol{\sigma}$ is eliminated. The LDG weak form of the Stokes problem is then: find $\boldsymbol{u}_h\in\boldsymbol{\mathcal{V}}^h$ and $p_h\in\mathcal{Q}^h$ such that

$$\begin{cases} a_{\mathtt{LDG}}(\boldsymbol{u}_h,\boldsymbol{v}) + b(\boldsymbol{v},p_h) + \big(\{p_h\},\llbracket\boldsymbol{n}\cdot\boldsymbol{v}\rrbracket\big)_{\Gamma\cup\Gamma_D} = l_{\mathtt{LDG}}(\boldsymbol{v}) & \forall\,\boldsymbol{v}\in\boldsymbol{\mathcal{V}}^h, \\ b(\boldsymbol{u}_h,q) + \big(\{q\},\llbracket\boldsymbol{n}\cdot\boldsymbol{u}_h\rrbracket\big)_{\Gamma\cup\Gamma_D} = \big(q,\boldsymbol{n}\cdot\boldsymbol{u}_D\big)_{\Gamma_D} & \forall\,q\in\mathcal{Q}^h, \end{cases} \quad \text{(B.14)}$$

with

$$\begin{aligned}a_{\mathtt{LDG}}(\boldsymbol{u},\boldsymbol{v}) := a_{\mathtt{IP}}(\boldsymbol{u},\boldsymbol{v}) - \big(2\nu\boldsymbol{C}_{12}\otimes\llbracket\boldsymbol{n}\cdot\boldsymbol{\nabla}^{\mathtt{S}}\boldsymbol{v}\rrbracket,\llbracket\boldsymbol{n}\otimes\boldsymbol{u}\rrbracket\big)_\Gamma - \big(2\nu\boldsymbol{C}_{12}\otimes\llbracket\boldsymbol{n}\cdot\boldsymbol{\nabla}^{\mathtt{S}}\boldsymbol{u}\rrbracket,\llbracket\boldsymbol{n}\otimes\boldsymbol{v}\rrbracket\big)_\Gamma \\ + \Big(2\nu\big(r(\llbracket\boldsymbol{n}\otimes\boldsymbol{u}\rrbracket) + s(\boldsymbol{C}_{12}\cdot\llbracket\boldsymbol{n}\otimes\boldsymbol{u}\rrbracket)\big), r(\llbracket\boldsymbol{n}\otimes\boldsymbol{v}\rrbracket) + s(\boldsymbol{C}_{12}\cdot\llbracket\boldsymbol{n}\otimes\boldsymbol{v}\rrbracket)\Big) \quad \text{(B.15a)}\end{aligned}$$

$$l_{\mathtt{LDG}}(\boldsymbol{v}) := l_{\mathtt{IP}}(\boldsymbol{v}) + \Big(2\nu\, r(\boldsymbol{n}\otimes\boldsymbol{v}), r(\boldsymbol{n}\otimes\boldsymbol{u}_D)\Big) \quad \text{(B.15b)}$$

and the forms defined in (2.4). The obtention of the weak form will be further detailed for the CDG formulation in Section B.2. Note that LDG has attractive properties since it is symmetric, conservative and adjoint consistent. Nevertheless the product of lifting operators in (B.15a) makes the resulting descretization non-compact. The equation corresponding to a given degree of freedom may involve degrees of freedom that belong to elements that are not immediate neighbors. To avoid this lost of compactness, a

Compact Discontinuous Galerkin (CDG) formulation is presented next.

B.2 CDG formulation

LDG presents attractive features but also the main desadvantage of a non-compact formulation. The objective of the CDG formulation is to modificate the expression of the lifting operators so that their product, see (B.15a) does not generate a bigger stencil. To do so, a stress field $\boldsymbol{\sigma}_h^e$ is defined for each face Γ_e as

$$\boldsymbol{\sigma}_h^e = 2\nu \boldsymbol{\nabla}^{\mathbf{S}} \boldsymbol{u}_h - \bar{\boldsymbol{\sigma}}_h^e,$$

where $\bar{\boldsymbol{\sigma}}_h^e$ is defined on a localized support

$$\bar{\boldsymbol{\sigma}}_h^e = 2\nu \left(r^e([\![\boldsymbol{n} \otimes \boldsymbol{u}_h]\!]) + s^e(\boldsymbol{C}_{12} \cdot [\![\boldsymbol{n} \otimes \boldsymbol{u}_h]\!]) \right) \quad \text{for } e \in \Gamma,$$

and

$$\bar{\boldsymbol{\sigma}}_h^e = -2\nu r^e\big(\boldsymbol{n} \otimes (\boldsymbol{u}_D - \boldsymbol{u}_h)\big) \quad \text{for } e \in \Gamma_D.$$

The main difference with LDG is thus that in order to compute $\hat{\boldsymbol{\sigma}}_h$ on a given face Γ_e, CDG requires to evaluate first a stress field $\boldsymbol{\sigma}_h^e$ associated to this face, through local lifting operators r^e and s^e defined next. As usual in CDG (Peraire and Persson, 2008), the liftings operators introduced in (B.11) and (B.12) are now decomposed into facewise contributions. For all sides $\Gamma_e \subset \Gamma \cup \Gamma_D$, the lifting $r^e : [\mathcal{L}_2(\Gamma_e)]^{\mathtt{n_{sd}^2}} \to \boldsymbol{\Sigma}^h$ is defined by

$$\int_\Omega r^e(\boldsymbol{\sigma}) : \boldsymbol{\tau} \, d\Omega = \int_{\Gamma_e} \boldsymbol{\sigma} : \{\boldsymbol{\tau}\} d\Gamma \quad \forall \boldsymbol{\tau} \in \boldsymbol{\Sigma}^h. \tag{B.16}$$

The second lifting, $s^e : [\mathcal{L}_2(\Gamma_e)]^{\mathtt{n_{sd}}} \to \boldsymbol{\Sigma}^h$, is set to zero for all boundary sides, $s^e(\boldsymbol{v}) = \mathbf{0}$ $\forall \boldsymbol{v} \in [\mathcal{L}_2(\Gamma_e)]^{\mathtt{n_{sd}}}$ for $\Gamma_e \subset \Gamma_D$, and it is defined by

$$\int_\Omega s^e(\boldsymbol{v}) : \boldsymbol{\tau} \, d\Omega = \int_{\Gamma_e} \boldsymbol{v} \cdot [\![\boldsymbol{n} \cdot \boldsymbol{\tau}]\!] d\Gamma \quad \forall \boldsymbol{\tau} \in \boldsymbol{\Sigma}^h, \tag{B.17}$$

for all interior sides $\Gamma_e \subset \Gamma$. Note that for all $\boldsymbol{\sigma} \in [\mathcal{L}_2(\Gamma_e)]^{\mathtt{n}_{\mathtt{sd}}^2}$ and $\boldsymbol{v} \in [\mathcal{L}_2(\Gamma_e)]^{\mathtt{n}_{\mathtt{sd}}}$

$$r(\boldsymbol{\sigma}) = \sum_{e \in \Gamma \cup \Gamma_D} r^e(\boldsymbol{\sigma}) \text{ and } s(\boldsymbol{v}) = \sum_{e \in \Gamma} s^e(\boldsymbol{v}).$$

Note that the diffusive flux $\hat{\boldsymbol{\sigma}}_h$ on a given face is defined for CDG as

$$\hat{\boldsymbol{\sigma}}_h = \{\boldsymbol{\sigma}_h^e\} - C_{11}[\![\boldsymbol{n} \otimes \boldsymbol{u}_h]\!] + \boldsymbol{C}_{12} \otimes [\![\boldsymbol{n} \cdot \boldsymbol{\sigma}_h^e]\!] \quad \text{on } \Gamma,$$

and

$$\hat{\boldsymbol{\sigma}}_h = \boldsymbol{\sigma}_h^e - C_{11}(\boldsymbol{u}_h - \boldsymbol{u}_D) \otimes \boldsymbol{n} \quad \text{on } \Gamma_D$$

C_{11} and $\boldsymbol{C}_{12}$ are the same parameters as the ones previously defined. The numerical fluxes $\hat{\boldsymbol{u}}_h^\sigma$, $\hat{\boldsymbol{u}}_h^p$ and $\hat{p}_h$ for CDG are the same ones as the ones defined in (B.5)-(B.9).

The obtention of the CDG weak form is now detailed. From the definition of the fluxes and of the local lifting operators, the terms involving the flux $\hat{\boldsymbol{\sigma}}_h$ in (B.13), can be written as: on Γ

$$\int_\Gamma \hat{\boldsymbol{\sigma}}_h : [\![\boldsymbol{n} \otimes \boldsymbol{v}]\!] = \sum_{\Gamma_e \subset \Gamma} \int_{\Gamma_e} (\{\boldsymbol{\sigma}_h^e\} - C_{11}[\![\boldsymbol{n} \otimes \boldsymbol{u}_h]\!] + \boldsymbol{C}_{12} \otimes [\![\boldsymbol{n} \cdot \boldsymbol{\sigma}_h^e]\!]) : [\![\boldsymbol{n} \otimes \boldsymbol{v}]\!] d\Gamma$$

$$\begin{aligned} &= \int_\Gamma \{2\nu \boldsymbol{\nabla}^{\mathtt{S}} \boldsymbol{u}_h\} : [\![\boldsymbol{n} \otimes \boldsymbol{v}]\!] d\Gamma + \int_\Gamma \left(\boldsymbol{C}_{12} \otimes [\![\boldsymbol{n} \cdot 2\nu \boldsymbol{\nabla}^{\mathtt{S}} \boldsymbol{u}_h]\!]\right) : [\![\boldsymbol{n} \otimes \boldsymbol{v}]\!] d\Gamma \\ -C_{11} &\int_\Gamma [\![\boldsymbol{n} \otimes \boldsymbol{u}_h]\!] : [\![\boldsymbol{n} \otimes \boldsymbol{v}]\!] d\Gamma - \sum_{\Gamma_e \subset \Gamma} \int_{\Gamma_e} \{\bar{\boldsymbol{\sigma}}_h^e\} : [\![\boldsymbol{n} \otimes \boldsymbol{v}]\!] d\Gamma - \sum_{\Gamma_e \subset \Gamma} \int_{\Gamma_e} [\![\boldsymbol{n} \cdot \bar{\boldsymbol{\sigma}}_h^e]\!] \cdot (\boldsymbol{C}_{12} \cdot [\![\boldsymbol{n} \otimes \boldsymbol{v}]\!]) d\Gamma \end{aligned}$$

$$\begin{aligned} &= \int_\Gamma \{2\nu \boldsymbol{\nabla}^{\mathtt{S}} \boldsymbol{u}_h\} : [\![\boldsymbol{n} \otimes \boldsymbol{v}]\!] d\Gamma + \int_\Gamma \left(\boldsymbol{C}_{12} \otimes [\![\boldsymbol{n} \cdot 2\nu \boldsymbol{\nabla}^{\mathtt{S}} \boldsymbol{u}_h]\!]\right) : [\![\boldsymbol{n} \otimes \boldsymbol{v}]\!] d\Gamma \\ &- C_{11} \int_\Gamma [\![\boldsymbol{n} \otimes \boldsymbol{u}_h]\!] : [\![\boldsymbol{n} \otimes \boldsymbol{v}]\!] d\Gamma - \sum_{\Gamma_e \subset \Gamma} \int_\Omega \bar{\boldsymbol{\sigma}}_h^e : \left(r^e([\![\boldsymbol{n} \otimes \boldsymbol{v}]\!]) + s^e(\boldsymbol{C}_{12} \cdot [\![\boldsymbol{n} \otimes \boldsymbol{v}]\!])\right) d\Omega \end{aligned}$$

$$= \int_\Gamma \{2\nu\boldsymbol{\nabla}^{\mathtt{S}}\boldsymbol{u}_h\} : [\![\boldsymbol{n}\otimes\boldsymbol{v}]\!]d\Gamma + \int_\Gamma (\boldsymbol{C}_{12}\otimes[\![\boldsymbol{n}\cdot 2\nu\boldsymbol{\nabla}^{\mathtt{S}}\boldsymbol{u}_h]\!]) : [\![\boldsymbol{n}\otimes\boldsymbol{v}]\!]d\Gamma - C_{11}\int_\Gamma [\![\boldsymbol{n}\otimes\boldsymbol{u}_h]\!] : [\![\boldsymbol{n}\otimes\boldsymbol{v}]\!]d\Gamma$$
$$- \sum_{\Gamma_e\subset\Gamma}\int_\Omega 2\nu\big(r^e([\![\boldsymbol{n}\otimes\boldsymbol{u}_h]\!]) + s^e(\boldsymbol{C}_{12}\cdot[\![\boldsymbol{n}\otimes\boldsymbol{u}_h]\!])\big) : \big(r^e([\![\boldsymbol{n}\otimes\boldsymbol{v}]\!]) + s^e(\boldsymbol{C}_{12}\cdot[\![\boldsymbol{n}\otimes\boldsymbol{v}]\!])\big)d\Omega$$

and on Γ_D

$$\int_{\Gamma_D} \hat{\boldsymbol{\sigma}}_h : (\boldsymbol{n}\otimes\boldsymbol{v})d\Gamma = \sum_{\Gamma_e\subset\Gamma_D}\int_{\Gamma_e} (\boldsymbol{\sigma}_h^e - C_{11}(\boldsymbol{u}_h - \boldsymbol{u}_D)\otimes\boldsymbol{n}) : (\boldsymbol{n}\otimes\boldsymbol{v})d\Gamma$$

$$= \int_{\Gamma_D} 2\nu\boldsymbol{\nabla}^{\mathtt{S}}\boldsymbol{u}_h : (\boldsymbol{n}\otimes\boldsymbol{v})d\Gamma - \int_{\Gamma_D} C_{11}(\boldsymbol{n}\otimes(\boldsymbol{u}_h - \boldsymbol{u}_D)) : (\boldsymbol{n}\otimes\boldsymbol{v})d\Gamma - \sum_{\Gamma_e\subset\Gamma_D}\int_{\Gamma_e} \bar{\boldsymbol{\sigma}}_h^e : (\boldsymbol{n}\otimes\boldsymbol{v})d\Gamma$$

$$= \int_{\Gamma_D} 2\nu\boldsymbol{\nabla}^{\mathtt{S}}\boldsymbol{u}_h : (\boldsymbol{n}\otimes\boldsymbol{v})d\Gamma - \int_{\Gamma_D} C_{11}(\boldsymbol{n}\otimes(\boldsymbol{u}_h - \boldsymbol{u}_D)) : (\boldsymbol{n}\otimes\boldsymbol{v})d\Gamma - \sum_{\Gamma_e\subset\Gamma_D}\int_\Omega \bar{\boldsymbol{\sigma}}_h^e : r^e(\boldsymbol{n}\otimes\boldsymbol{v})d\Omega$$

$$= \int_{\Gamma_D} 2\nu\boldsymbol{\nabla}^{\mathtt{S}}\boldsymbol{u}_h : (\boldsymbol{n}\otimes\boldsymbol{v})d\Gamma - \int_{\Gamma_D} C_{11}(\boldsymbol{n}\otimes(\boldsymbol{u}_h - \boldsymbol{u}_D)) : (\boldsymbol{n}\otimes\boldsymbol{v})d\Gamma$$
$$+ \sum_{\Gamma_e\subset\Gamma_D}\int_\Omega 2\nu r^e\big(\boldsymbol{n}\otimes(\boldsymbol{u}_D - \boldsymbol{u}_h)\big) : r^e(\boldsymbol{n}\otimes\boldsymbol{v})d\Omega$$

Therefore sustituting these expressions in equation (B.13), the CDG scheme for the steady incompressible Stokes equations is obtained: find $\boldsymbol{u}_h \in \boldsymbol{\mathcal{V}}^h$ and $p_h \in \mathcal{Q}^h$ such that

$$a_{\mathtt{CDG}}\big(\boldsymbol{u}_h, \boldsymbol{v}\big) + b\big(\boldsymbol{v}, p_h\big) + \big(\{p_h\}, [\![\boldsymbol{n}\cdot\boldsymbol{v}]\!]\big)_{\Gamma\cup\Gamma_D} = l_{\mathtt{CDG}}\big(\boldsymbol{v}\big) \quad \forall\, \boldsymbol{v} \in \boldsymbol{\mathcal{V}}^h, \tag{B.20}$$

with

$$a_{\mathtt{CDG}}(\boldsymbol{u},\boldsymbol{v}) := a_{\mathtt{IP}}(\boldsymbol{u},\boldsymbol{v}) - \big(2\nu\boldsymbol{C}_{12}\otimes[\![\boldsymbol{n}\cdot\boldsymbol{\nabla}^{\mathtt{S}}\boldsymbol{v}]\!],[\![\boldsymbol{n}\otimes\boldsymbol{u}]\!]\big)_{\Gamma} - \big(2\nu\boldsymbol{C}_{12}\otimes[\![\boldsymbol{n}\cdot\boldsymbol{\nabla}^{\mathtt{S}}\boldsymbol{u}]\!],[\![\boldsymbol{n}\otimes\boldsymbol{v}]\!]\big)_{\Gamma} + \sum_{\Gamma_e\subset\Gamma\cup\Gamma_D}\Big(2\nu\big(r^e([\![\boldsymbol{n}\otimes\boldsymbol{u}]\!])+s^e(\boldsymbol{C}_{12}\cdot[\![\boldsymbol{n}\otimes\boldsymbol{u}]\!])\big), r^e([\![\boldsymbol{n}\otimes\boldsymbol{v}]\!])+s^e(\boldsymbol{C}_{12}\cdot[\![\boldsymbol{n}\otimes\boldsymbol{v}]\!])\Big) \tag{B.21a}$$

$$l_{\mathtt{CDG}}(\boldsymbol{v}) := l_{\mathtt{IP}}(\boldsymbol{v}) + \sum_{\Gamma_e\subset\Gamma_D}\Big(2\nu\, r^e(\boldsymbol{n}\otimes\boldsymbol{v}), r^e(\boldsymbol{n}\otimes\boldsymbol{u}_D)\Big) \tag{B.21b}$$

and the forms defined in (2.4).

Using the following identity for any $\boldsymbol{v}\in[\mathcal{H}^1(\widehat{\Omega})]^{\mathtt{n_{sd}}}$ and any $q\in\mathcal{L}_2(\Omega)$

$$-\int_{\Omega} q\boldsymbol{\nabla}\cdot\boldsymbol{v}d\Omega + \int_{\Gamma\cup\partial\Omega}\{q\}[\![\boldsymbol{n}\cdot\boldsymbol{v}]\!]d\Gamma = \int_{\Omega}\boldsymbol{v}\cdot\boldsymbol{\nabla}q d\Omega - \int_{\Gamma\cup\partial\Omega}[\![q\boldsymbol{n}]\!]\{\boldsymbol{v}\}d\Gamma,$$

the incompressibility equation (B.3c) can be rewritten as

$$b(\boldsymbol{u}_h,q) + \big(\{q\},[\![\boldsymbol{n}\cdot\boldsymbol{u}_h]\!]\big)_{\Gamma\cup\Gamma_D} = \big(q,\boldsymbol{n}\cdot\boldsymbol{u}_D\big)_{\Gamma_D} \quad \forall\, q\in\mathcal{Q}^h. \tag{B.22}$$

It is straightforward to verify that the bilinear form (B.21a) is symmetric. Also the conservative form of the numerical fluxes guarantees that CDG is conservative and adjoint consistent, see Peraire and Persson (2008). Both thus share the same attractive properties. But while LDG's weak form involves product of non local lifting operators, CDG involves product of local lifting operators, see (B.21a), which does not increase the stencil of the diffusion operator.

Appendix C

Explicit Runge-Kutta methods for incompressible flows

This appendix shows how to apply explicit Runge-Kutta (RK) methods to DAE problems, such as incompressible Stokes or Navier-Stokes equations. As commented in Section 3.1.1 explicit RK methods can not be directly applied to DAE the same way implicit or semi-implicit RK are formulated in (3.5)-(3.6), because the resulting system of equations (3.6) is under-determined. Pereira et al. (2001) propose an explicit RK formulation for the incompressible Navier-Stokes equations. As will be commented next, the scheme is very similar to the one obtained for an ODE, but at each stage the incompressibility constraint is added.

For simplicity purpose the Stokes equations are considered, but the formulation would be equivalent for non-linear incompressible problems such as Navier-Stokes. Let us consider the incompressible unsteady Stokes equations in discrete form

$$\begin{cases} \mathbf{M\dot{u}} + \mathbf{Ku} + \mathbf{Gp} = \mathbf{f} \\ \mathbf{G^T u} = \mathbf{0} \end{cases} \tag{C.1}$$

Following Pereira et al. (2001), the 4-stage explicit method with Butcher array seen in Table C.1, leads to the scheme

0				
$\frac{1}{2}$	$\frac{1}{2}$			
$\frac{1}{2}$	0	$\frac{1}{2}$		
1	0	0	$\frac{1}{2}$	
	$\frac{1}{6}$	$\frac{1}{3}$	$\frac{1}{3}$	$\frac{1}{6}$

Table C.1: Butcher array for 4-stage explicit Runge-Kutta method

$$\begin{cases} \mathbf{u}^{n+1} = \mathbf{u}^n + \Delta t \sum_{i=1}^{4} \left(\mathbf{f}(t^n + b_i \Delta t) - b_i \mathbf{K u_i}\right) - \Delta t \mathbf{G p}^{n+1} \\ \mathbf{G^T u}^{n+1} = \mathbf{0} \end{cases} \tag{C.2}$$

with

$$\mathbf{u_1} = \mathbf{u}^n \tag{C.3a}$$

$$\begin{cases} \mathbf{M u_2} = \mathbf{u}^n + \dfrac{\Delta t}{2}\left(\mathbf{f}\left(t^n + \dfrac{\Delta t}{2}\right) - \mathbf{K u_1}\right) - \Delta t \mathbf{G p_2} \\ \mathbf{G^T u_2} = \mathbf{0} \end{cases} \tag{C.3b}$$

$$\begin{cases} \mathbf{M u_3} = \mathbf{u}^n + \dfrac{\Delta t}{2}\left(\mathbf{f}\left(t^n + \dfrac{\Delta t}{2}\right) - \mathbf{K u_2}\right) - \Delta t \mathbf{G p_3} \\ \mathbf{G^T u_3} = \mathbf{0} \end{cases} \tag{C.3c}$$

$$\begin{cases} \mathbf{M u_4} = \mathbf{u}^n + \dfrac{\Delta t}{2}\left(\mathbf{f}\left(t^n + \Delta t\right) - \mathbf{K u_3}\right) - \Delta t \mathbf{G p_4} \\ \mathbf{G^T u_4} = \mathbf{0} \end{cases} \tag{C.3d}$$

A simple example with analytical solution is now used to check the orders of convergence of explicit RK methods:

$$\mathbf{M} = \begin{pmatrix} 1 & 0 \\ 0 & 1 \end{pmatrix}, \quad \mathbf{K} = \begin{pmatrix} 3 & 4 \\ 5 & 6 \end{pmatrix}, \quad \mathbf{G} = \begin{pmatrix} 1 \\ -2 \end{pmatrix},$$

are considered, with a body force

$$\mathbf{f} = \begin{pmatrix} 2cos(t) + 10sin(t) + e^{-t} \\ cos(t) + 16sin(t) - 2e^{-t} \end{pmatrix}$$

imposed in order to have the exact solution

$$\mathbf{u} = \begin{pmatrix} 2sin(t) \\ sin(t) \end{pmatrix}, \quad p = e^{-t}.$$

Figure C.1 shows the errors for velocity and pressure for the 2-stage Heune's method and the 4-stage explicit RK method. Though a slightly better accuracy is obtained us-

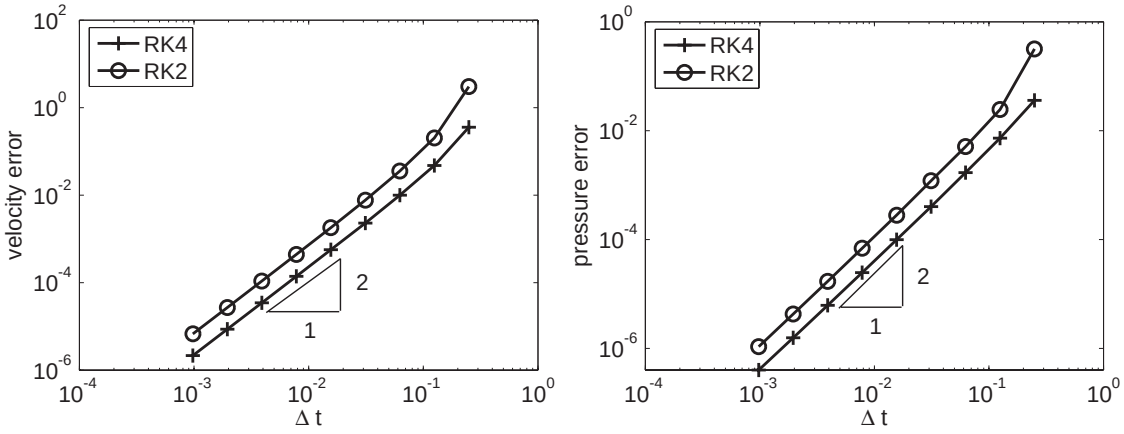

Figure C.1: Velocity and pressure error for fourth (RK4) and second (RK2) order explicit Runge-Kutta methods.

ing 4-stage explicit RK, second order convergence is reached for velocity and pressure errors with both methods. That is a high number of stages for explicit RK applied to DAE systems does not allow to reach the same high orders of convergence than when applied to ODE. Here the 2-stage Heune's would be preferred since its cost is less than the 4-stage explicit RK and both accuracy are equivalent. Furthermore, 2-stage Heune's method has an equivalent cost as a fractional-step (FS) method for incompressible flow. FS generally reaches second order in time for velocity but only first order for pressure, see for example Guermond et al. (2006). Thus 2-stage Heune's

method is a more efficient explicit method for incompressible flows than FS.

A discontinuous Galerkin method with divergence-free interpolation for the incompressible Stokes equations

A. Montlaur, S. Fernández-Méndez and A. Huerta

International Journal for Numerical Methods in Fluids,
Vol. 57, Issue 9, p p1071-1092, 2008

INTERNATIONAL JOURNAL FOR NUMERICAL METHODS IN FLUIDS
Int. J. Numer. Meth. Fluids 2008; **57**:1071–1092
Published online 14 April 2008 in Wiley InterScience (www.interscience.wiley.com). DOI: 10.1002/fld.1716

Discontinuous Galerkin methods for the Stokes equations using divergence-free approximations

A. Montlaur[1,2], S. Fernandez-Mendez[1,3] and A. Huerta[1,3,*,†]

[1]*Laboratori de Càlcul Numèric (LaCàN), Universitat Politècnica de Catalunya, Jordi Girona 1-3, 08034 Barcelona, Spain*
[2]*Escola Politècnica Superior de Castelldefels, Universitat Politècnica de Catalunya, Castelldefels, Spain*
[3]*Departament de Matemàtica Aplicada III, E.T.S. Ingenieros de Caminos, Universitat Politècnica de Catalunya, Jordi Girona 1, E-08034 Barcelona, Spain*

SUMMARY

A discontinuous Galerkin (DG) method with solenoidal approximation for the simulation of incompressible flow is proposed. It is applied to the solution of the Stokes equations. The interior penalty method is employed to construct the DG weak form. For every element, the approximation space for the velocity field is decomposed as the direct sum of a solenoidal space and an irrotational space. This allows to split the DG weak form into two uncoupled problems: the first one solves for the velocity and the hybrid pressure (pressure along the mesh edges) and the second one allows the computation of the pressure in the element interior. Furthermore, the introduction of an extra penalty term leads to an alternative DG formulation for the computation of solenoidal velocities with no presence of pressure terms. Pressure can then be computed as a post-process of the velocity solution. Numerical examples demonstrate the applicability of the proposed methodologies. Copyright © 2008 John Wiley & Sons, Ltd.

Received 30 July 2007; Revised 9 November 2007; Accepted 12 November 2007

KEY WORDS: discontinuous Galerkin; Stokes equations; incompressible flow; divergence-free; solenoidal; interior penalty method

1. INTRODUCTION

Research in finite element methods for the numerical solution of problems with incompressibility constraints has been very active in the past decades. These problems have a large number of applications ranging from the simulation of incompressible fluids to the solution of Maxwell's equations

*Correspondence to: A. Huerta, Departament de Matemàtica Aplicada III, E.T.S. Ingenieros de Caminos, Universitat Politècnica de Catalunya, Jordi Girona 1, E-08034 Barcelona, Spain.
†E-mail: antonio.huerta@upc.edu, www-lacan.upc.edu

Contract/grant sponsor: Ministerio de Educación y Ciencia; contract/grant numbers: BIA2007-66965, DPI2007-62395
Contract/grant sponsor: Generalitat de Catalunya AGAUR; contract/grant number: 2005SGR917

in electrodynamic problems. An interesting alternative is to use explicit divergence-free bases in order to solve problems with incompressibility. Crouzeix and Raviart [1] were the first to construct divergence-free elements in order to eliminate the pressure in the final equation. They used triangular conforming and non-conforming elements where the incompressibility condition was only approximately satisfied. Griffiths [2] proposed an element-level divergence-free basis for several finite element schemes on triangular and quadrilateral elements. Nevertheless, a major limitation of these techniques is that continuous and *weakly divergence-free* (or discretely divergence-free following the notation of [3]) approximation spaces are difficult to generalize for higher-order approximations.

More recently, several authors have focused their attention on *discontinuous Galerkin* (DG) formulations for computational fluid dynamics [4] and in particular for the Stokes equations [5–7]. The attractiveness of DG method is mainly due to its stability properties in convection-dominated problems, its efficiency for high-order computations, which allows *hp*-adaptive refinement, and local conservation properties. Moreover, in a DG framework, divergence-free high-order approximations can be easily defined: an element-by-element discontinuous approximation with a divergence-free polynomial base in each element can be considered with a straightforward definition for high-order approximations [5, 6]. Because of the important costs of DG methods, the reduction in degrees of freedom (both in velocity and pressure) induced by a divergence-free approach is very interesting from a computational point of view.

In the 1990s, Baker *et al*. [5] and Karakashian and Jureidini [8] developed and analyzed a DG formulation with a piecewise polynomial divergence-free velocity, with optimal error bounds. Nevertheless, this formulation has some limitations: it requires the use of continuous pressure approximations; only Dirichlet boundary conditions are considered (in fact, natural boundary conditions cannot be easily imposed), and different computational meshes (with different mesh sizes) must be considered for velocity and pressure to ensure stability.

A DG method for the Stokes equations with piecewise polynomial approximations was also proposed and analyzed by Toselli [7], but without the pointwise imposition of the divergence-free condition. This DG formulation shows better stability properties than continuous Galerkin approximations, and uniform divergence stability is proven when velocity is approximated one or two degrees higher than pressure. In fact, equal-order interpolation numerical results show no spurious pressure modes although no uniform stability properties are proven. Unfortunately, the bilinear form related with velocities is non-symmetric, and the DG advantages for the definition of piecewise solenoidal approximations are not exploited.

More recently, Cockburn and coworkers propose [6, 9, 10] a DG formulation with solenoidal piecewise polynomial approximations. It is derived from a *local discontinuous Galerkin* (LDG) rationale based on a mixed formulation of the problem (with velocity, vorticity and pressure), and with the introduction of numerical traces. The concept of *hybrid pressures* is also introduced, that is, pressures along the element sides. Pressures in the interior of the elements are computed as a post-process of the LDG solution. For analysis purposes, the LDG formulation is expressed in compact form in [9]. With the introduction of proper lifting operators, the vorticity is replaced in the LDG formulation leading to a velocity–pressure formulation with symmetric and coercive bilinear form for velocities.

In this work, a new DG formulation with piecewise solenoidal polynomial velocity and hybrid pressures is proposed. It is derived from an *interior penalty method* (IPM) rationale [11, 12], leading also to a symmetric and coercive bilinear form for velocities. As for the LDG formulation, the approximation space for the velocity field is decomposed in every element as direct sum of

DOI: 10.1002/fld

solenoidal and irrotational polynomial spaces. This also allows to split the IPM weak form into two uncoupled problems: the first one solves for velocity and hybrid pressure and the second one allows the evaluation of pressures in the interior of the elements. The resulting method has many points in common with the LDG formulation in *compact* form stated in [9]. Namely, both are formulated in terms of piecewise solenoidal velocities and hybrid pressures, the bilinear form is symmetric and positive definite, and the pressure in the interior of the elements is computed as a post-process of the solution. Nevertheless, different rationales are followed for the LDG and IPM methods, leading to completely different formulations. For instance, one of the most remarkable differences is that the IPM formulation proposed here does not involve lifting operators that induce an *approximate orthogonality* property in the LDG formulation [9].

The IPM weak problem is also reformulated as a minimization problem subject to the constraint of normal continuity of the velocity field. The solution of this optimization problem with the introduction of a non-consistent penalty leads to an alternative DG formulation for the computation of solenoidal velocities with no presence of pressure terms (i.e. solving a system with symmetric positive-definite matrix). Pressure can then be computed as a post-process of the velocity solution. This second IPM method exactly coincides with the DG method proposed in [13], where different alternatives for the approximation, based on the definition of a piecewise continuous stream function spaces, are also proposed and analyzed. In fact, it is worth noting the contributions in solid mechanics by Hansbo and co-workers [12, 14, 15], which have inspired several authors (see, for instance, [16] for the solution of the Navier–Stokes equations) and in particular this paper.

The contributions of this paper are presented as follows. The derivation of a new DG IPM formulation for the solution of Stokes problems, with Dirichlet and Neumann boundary conditions, is presented in detail in Section 3.1. The particularization of the IPM weak form with a splitting of the velocity space in solenoidal and irrotational parts is presented and analyzed in Section 3.2. In Section 3.3, the DG method initially proposed by Hansbo and Larson in [13] is presented with an alternative derivation. The implementation of Neumann boundary conditions is included in the formulation, and a methodology for the computation of pressures as a post-process of the velocity solution is proposed. Numerical tests demonstrate the applicability of both methodologies (IPM and IPM with non-consistent penalty) for the solution of the Stokes equations in Section 5. The selection of the penalization parameters in order to achieve optimal convergence rates is also studied. Finally, the IPM formulation is used for the simulation of a fluid flow through a porous medium.

2. THE STOKES PROBLEM

Let $\Omega \subset \mathbb{R}^{\mathtt{n_{sd}}}$ be an open bounded domain with piecewise linear boundary $\partial\Omega$ and $\mathtt{n_{sd}}$ the number of spatial dimensions. Suppose that Ω is partitioned in $\mathtt{n_{el}}$ disjoint subdomains Ω_i, which for example correspond to different materials, with also piecewise linear boundaries $\partial\Omega_i$ which define an internal interphase Γ; the following definitions and notations are used:

$$\overline{\Omega} = \bigcup_{i=1}^{\mathtt{n_{el}}} \overline{\Omega}_i, \quad \Omega_i \cap \Omega_j = \emptyset \quad \text{for } i \neq j$$

$$\widehat{\Omega} := \bigcup_{i=1}^{\mathtt{n_{el}}} \Omega_i \quad \text{and} \quad \Gamma := \bigcup_{\substack{i,j=1 \\ i \neq j}}^{\mathtt{n_{el}}} \overline{\Omega}_i \cap \overline{\Omega}_j = \left[\bigcup_{i=1}^{\mathtt{n_{el}}} \partial\Omega_i \right] \Big\backslash \partial\Omega$$

DOI: 10.1002/fld

The strong form of the homogeneous Stokes problem can be expressed as

$$-\nabla\cdot\boldsymbol{\sigma}=\mathbf{s} \quad \text{in } \widehat{\Omega} \tag{1a}$$

$$\nabla\cdot\mathbf{u}=0 \quad \text{in } \widehat{\Omega} \tag{1b}$$

$$\mathbf{u}=\mathbf{u}_{\mathrm{D}} \quad \text{on } \Gamma_{\mathrm{D}} \tag{1c}$$

$$\mathbf{n}\cdot\boldsymbol{\sigma}=\mathbf{t} \quad \text{on } \Gamma_{\mathrm{N}} \tag{1d}$$

$$[\![\mathbf{n}\otimes\mathbf{u}]\!]=\mathbf{0} \quad \text{on } \Gamma \tag{1e}$$

$$[\![\mathbf{n}\cdot\boldsymbol{\sigma}]\!]=\mathbf{0} \quad \text{on } \Gamma \tag{1f}$$

where $\partial\Omega=\overline{\Gamma}_{\mathrm{D}}\cup\overline{\Gamma}_{\mathrm{N}}$, $\Gamma_{\mathrm{D}}\cap\Gamma_{\mathrm{N}}=\emptyset$, $\mathbf{s}\in\mathcal{L}_2(\Omega)$ is a source term, $\boldsymbol{\sigma}$ is the ('dynamic' or 'density-scaled') Cauchy stress, which is related to velocity, $\mathbf{u}$, and pressure, p, by the linear Stokes' law

$$\boldsymbol{\sigma}=-p\,\mathbf{I}+2\nu\,\nabla^{\mathrm{s}}\mathbf{u} \tag{2}$$

with ν being the kinematic viscosity and $\nabla^{\mathrm{s}}=\frac{1}{2}(\nabla+\nabla^{\mathrm{T}})$.

The jump $[\![\cdot]\!]$ and the mean $\{\cdot\}$ operators are defined along the interface Γ using values from the elements to the left and right of the interface—say, Ω_i and Ω_j—and are also extended along the exterior boundary—only values in the interior of Ω are employed—namely

$$[\![\circledcirc]\!]=\begin{cases}\circledcirc_i+\circledcirc_j & \text{on } \Gamma\\ \circledcirc & \text{on } \partial\Omega\end{cases} \quad \text{and} \quad \{\circledcirc\}=\begin{cases}\kappa_i\circledcirc_i+\kappa_j\circledcirc_j & \text{on } \Gamma\\ \circledcirc & \text{on } \partial\Omega\end{cases}$$

Usually $\kappa_i=\kappa_j=\frac{1}{2}$ but, in general, these two scalars are only required to verify $\kappa_i+\kappa_j=1$, see, for instance, [12]. Note that definitions such as

$$\kappa_i=\begin{cases}1 & \text{if } \Omega_i \text{ is the largest}\\ 0 & \text{otherwise}\end{cases}$$

are also possible.

The major difference between the mean and the jump operator is that the latter always involves the normal to the interface or to the domain. Given two contiguous subdomains Ω_i and Ω_j, their exterior unit normals are denoted by, respectively, $\mathbf{n}_i$ and $\mathbf{n}_j$ (recall that $\mathbf{n}_i=-\mathbf{n}_j$) and along $\partial\Omega$ the exterior unit normal is denoted by $\mathbf{n}$. In what follows, the jump operator as defined previously will appear in these three cases:

$$[\![p\,\mathbf{n}]\!]=\begin{cases}p_i\,\mathbf{n}_i+p_j\,\mathbf{n}_j=\mathbf{n}_i(p_i-p_j) & \text{on } \Gamma\\ p\,\mathbf{n} & \text{on } \partial\Omega\end{cases} \quad \text{for scalars} \tag{3}$$

$$[\![\mathbf{n}\otimes\mathbf{v}]\!]=\begin{cases}\mathbf{n}_i\otimes\mathbf{v}_i+\mathbf{n}_j\otimes\mathbf{v}_j=\mathbf{n}_i\otimes(\mathbf{v}_i-\mathbf{v}_j) & \text{on } \Gamma\\ \mathbf{n}\otimes\mathbf{v} & \text{on } \partial\Omega\end{cases} \quad \text{or} \tag{4}$$

DOI: 10.1002/fld

$$[\![\mathbf{n}\cdot\mathbf{v}]\!]=\begin{cases}\mathbf{n}_i\cdot\mathbf{v}_i+\mathbf{n}_j\cdot\mathbf{v}_j=\mathbf{n}_i\cdot(\mathbf{v}_i-\mathbf{v}_j) & \text{on } \Gamma\\ \mathbf{n}\cdot\mathbf{v} & \text{on } \partial\Omega\end{cases} \quad \text{for vectors} \tag{5}$$

$$[\![\mathbf{n}\cdot\boldsymbol{\sigma}]\!]=\begin{cases}\mathbf{n}_i\cdot\boldsymbol{\sigma}_i+\mathbf{n}_j\cdot\boldsymbol{\sigma}_j=\mathbf{n}_i\cdot(\boldsymbol{\sigma}_i-\boldsymbol{\sigma}_j) & \text{on } \Gamma\\ \mathbf{n}\cdot\boldsymbol{\sigma} & \text{on } \partial\Omega\end{cases} \quad \text{for second-order tensors} \tag{6}$$

This definition of the jump was previously considered by other authors, see, for instance, [9], and presents two important advantages: first, it does not depend on a selection of a privileged normal sign on the edges in 2D or faces in 3D, and second, the input and output spaces for the operator coincide, that is, the jump of a scalar is a scalar, the jump of a vector is a vector, etc. Other definitions have been more popular in the past, but do not have these advantages. For instance, the jump at an edge Γ_E, shared by two elements Ω_i and Ω_j with $i<j$, could be defined as $[\![u]\!]=u_i-u_j$, see [5] among others. This definition involves the decision of a privileged normal sign; therefore, it may lead to weak definitions with a not desirable dependency on this choice. Another alternative definition would be $[\![u]\!]=u_i\mathbf{n}_i+u_j\mathbf{n}_j$ for scalar u, $[\![\mathbf{u}]\!]=\mathbf{u}_i\cdot\mathbf{n}_i+\mathbf{u}_j\cdot\mathbf{n}_j$ for vector $\mathbf{u}$, etc., see, for instance, [17]. It also does not require the selection of a normal sign, but it has different spaces for the input and the output: the jump of a scalar is a vector and the jump of a vector is a scalar. Moreover, the use of this definition camouflages the presence of the normal in the weak formulation: note that the evaluation of $[\![u]\!]$ involves the normal, although the normal does not explicitly appear in the weak form. Thus, in the authors' opinion the jump operator (3) leads to more easily readable weak formulations. Nevertheless, there is one situation where jump (3) or the definition used in [17] present some limitations: the computation of the jump of a scalar function with no presence of the normal vector. In the following, this computation appears only for terms of the form $(\mathbf{u}_i-\mathbf{u}_j,\mathbf{v}_i-\mathbf{v}_j)_{\Gamma_E}$, where Ω_i and Ω_j are the elements sharing the interface Γ_E, and the following identity is used:

$$(\mathbf{u}_i-\mathbf{u}_j,\mathbf{v}_i-\mathbf{v}_j)_{\Gamma_E}=([\![\mathbf{n}\otimes\mathbf{u}]\!],[\![\mathbf{n}\otimes\mathbf{v}]\!])_{\Gamma_E}$$

3. THE WEAK FORM OF THE STOKES PROBLEM

Following the usual methodology in the DG framework, the weak problem from the strong form defined by (1) is considered for each domain Ω_i. That is, find $\mathbf{u}_i\in[\mathcal{H}^1(\Omega_i)]^{\mathtt{n_{sd}}}$ and $p_i\in\mathcal{L}_2(\Omega_i)$ for $i=1,\ldots,\mathtt{n_{el}}$, which comply the boundary conditions (1c), (1e) and (1f) such that

$$a_{\Omega_i}(\mathbf{u}_i,\mathbf{v})+b_{\Omega_i}(\mathbf{v},p_i)-(\mathbf{n}_i\cdot\boldsymbol{\sigma}(\mathbf{u}_i,p_i),\mathbf{v})_{\partial\Omega_i\setminus\Gamma_N}+b_{\Omega_i}(\mathbf{u}_i,q)=l_{\Omega_i}(\mathbf{v})+(\mathbf{t},\mathbf{v})_{\partial\Omega_i\cap\Gamma_N} \tag{7}$$

for all $(\mathbf{v},q)\in[\mathcal{H}^1(\Omega_i)]^{\mathtt{n_{sd}}}\times\mathcal{L}_2(\Omega_i)$, where

$$a_{\Omega_i}(\mathbf{v},\mathbf{w})=\int_{\Omega_i}2\nu\,\nabla^{\mathrm{s}}\mathbf{v}:\nabla^{\mathrm{s}}\mathbf{w}\,\mathrm{d}\Omega,\quad b_{\Omega_i}(\mathbf{v},q)=-\int_{\Omega_i}q\,\nabla\cdot\mathbf{v}\,\mathrm{d}\Omega$$

$$l_{\Omega_i}(\mathbf{v})=\int_{\Omega_i}\mathbf{s}\mathbf{v}\,\mathrm{d}\Omega$$

DOI: 10.1002/fld

In the previous and the following equations, $(\cdot,\cdot)_\Upsilon$ denotes the $\mathcal{L}_2$ scalar product in any domain $\Upsilon\subset\Gamma\cup\partial\Omega$, that is

$$(p,q)_\Upsilon=\int_\Upsilon p\,q\,\mathrm{d}\Gamma \quad \text{for scalars}$$

$$(\mathbf{u},\mathbf{v})_\Upsilon=\int_\Upsilon \mathbf{u}\cdot\mathbf{v}\,\mathrm{d}\Gamma \quad \text{for vectors}$$

$$(\boldsymbol{\sigma},\boldsymbol{\tau})_\Upsilon=\int_\Upsilon \boldsymbol{\sigma}:\boldsymbol{\tau}\,\mathrm{d}\Gamma \quad \text{for second-order tensors}$$

In order to rewrite all $\mathtt{n_{el}}$ weak problems defined in (7) as one weak problem, let $\mathbf{u}$ be such that its restriction to Ω_i is $\mathbf{u}_i$, namely $\mathbf{u}\in[\mathcal{H}^1(\widehat{\Omega})]^{\mathtt{n_{sd}}}$ with

$$[\mathcal{H}^1(\widehat{\Omega})]^{\mathtt{n_{sd}}}:=\{\mathbf{v}\in[\mathcal{L}_2(\Omega)]^{\mathtt{n_{sd}}}\,|\,\mathbf{v}|_{\Omega_i}\in[\mathcal{H}^1(\Omega_i)]^{\mathtt{n_{sd}}}\ \text{for}\ i=1,\ldots,\mathtt{n_{el}}\}$$

and, similarly, $p\in\mathcal{L}_2(\Omega)$ is such that its restriction to Ω_i is p_i. Differential operators are assumed to act on these functions piecewise and not in the sense of distributions. Thus, adding equations (7) for $i=1,\ldots,\mathtt{n_{el}}$, the unique weak problem becomes: find $\mathbf{u}$ and p such that

$$a(\mathbf{u},\mathbf{v})+b(\mathbf{v},p)-\sum_{i=1}^{\mathtt{n_{el}}}(\mathbf{n}_i\cdot\boldsymbol{\sigma}(\mathbf{u}_i,p_i),\mathbf{v})_{\partial\Omega_i\setminus\Gamma_\mathrm{N}}+b(\mathbf{u},q)=l(\mathbf{v}) \tag{8}$$

for all test functions $\mathbf{v}\in[\mathcal{H}^1(\widehat{\Omega})]^{\mathtt{n_{sd}}}$ and $q\in\mathcal{L}_2(\Omega)$; where the bilinear forms are now integrated over the whole domain Ω, namely

$$a(\mathbf{v},\mathbf{w})=\int_\Omega 2\nu\,\boldsymbol{\nabla}^\mathrm{s}\mathbf{v}:\boldsymbol{\nabla}^\mathrm{s}\mathbf{w}\,\mathrm{d}\Omega,\quad b(\mathbf{v},q)=-\int_\Omega q\,\boldsymbol{\nabla}\cdot\mathbf{v}\,\mathrm{d}\Omega$$

and

$$l(\mathbf{v})=\int_\Omega \mathbf{s}\mathbf{v}\,\mathrm{d}\Omega+(\mathbf{t},\mathbf{v})_{\Gamma_\mathrm{N}}$$

For two contiguous subdomains, Ω_i and Ω_j, with a common boundary $\Gamma_\mathrm{e}\subset\Gamma$ it is easy to check that

$$\begin{aligned}&(\mathbf{n}_i\cdot\boldsymbol{\sigma}(\mathbf{u}_i,p_i),\mathbf{v}_i)_{\Gamma_\mathrm{e}}+(\mathbf{n}_j\cdot\boldsymbol{\sigma}(\mathbf{u}_j,p_j),\mathbf{v}_j)_{\Gamma_\mathrm{e}}\\&\quad=(\{\boldsymbol{\sigma}(\mathbf{u},p)\},[\![\mathbf{n}\otimes\mathbf{v}]\!])_{\Gamma_\mathrm{e}}+([\![\mathbf{n}\cdot\boldsymbol{\sigma}(\mathbf{u},p)]\!],\kappa_j\mathbf{v}_i+\kappa_i\mathbf{v}_j)_{\Gamma_\mathrm{e}}\end{aligned}$$

Moreover, the boundary condition (1f) simplifies the previous equation because the last term is zero. Thus, from the previous equation the weak form (8) can be rewritten as

$$a(\mathbf{u},\mathbf{v})+b(\mathbf{v},p)-(\{\boldsymbol{\sigma}(\mathbf{u},p)\},[\![\mathbf{n}\otimes\mathbf{v}]\!])_\Gamma-(\mathbf{n}\cdot\boldsymbol{\sigma}(\mathbf{u},p),\mathbf{v})_{\Gamma_\mathrm{D}}+b(\mathbf{u},q)=l(\mathbf{v})$$

This expression can be further simplified using the extension of the jump and mean operators on the exterior boundary, in particular, in this case along Γ_D, and the identity $\mathbf{n}\cdot\boldsymbol{\sigma}\cdot\mathbf{v}=\boldsymbol{\sigma}:(\mathbf{n}\otimes\mathbf{v})$. The weak problem equivalent to (1) becomes: find $\mathbf{u}\in[\mathcal{H}^1(\widehat{\Omega})]^{\mathtt{n_{sd}}}$ and $p\in\mathcal{L}_2(\Omega)$ subject to the boundary conditions defined by (1c) and (1e) such that

$$a(\mathbf{u},\mathbf{v})+b(\mathbf{v},p)-(\{\boldsymbol{\sigma}(\mathbf{u},p)\},[\![\mathbf{n}\otimes\mathbf{v}]\!])_{\Gamma\cup\Gamma_\mathrm{D}}+b(\mathbf{u},q)=l(\mathbf{v}) \tag{9}$$

for all test functions $\mathbf{v}\in[\mathcal{H}^1(\widehat{\Omega})]^{\mathtt{n_{sd}}}$ and $q\in\mathcal{L}_2(\Omega)$.

DOI: 10.1002/fld

3.1. The IPM formulation

Following the standard approach of IPM [11], the previous weak problem (9) is symmetrized and a new term is added to ensure a coercive bilinear form for the velocity. In this process, the boundary conditions (1c) and (1e)—not yet imposed—are used in order to maintain the consistency of the weak problem (i.e. the solution of (1) is the solution of the weak problem). The resulting IPM weak problem can then be expressed as: find $\mathbf{u}\in[\mathcal{H}^1(\widehat{\Omega})]^{\mathtt{n_{sd}}}$ and $p\in\mathcal{L}_2(\Omega)$ such that

$$a(\mathbf{u},\mathbf{v})+b(\mathbf{v},p)+b(\mathbf{u},q)-(\{\boldsymbol{\sigma}(\mathbf{u},p)\},[\![\mathbf{n}\otimes\mathbf{v}]\!])_{\Gamma\cup\Gamma_{\mathrm{D}}}-([\![\mathbf{n}\otimes\mathbf{u}]\!],\{\boldsymbol{\sigma}(\mathbf{v},q)\})_{\Gamma\cup\Gamma_{\mathrm{D}}}$$
$$+\gamma(l_{\mathrm{e}}^{-1}[\![\mathbf{n}\otimes\mathbf{u}]\!],[\![\mathbf{n}\otimes\mathbf{v}]\!])_{\Gamma\cup\Gamma_{\mathrm{D}}}=l(\mathbf{v})-(\mathbf{u}_{\mathrm{D}},\mathbf{n}\cdot\boldsymbol{\sigma}(\mathbf{v},q))_{\Gamma_{\mathrm{D}}}+\gamma(l_{\mathrm{e}}^{-1}\mathbf{u}_{\mathrm{D}},\mathbf{v})_{\Gamma_{\mathrm{D}}}$$

for all $\mathbf{v}\in[\mathcal{H}^1(\widehat{\Omega})]^{\mathtt{n_{sd}}}$ and $q\in\mathcal{L}_2(\Omega)$, where l_{e} is a measure of each interface Γ_{e} (edge in 2D, face in 3D) and γ is a scalar parameter, which must be *sufficiently* large (to ensure coercivity of the form $a_{\mathtt{IP}}(\cdot,\cdot)$ defined below, see Remark 1). Note that boundary conditions (1c) and (1e) are no longer explicitly mentioned because they are now imposed in weak form.

Using the constitutive law (2) in the previous equation, the weak problem, which presents a symmetric structure, can be expressed as: find $\mathbf{u}\in[\mathcal{H}^1(\widehat{\Omega})]^{\mathtt{n_{sd}}}$ and $p\in\mathcal{L}_2(\Omega)$ such that

$$\begin{aligned}&a_{\mathtt{IP}}(\mathbf{u},\mathbf{v})+b(\mathbf{v},p)+(\{p\},[\![\mathbf{n}\cdot\mathbf{v}]\!])_{\Gamma\cup\Gamma_{\mathrm{D}}}\\&\quad+b(\mathbf{u},q)+(\{q\},[\![\mathbf{n}\cdot\mathbf{u}]\!])_{\Gamma\cup\Gamma_{\mathrm{D}}}=l_{\mathtt{IP}}(\mathbf{v})+(q,\mathbf{n}\cdot\mathbf{u}_{\mathrm{D}})_{\Gamma_{\mathrm{D}}}\end{aligned}\tag{10}$$

for all $\mathbf{v}\in[\mathcal{H}^1(\widehat{\Omega})]^{\mathtt{n_{sd}}}$ and $q\in\mathcal{L}_2(\Omega)$, with

$$\begin{aligned}a_{\mathtt{IP}}(\mathbf{u},\mathbf{v}):=&\,a(\mathbf{u},\mathbf{v})-(2\nu\{\nabla^{\mathrm{s}}\mathbf{u}\},[\![\mathbf{n}\otimes\mathbf{v}]\!])_{\Gamma\cup\Gamma_{\mathrm{D}}}\\&-([\![\mathbf{n}\otimes\mathbf{u}]\!],2\nu\{\nabla^{\mathrm{s}}\mathbf{v}\})_{\Gamma\cup\Gamma_{\mathrm{D}}}+\gamma(l_{\mathrm{e}}^{-1}[\![\mathbf{n}\otimes\mathbf{u}]\!],[\![\mathbf{n}\otimes\mathbf{v}]\!])_{\Gamma\cup\Gamma_{\mathrm{D}}}\end{aligned}\tag{11a}$$

and

$$l_{\mathtt{IP}}(\mathbf{v}):=l(\mathbf{v})-(\mathbf{u}_{\mathrm{D}},2\nu\mathbf{n}\cdot\nabla^{\mathrm{s}}\mathbf{v})_{\Gamma_{\mathrm{D}}}+\gamma(l_{\mathrm{e}}^{-1}\mathbf{u}_{\mathrm{D}},\mathbf{v})_{\Gamma_{\mathrm{D}}}\tag{11b}$$

This weak form is close to the formulation proposed in [7] where stability is also studied. It clearly identifies pressure with the Lagrange multiplier that imposes both a weakly solenoidal field inside each element and a continuous normal component along Γ. However, the IPM provides a symmetric bilinear form for the velocity, see Equation (11a), whereas the formulation proposed in [7] does not.

An alternative IPM formulation that does not require the evaluation of the divergence of the velocity field can also be obtained from (10). The divergence term is replaced using the following identity valid for any $\mathbf{v}\in[\mathcal{H}^1(\widehat{\Omega})]^{\mathtt{n_{sd}}}$ and $q\in\mathcal{L}_2(\Omega)$:

$$b(\mathbf{v},q)+(\{q\},[\![\mathbf{n}\cdot\mathbf{v}]\!])_{\Gamma\cup\partial\Omega}=(\mathbf{v},\nabla q)_{\Omega}-([\![q\,\mathbf{n}]\!],\{\!\{\mathbf{v}\}\!\})_{\Gamma}$$

where the operator $\{\!\{\cdot\}\!\}$ is defined at any interior edge $\Gamma_{\mathrm{E}}=\Omega_i\cap\Omega_j$ as

$$\{\!\{\mathbf{v}\}\!\}=\kappa_j\mathbf{v}_i+\kappa_i\mathbf{v}_j$$

Using this identity and its particularization for $\mathbf{v}=\mathbf{u}$, the solution of the problem (which is continuous and verifies (1c)), i.e.

$$b(\mathbf{u},q)+(q,\mathbf{n}\cdot\mathbf{u})_{\Gamma_{\mathrm{N}}}=(\mathbf{u},\nabla q)_{\Omega}-(\mathbf{n}\cdot\mathbf{u}_{\mathrm{D}},q)_{\Gamma_{\mathrm{D}}}-([\![q\,\mathbf{n}]\!],\{\!\{\mathbf{u}\}\!\})_{\Gamma}$$

DOI: 10.1002/fld

the IPM weak formulation (10) can be expressed as: find $\mathbf{u}\in[\mathcal{H}^1(\widehat{\Omega})]^{\mathtt{n_{sd}}}$ and $p\in\mathcal{L}_2(\Omega)$ such that

$$a_{\mathtt{IP}}(\mathbf{u},\mathbf{v})+(\mathbf{v},\nabla p)_\Omega-(p,\mathbf{n}\cdot\mathbf{v})_{\Gamma_\mathrm{N}}-(\llbracket p\,\mathbf{n}\rrbracket,\{\!\{\mathbf{v}\}\!\})_\Gamma$$
$$+(\mathbf{u},\nabla q)_\Omega-(q,\mathbf{n}\cdot\mathbf{u})_{\Gamma_\mathrm{N}}-(\llbracket q\,\mathbf{n}\rrbracket,\{\!\{\mathbf{u}\}\!\})_\Gamma=l_{\mathtt{IP}}(\mathbf{v})+(\mathbf{n}\cdot\mathbf{u}_\mathrm{D},q)_{\Gamma_\mathrm{D}}$$

for all $\mathbf{v}\in[\mathcal{H}^1(\widehat{\Omega})]^{\mathtt{n_{sd}}}$ and $q\in\mathcal{L}_2(\Omega)$. The structure of this formulation suggests the use of continuous pressures to simplify the equation, removing the terms with the $\{\!\{\cdot\}\!\}$ operator. The resulting formulation is more closely related to the work presented in [5, 8], where the proposed bilinear form is also symmetric and with no presence of divergence terms. Nevertheless, the weak formulation proposed in [5, 8] has some limitations: as commented, it requires the use of continuous approximations for the pressure, it is developed only for Dirichlet boundary conditions and natural boundary conditions cannot be directly imposed, and different computational meshes (with different mesh size) must be considered for velocity and pressure to ensure stability.

In this paper, the IPM formulation (10) is preferred because discontinuous approximations for the pressure are considered and, more importantly, because this weak formulation can be further simplified using piecewise solenoidal approximations.

3.2. The IPM formulation with solenoidal space

It is well known that any function in $[\mathcal{H}^1(\Omega_i)]^{\mathtt{n_{sd}}}$ can be expressed as the sum of a solenoidal part and an irrotational one. Thus, the functional space for the velocity can be split into the direct sum: $[\mathcal{H}^1(\widehat{\Omega})]^{\mathtt{n_{sd}}}=\mathcal{S}\oplus\mathcal{I}$ where

$$\mathcal{S}:=\{\mathbf{v}\in[\mathcal{H}^1(\widehat{\Omega})]^{\mathtt{n_{sd}}}\,|\,\nabla\cdot\mathbf{v}|_{\Omega_i}=0\text{ for }i=1,\ldots,\mathtt{n_{el}}\}$$

$$\mathcal{I}\subset\{\mathbf{v}\in[\mathcal{H}^1(\widehat{\Omega})]^{\mathtt{n_{sd}}}\,|\,\nabla\times\mathbf{v}|_{\Omega_i}=\mathbf{0}\text{ for }i=1,\ldots,\mathtt{n_{el}}\}$$

Note also that $\mathbf{u}$, the solution of the original problem (1) and (10), belongs to $\mathcal{S}$. Under these circumstances, problem (10) can be split into two *uncoupled* problems, for test functions in $\mathcal{S}$ and $\mathcal{I}$, respectively.

First, *divergence-free* solution and test functions, $\mathbf{u},\mathbf{v}\in\mathcal{S}$, are considered in the IPM formulation (10), leading to a simplified IPM formulation with no divergence terms

$$a_{\mathtt{IP}}(\mathbf{u},\mathbf{v})+(\{p\},\llbracket\mathbf{n}\cdot\mathbf{v}\rrbracket)_{\Gamma\cup\Gamma_\mathrm{D}}+(\{q\},\llbracket\mathbf{n}\cdot\mathbf{u}\rrbracket)_{\Gamma\cup\Gamma_\mathrm{D}}=l_{\mathtt{IP}}(\mathbf{v})+(q,\mathbf{n}\cdot\mathbf{u}_\mathrm{D})_{\Gamma_\mathrm{D}}\tag{12}$$

for all $\mathbf{v}\in\mathcal{S}$ and $q\in\mathcal{L}_2(\Omega)$. This formulation is further simplified with the introduction of the space of the so-called *hybrid pressures*, that is

$$\mathcal{P}:=\{\hat{p}\,|\,\hat{p}:\Gamma\cup\Gamma_\mathrm{D}\longrightarrow\mathbb{R}\text{ and }\hat{p}=\llbracket\mathbf{n}\cdot\mathbf{v}\rrbracket\text{ for some }\mathbf{v}\in\mathcal{S}\}\tag{13}$$

see [6] for details.

Thus, the first problem for *divergence-free* velocities and *hybrid pressures* becomes: find $\mathbf{u}\in\mathcal{S}$ and $\hat{p}\in\mathcal{P}$ such that

$$\begin{aligned}a_{\mathtt{IP}}(\mathbf{u},\mathbf{v})+(\hat{p},\llbracket\mathbf{n}\cdot\mathbf{v}\rrbracket)_{\Gamma\cup\Gamma_\mathrm{D}}&=l_{\mathtt{IP}}(\mathbf{v})\quad\forall\mathbf{v}\in\mathcal{S}\\(\hat{q},\llbracket\mathbf{n}\cdot\mathbf{u}\rrbracket)_{\Gamma\cup\Gamma_\mathrm{D}}&=(\hat{q},\mathbf{n}\cdot\mathbf{u}_\mathrm{D})_{\Gamma_\mathrm{D}}\quad\forall\hat{q}\in\mathcal{P}\end{aligned}\tag{14a}$$

DOI: 10.1002/fld

The second problem, which requires the solution of the previous one, i.e. the velocity $\mathbf{u}$ and the hybrid pressure $\hat{p}$, determines the *interior pressure*: find $p \in \mathcal{L}_2(\widehat{\Omega})$

$$b(\mathbf{v}, p) = l_{\mathrm{IP}}(\mathbf{v}) - a_{\mathrm{IP}}(\mathbf{u}, \mathbf{v}) - (\hat{p}, [\![\mathbf{n}\cdot\mathbf{v}]\!])_{\Gamma\cup\Gamma_{\mathrm{D}}} \quad \forall \mathbf{v} \in \mathcal{T} \tag{14b}$$

Note that this second problem would allow an independent computation of the interior pressure in every domain Ω_i.

The IPM formulation with solenoidal and irrotational spaces proposed here has many points in common with the LDG formulation in *compact form* presented in [9]. Both consider piecewise polynomial approximations, see Section 4, and a splitting of the approximation space as a sum of solenoidal and irrotational parts, leading to two uncoupled problems: the first for velocities and hybrid pressures, and the second for the computation of pressures in the interior of the elements. Moreover, the bilinear form is symmetric, continuous and coercive in both formulations (see Remark 1). Nevertheless, the IPM and the LDG methods correspond to different formulations. In fact, none of the two methods can be expressed as a particular case of the other one. The LDG method is deduced from a mixed formulation of the Stokes problem with velocity, vorticity and pressure, and it is expressed in *compact form* using proper lifting operators to replace the vorticity. In fact, the presence of lifting operators in the weak form is an important difference with the IPM method, with consequences in the consistency of the formulation. The IPM formulation is a consistent formulation in the sense that the solution of the Stokes problem (1) is also a solution of the IPM weak form, whereas the LDG formulation only verifies an *approximate orthogonality* property, see [9] for details.

Remark 1

For γ large enough, the IPM bilinear form $a_{\mathrm{IP}}(\cdot,\cdot)$ defined in (11a) is continuous and coercive, that is

$$a_{\mathrm{IP}}(\mathbf{u}, \mathbf{v}) \leqslant |||\mathbf{u}|||\,|||\mathbf{v}||| \quad \forall \mathbf{v} \in \mathcal{S} \tag{15}$$

and

$$m|||\mathbf{v}||| \leqslant a_{\mathrm{IP}}(\mathbf{v}, \mathbf{v}) \quad \forall \mathbf{v} \in \mathcal{S} \tag{16}$$

for some constant $m>0$ independent of the mesh size h, where

$$|||\mathbf{v}|||^2 = \|\nabla^{\mathrm{s}}\mathbf{v}\|_{\Omega}^2 + \|h^{1/2}\mathbf{n}\cdot\{\nabla^{\mathrm{s}}\mathbf{v}\}\|_{\Gamma\cup\Gamma_{\mathrm{D}}}^2 + \|h^{-1/2}[\![\mathbf{n}\otimes\mathbf{v}]\!]\|_{\Gamma\cup\Gamma_{\mathrm{D}}}^2 \tag{17}$$

and the $\mathcal{L}^2$ norms are defined as

$$\|\mathbf{f}\|_{\Omega}^2 = \sum_i \int_{\Omega_i} \mathbf{f}:\mathbf{f}\,\mathrm{d}\Omega, \quad \|f\|_{\Gamma\cup\Gamma_{\mathrm{D}}}^2 = (f, f)_{\Gamma\cup\Gamma_{\mathrm{D}}} \tag{18}$$

These properties can be proved following standard arguments, see [13, 14] for details.

3.3. IPM formulation with penalization of the discontinuity

The IPM formulation with solenoidal spaces presented in the previous section, see Equation (14a), allows a computation of the velocity solution involving the pressure only in the boundary of the domains Ω_i, i.e. the hybrid pressure. The aim of this section is more ambitious: to obtain a completely decoupled formulation allowing the computation of the solenoidal velocity, but with

DOI: 10.1002/fld

no presence of pressures at all. As proposed in [13], the introduction of a new penalty in the weak formulation achieves this purpose. However, the price of a totally decoupled velocity–pressure formulation is the loss of consistency, which provokes the ill-conditioning typical for non-consistent penalty formulations.

The DG formulation initially proposed and analyzed in [13] is deduced next from an alternative rationale, based on the IPM formulation (14a) and the introduction of a non-consistent penalty. The IPM formulation with solenoidal velocities (14a) can be rewritten as a saddle-point problem, namely

$$(\mathbf{u}, \hat{p}) = \arg \min_{\mathbf{v} \in \mathcal{S}} \max_{\hat{q} \in \mathcal{P}} \tfrac{1}{2} a_{\mathtt{IP}}(\mathbf{v}, \mathbf{v}) - l_{\mathtt{IP}}(\mathbf{v}) + (\hat{q}, [\![\mathbf{n} \cdot \mathbf{v}]\!])_{\Gamma \cup \Gamma_{\mathrm{D}}} - (\hat{q}, \mathbf{n} \cdot \mathbf{u}_{\mathrm{D}})_{\Gamma_{\mathrm{D}}} \tag{19}$$

or, equivalently, as a minimization problem subject to normal continuity constraints,

$$\mathbf{u} = \arg \min_{\substack{\mathbf{v} \in \mathcal{S} \\ \text{s.t.} [\![\mathbf{n} \cdot \mathbf{v}]\!] = 0 \text{ on } \Gamma \\ \mathbf{n} \cdot \mathbf{v} = \mathbf{n} \cdot \mathbf{u}_{\mathrm{D}} \text{ on } \Gamma_{\mathrm{D}}}} \tfrac{1}{2} a_{\mathtt{IP}}(\mathbf{v}, \mathbf{v}) - l_{\mathtt{IP}}(\mathbf{v}) \tag{20}$$

Note that the terms with pressures are canceled, thanks to the imposed continuity constraints. As usual in constrained minimization problems, the previous optimization problem can be solved using a *non-consistent penalty*, see, for instance, [18]. The corresponding minimization problem with penalty is

$$\mathbf{u} = \arg \min_{\mathbf{v} \in \mathcal{S}} \tfrac{1}{2} a_{\mathtt{IP}}(\mathbf{v}, \mathbf{v}) - l_{\mathtt{IP}}(\mathbf{v}) + \beta [([\![\mathbf{n} \cdot \mathbf{v}]\!], [\![\mathbf{n} \cdot \mathbf{v}]\!])_{\Gamma} - (\mathbf{n} \cdot (\mathbf{u}_{\mathrm{D}} - \mathbf{v}), \mathbf{n} \cdot (\mathbf{u}_{\mathrm{D}} - \mathbf{v}))_{\Gamma_{\mathrm{D}}}]$$

where β is a scalar penalty to be chosen. The solution of this optimization problem is the solution of the following IPM weak formulation with penalty: find $\mathbf{u}_\beta \in \mathcal{S}$ such that

$$a_{\mathtt{IP}}(\mathbf{u}_\beta, \mathbf{v}) + \beta([\![\mathbf{n} \cdot \mathbf{u}_\beta]\!], [\![\mathbf{n} \cdot \mathbf{v}]\!])_{\Gamma \cup \Gamma_{\mathrm{D}}} = l_{\mathtt{IP}}(\mathbf{v}) + \beta(\mathbf{n} \cdot \mathbf{v}, \mathbf{n} \cdot \mathbf{u}_{\mathrm{D}})_{\Gamma_{\mathrm{D}}} \tag{21}$$

for all $\mathbf{v} \in \mathcal{S}$. In the following, we refer to this weak formulation as *interior penalty method with penalty* (IPMP) in front of the IPM formulation described in (14).

Once the velocity is obtained, pressure can be computed as a post-process with two steps. First, an approximation of the hybrid pressure can be obtained introducing the solution of (21) in (14a), namely

$$\hat{p}_\beta = \begin{cases} \beta [\![\mathbf{n} \cdot \mathbf{u}_\beta]\!] & \text{on } \Gamma \\ \beta \mathbf{n} \cdot [\mathbf{u}_\beta - \mathbf{u}_{\mathrm{D}}] & \text{on } \Gamma_{\mathrm{D}} \end{cases}$$

Then, with $\mathbf{u}_\beta$ and $\hat{p}_\beta$ the interior pressure can be determined as the solution of (14b).

It is important to remark that the IPMP formulation (21) involves two different penalties with important differences. The first one is inherited from the IPM formulation, i.e. γ / l_{e} in the bilinear form $a_{\mathtt{IP}}(\cdot, \cdot)$ defined in (11a). It is a consistent penalty in the sense that the solution of the original problem (1) is the solution of the IPM formulation (14a); therefore, as usual in IPM formulations, in practice moderate values of the constant parameter γ provide accurate and optimally convergent results. This is not the case for the second penalty. The penalty β in the IPMP formulation (21) is a non-consistent penalty: the solution of the IPMP formulation verifies the continuity of the normal component of the velocity and the Dirichlet boundary conditions only in the limit, for β going to infinity. This lack of consistency is the origin of the usual drawbacks of penalty

DOI: 10.1002/fld

techniques: the tuning of the penalty parameter affects the accuracy of the solution and, in practice, too large values of β are needed, leading to ill-conditioned systems of equations. In fact, as proved in [18] in the context of boundary conditions, and as it is seen in the numerical examples, the penalty parameter β has to be of order h^{-k} in order to keep the optimal $\mathcal{H}^1$ convergence rate, with h the element size and k the degree of the approximation.

It is worth noting that an alternative and consistent methodology for the solution of the constrained minimization problem (20) would be the introduction of a Lagrange multiplier. That is,

$$(\mathbf{u},\lambda)=\arg\min_{\mathbf{v}\in\mathcal{S}}\max_{\lambda\in\Lambda}\tfrac{1}{2}a_{\mathtt{IP}}(\mathbf{v},\mathbf{v})-l_{\mathtt{IP}}(\mathbf{v})+(\lambda,[\![\mathbf{n}\cdot\mathbf{v}]\!])_{\Gamma}-(\lambda,\mathbf{n}\cdot(\mathbf{v}-\mathbf{u}_{\mathrm{D}}))_{\Gamma_{\mathrm{D}}}$$

where λ is the Lagrange multiplier defined at $\Gamma\cup\Gamma_{\mathrm{D}}$. This formulation corresponds exactly to (19), or equivalently to the IPM formulation (14a), demonstrating that the hybrid pressure plays the role of a Lagrange multiplier to impose the continuity of the normal velocity.

4. FINITE-DIMENSIONAL SPACES

In practice, approximations to the exact solution are obtained using finite-dimensional spaces. In particular, standard finite-dimensional polynomial spaces may be introduced in each element (standard DG) for all the previously defined weak problems, namely

$$\mathcal{V}^h:=\{\mathbf{v}\in[\mathcal{H}^1(\widehat{\Omega})]^{\mathtt{n_{sd}}}\,|\,\mathbf{v}|_{\Omega_i}\in[\mathbb{P}^k(\Omega_i)]^{\mathtt{n_{sd}}}\ \text{for}\ i=1,\ldots,\mathtt{n_{el}}\}$$

and

$$\mathcal{Q}^h:=\{p\in\mathcal{L}_2(\Omega)\,|\,p|_{\Omega_i}\in\mathbb{P}^{k-1}(\Omega_i)\ \text{for}\ i=1,\ldots,\mathtt{n_{el}}\}$$

where $\mathbb{P}^m$ denotes the space of complete polynomials of degree less than or equal to m. The finite counterparts of $\mathcal{S}$ and $\mathcal{I}$ are

$$\mathcal{S}^h=\{\mathbf{v}\in[\mathcal{H}^1(\widehat{\Omega})]^{\mathtt{n_{sd}}}\,|\,\mathbf{v}|_{\Omega_i}\in[\mathbb{P}^k(\Omega_i)]^{\mathtt{n_{sd}}},\quad \nabla\cdot\mathbf{v}|_{\Omega_i}=0\ \text{for}\ i=1,\ldots,\mathtt{n_{el}}\}$$

$$\mathcal{I}^h\subset\{\mathbf{v}\in[\mathcal{H}^1(\widehat{\Omega})]^{\mathtt{n_{sd}}}\,|\,\mathbf{v}|_{\Omega_i}\in[\mathbb{P}^k(\Omega_i)]^{\mathtt{n_{sd}}},\quad \nabla\times\mathbf{v}|_{\Omega_i}=\mathbf{0}\ \text{for}\ i=1,\ldots,\mathtt{n_{el}}\}$$

such that $\mathcal{I}^h\subset\mathcal{I}$. Note that the following relations and inclusions are verified: $\mathcal{V}^h=\mathcal{S}^h\oplus\mathcal{I}^h$, $\mathcal{V}^h\subset[\mathcal{H}^1(\widehat{\Omega})]^{\mathtt{n_{sd}}}$, $\mathcal{Q}^h\subset\mathcal{L}_2(\Omega)$ and $\mathcal{S}^h\subset\mathcal{S}$. The finite-dimensional subspace associated with the hybrid pressures, $\mathcal{P}^h\subset\mathcal{P}$, can be defined directly from (13) restricting velocities to $\mathcal{S}^h$. In fact, Reference [6] also demonstrates that $\mathcal{P}^h$ corresponds to piecewise polynomial pressures in the element edges in 2D or faces in 3D.

It is worth noting that the definition of the solenoidal and irrotational polynomial bases to be used at each element is an easy task. For instance, a solenoidal base in a 2D triangle for an approximation of degree $k=2$ is

$$\mathcal{S}^h=\left\langle\begin{pmatrix}1\\0\end{pmatrix},\begin{pmatrix}0\\1\end{pmatrix},\begin{pmatrix}0\\x\end{pmatrix},\begin{pmatrix}x\\-y\end{pmatrix},\begin{pmatrix}y\\0\end{pmatrix},\begin{pmatrix}0\\x^2\end{pmatrix},\begin{pmatrix}2xy\\-y^2\end{pmatrix},\begin{pmatrix}x^2\\-2xy\end{pmatrix},\begin{pmatrix}y^2\\0\end{pmatrix}\right\rangle$$

DOI: 10.1002/fld

The use of this polynomial basis defined with Cartesian coordinates was also proposed in [6]. An irrotational base for $k=2$ is

$$\mathcal{I}^h = \left\langle \begin{pmatrix} x \\ 0 \end{pmatrix}, \begin{pmatrix} x^2 \\ 0 \end{pmatrix}, \begin{pmatrix} 0 \\ y^2 \end{pmatrix} \right\rangle$$

In the numerical examples, to avoid ill-conditioning of the elemental matrices, all polynomials p of the base are centered and scaled at each element as $p((\mathbf{x}-\mathbf{c}_\mathrm{e})/h_\mathrm{e})$, where $\mathbf{c}_\mathrm{e}$ and h_e denote the center and the size of the element, respectively.

Remark 2
With these polynomial spaces, the numerical solution $\mathbf{u}_h$ of the IPM method presented in Section 3.2 verifies the following error bound:

$$|||\mathbf{u}-\mathbf{u}_h||| \leqslant K h^\alpha |\mathbf{u}|_{\mathcal{H}^{1+\alpha}(\Omega)} \tag{22}$$

for $\mathbf{u} \in \mathcal{H}^{1+\alpha}(\Omega)$, $1 \leqslant \alpha \leqslant k$ and some constant K. This result can be proved using the continuity and coercivity of the bilinear form, see Remark 1 in Section 3.2. Following [9], the space of piecewise divergence-free polynomial functions with continuity constraints for the normal velocity is considered

$$Z_h(\mathbf{u}_\mathrm{D}) = \{\mathbf{v} \in \mathcal{S}^h : (q, [\![\mathbf{n}\cdot\mathbf{v}]\!])_{\Gamma\cup\Gamma_\mathrm{D}} = (q, \mathbf{n}\cdot\mathbf{u}_\mathrm{D})_{\Gamma_\mathrm{D}} \ \forall q \in \mathcal{P}^h\} \subset \mathcal{S}^h$$

Note that although the LDG formulation analyzed in [9] verifies an approximate orthogonality with a residual $\mathcal{R}_h \neq 0$ (due to the introduction of the lifting operators), the IPM formulation is consistent and therefore the residual is in this case $\mathcal{R}_h = 0$. Thus, the particularization of the error bound stated in [9] is

$$|||\mathbf{u}-\mathbf{u}_h||| \leqslant (1+m) \inf_{\mathbf{v}\in Z_h(\mathbf{u}_\mathrm{D})} |||\mathbf{u}-\mathbf{v}|||$$

where m is the coercivity constant, see Remark 1. The error bound (22) is obtained considering the projection into the BDM_0 space (Brezzi–Douglas–Marini space of full polynomial approximations with normal continuity and zero elementwise divergence, see [19] for details), that is $\mathbf{v} = \pi^{\mathrm{BDM}}\mathbf{u}$. Note that $\mathrm{BDM}_0 \subset Z_h(\mathbf{u}_\mathrm{D})$, thus using the bound in [13] for the $|||\cdot|||$ norm, i.e.

$$|||\mathbf{u}-\pi^{\mathrm{BDM}}\mathbf{u}||| \leqslant C h^\alpha |u|_{\mathcal{H}^{1+\alpha}(\Omega)}$$

with some constant C, bound (22) is proved.

Remark 3
The convergence of the IPMP formulation, developed in Section 3.3, is analyzed in detail in [13] for different approximation spaces. For velocity approximation spaces including the BDM_0 space, the error bound is

$$|||\mathbf{u}-\mathbf{u}_h||| \leqslant C(h^\alpha |\mathbf{u}|_{\mathcal{H}^{1+\alpha}(\Omega)} + h\|p\|_{\mathcal{H}^1(\Omega)})$$

for some constant C, and $\mathbf{u} \in \mathcal{H}^{1+\alpha}(\Omega)$, with $1 \leqslant \alpha \leqslant k$.

DOI: 10.1002/fld

5. NUMERICAL EXAMPLES

To demonstrate the applicability of the two proposed methods, some numerical examples are shown in this section. In all tests, an approximation of order k for velocity and $k-1$ for pressure is considered. Triangular meshes are obtained by splitting a regular $n \times m$ Cartesian grid into a total of $2n \times m$ triangles for a rectangular domain, or $2n^2$ triangles for a square domain, giving uniform element size of $h = 1/n$.

5.1. Driven cavity example

A standard benchmark test for incompressible flows is considered first. A plane flow of an isothermal fluid in a lid-driven cavity is modeled in a 2D square domain $\Omega =]0, 1[\times]0, 1[$, with zero body force and one moving wall. A velocity $\mathbf{u} = (1, 0)^{\mathrm{T}}$ is imposed on the exterior upper boundary $\{y = 1\}$, and a zero velocity $\mathbf{u} = (0, 0)^{\mathrm{T}}$ is enforced on the other three sides.

Figure 1 shows the velocity vectors and the pressure fields of the flow for, respectively, the IPM and the IPMP formulations, with a discretization of order $k = 2$ for velocity and order $k - 1 = 1$ for pressure. Results fit to the expected solution; note that around the two upper corners the pressure

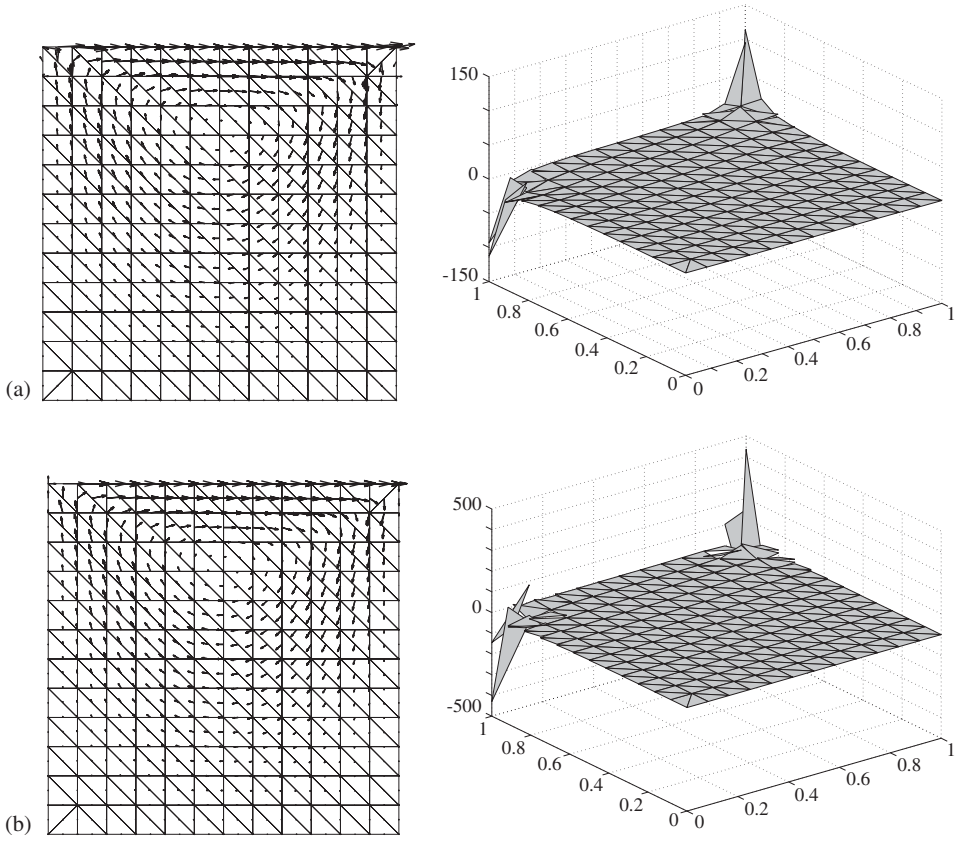

Figure 1. Driven cavity IPM (top) and IPMP (bottom) results for second-order velocity and linear pressure: (a) IPM velocity and pressure with $\gamma = 10$ and (b) IPMP velocity and pressure with $\gamma = 10$ and $\beta = 1000/h^2$.

DOI: 10.1002/fld

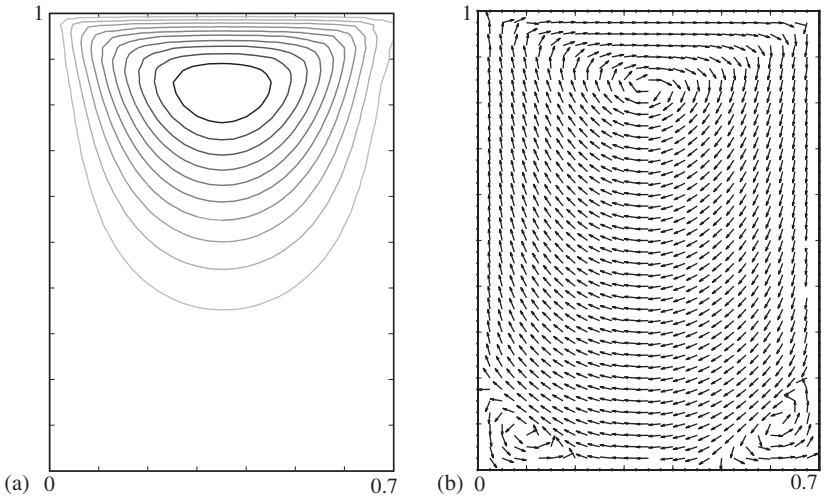

Figure 2. IPM velocity solution with 140 elements, fourth-order velocity approximation and $\gamma=20$: (a) velocity streamlines and (b) scaled velocity.

takes not bounded values because of the discontinuity of the velocity. Recall that the computation of velocity and pressure is completely decoupled using the IPMP, with the corresponding saving in computational cost. Nevertheless, it is worth noting that the use of the non-consistent parameter $\beta=1000/h^2$ in the IPMP considerably increases the condition number of the matrix. Moreover, although similar accuracy is obtained for the velocity field, for the same discretization the IPM provides more accurate and stable results for the pressure field than the IPMP.

The same example is now used for a rectangular cavity $\Omega=]0,0.7[\times]0,1[$. Figure 2 illustrates the results obtained using the IPM formulation. The results present the expected behavior. Contra-rotating vortices are created in the corners opposite to the moving wall. In the representation of the velocity vectors, only the direction of the flow is represented, all the arrows have the same length so that the contra-rotating vortices can be noticed. The velocity streamlines are represented as well to prove that the contra-rotating vortices have small amplitude compared with the main vortex movement.

5.2. Analytical example

An example with analytical solution is now considered to study the accuracy and convergence properties of the proposed methodologies. The Stokes equations are solved in a 2D square domain $\Omega=]0,1[\times]0,1[$ with Dirichlet boundary conditions on three edges, and a Neumann boundary condition on the fourth edge $\{y=0\}$. A body force

$$\mathbf{f}=\begin{pmatrix} 12(1-2y)x^4+24(-1+2y)x^3+12(-4y+6y^2-4y^3+1)x^2 \\ +(-2+24(y-3y^2+2y^3))x+1-4y+12y^2-8y^3 \\ 8(1-6y+6y^2)x^3+12(-1+6y-6y^2)x^2 \\ +(4+48(y^2-y^3)+24(y^4-y))x-12y^2+24y^3-12y^4 \end{pmatrix}$$

DOI: 10.1002/fld

is imposed in order to have the polynomial exact solution

$$\mathbf{u}=\begin{pmatrix} x^2(1-x)^2(2y-6y^2+4y^3) \\ -y^2(1-y)^2(2x-6x^2+4x^3) \end{pmatrix}$$

$$p=x(1-x)$$

5.2.1. IPM analysis. The behavior of the IPM formulation is first studied. In all examples, the consistent penalty term γ is set to a sufficiently large value to ensure the coercivity of the form $a_{\mathrm{IP}}(,)$, see Equation (11a). In practice, moderate values of this penalty term are required.

Figure 3 shows the IPM solution obtained with an approximation of degree $k=2$ and 4 for the velocity field ($k-1$ for pressure), with the same number of degrees of freedom. One of the advantages of the proposed method is that the order of the approximation can be easily increased, with a straightforward modification of the definition of the solenoidal and irrotational bases, see Section 4. As expected, the higher-order approximation provides more accurate results, with smaller discontinuities in the solution, especially for the pressure field.

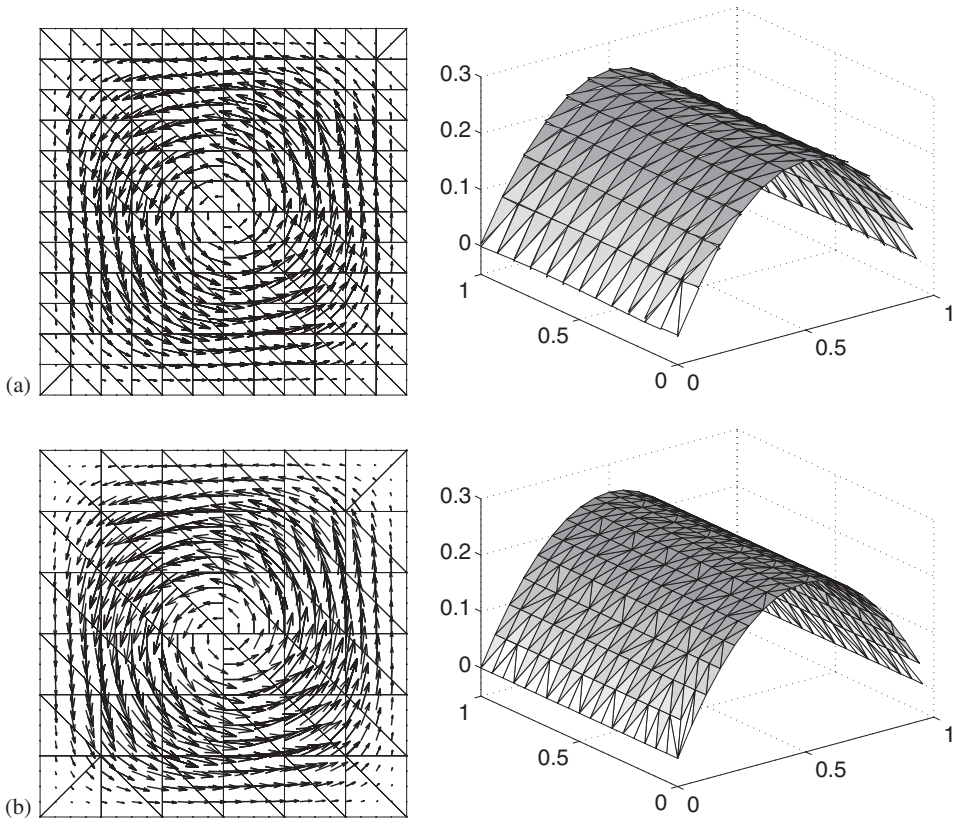

Figure 3. IPM velocity vectors and pressure field for two different orders of approximation: (a) velocity and pressure with degree $k=2$, 256 elements and $\gamma=10$ and (b) velocity and pressure with degree $k=4$, 72 elements and $\gamma=40$.

DOI: 10.1002/fld

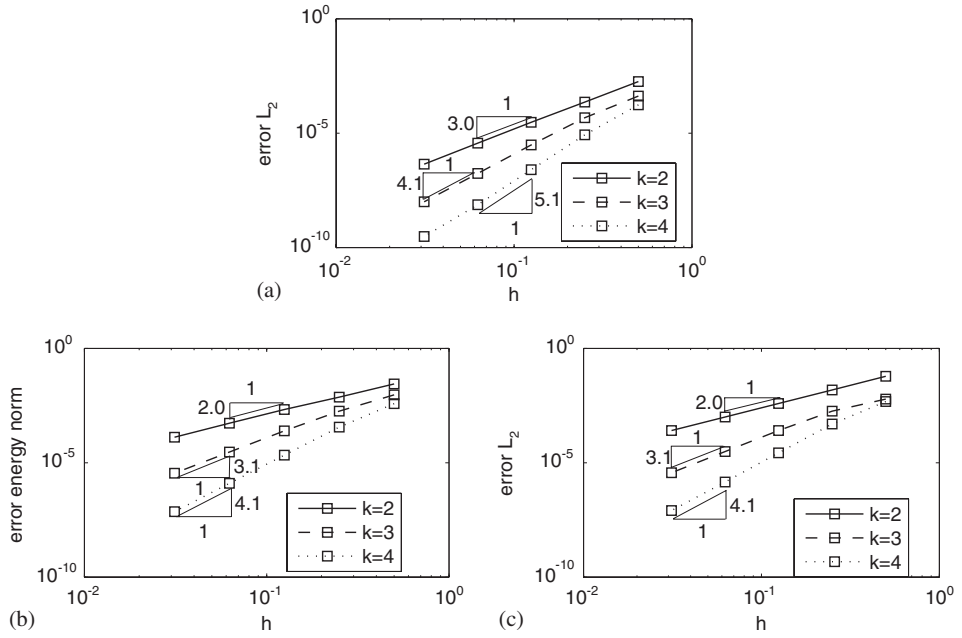

Figure 4. IPM convergence results with velocity approximation of degree $k=2,3,4$ and pressure interpolation of degree $k-1$, with $\gamma=10,20,40$, respectively: (a) velocity $\mathcal{L}_2$ error; (b) velocity energy error; and (c) pressure $\mathcal{L}_2$ error.

These results also confirm that the condition proposed in [20] to ensure the coercivity of the bilinear form is also valid for the IPM formulation with solenoidal approximation proposed here. The explicit formula used for the computation of the consistent penalty parameter is

$$\gamma \approx a\nu k^2 \tag{23}$$

where a is a positive constant and k is the degree of the velocity approximation.

Figure 4 shows the convergence under h-refinement, for different orders of approximation of the velocity and pressure. Optimal convergence is obtained using polynomials of degree k to approximate the velocity and $k-1$ for pressure; that is, convergence of order $k+1$ for the velocity $\mathcal{L}_2$ norm, order k for the energy norm, and order of k for the pressure $\mathcal{L}_2$ norm. As usual in consistent IPM formulations, a penalty term of order h^{-1}, i.e constant γ, suffices to maintain the optimal convergence rates for any order of approximation. As seen in the following examples, this is not the case for the non-consistent penalty β in the IPMP formulation.

5.2.2. IPMP analysis. The IPMP behavior is tested with the same analytical example. First, the influence of the non-consistent penalty term β is analyzed. The IPMP velocity for an approximation of degree $k=3$, with two different values of the non-consistent penalty parameter β is depicted in Figure 5. As previously commented, rather large values of β are necessary to ensure moderate discontinuities of the normal velocity.

Figure 6 shows the results for two different orders of approximation. Again, higher-order approximations provide more accurate results for the same number of degrees of freedom, especially for the pressure field that presents much better continuity.

DOI: 10.1002/fld

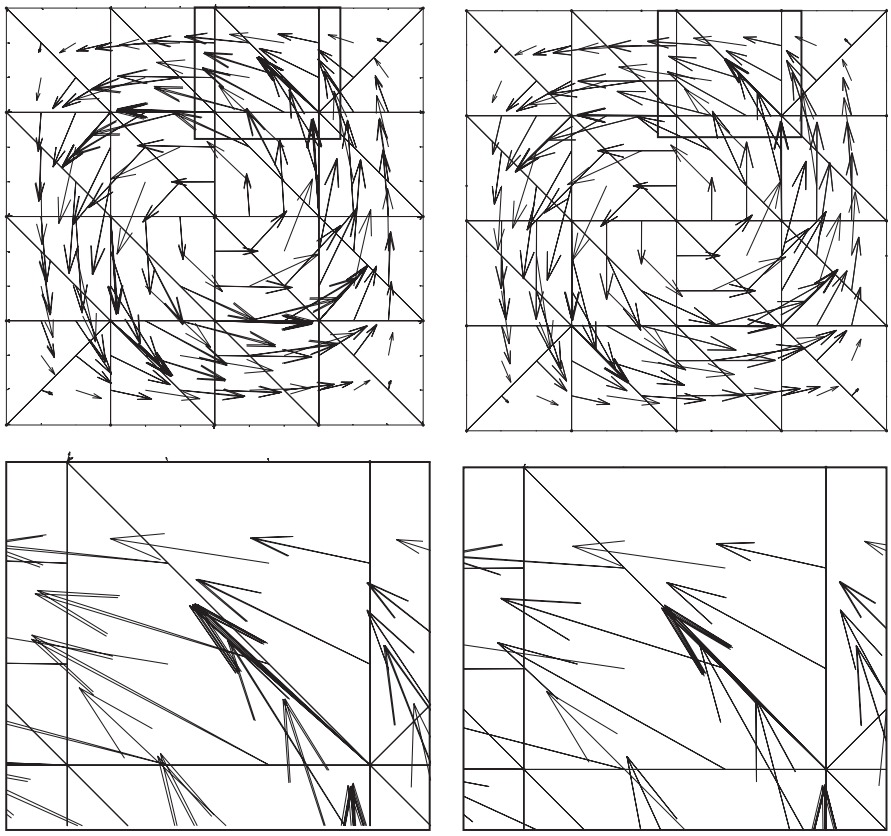

Figure 5. IPMP velocity solution (top) and detail (bottom) for two different values of the penalty term β with a third-order velocity approximation and 32 elements: (a) $\beta = 5/h^4$ and (b) $\beta = 2000/h^4$.

Figure 7 shows the evolution of the error under h-refinement for different orders of approximation of the velocity and pressure, using the IPMP formulation. As usual for non-consistent penalty formulations [18], almost optimal converge rates are achieved using a penalty term of order h^{-k}. As previously noted, the need of large values for the penalty β is the main drawback of the IPMP formulation, because of the ill-conditioning of the matrices in the solution with fine meshes. For instance, for a computation with fourth-order interpolation of the velocity and 72 elements, the dimension of the system of equations to be solved for the IPM (with velocity and hybrid pressures) is 1350, whereas for the IPMP (with only velocities) the dimension is 1308. The reduction in the number of degrees of freedom is thus appreciable for the IPMP case, but in return the condition number of the matrix is higher for the IPMP formulation: around 5×10^9 for the IPMP with $\gamma = 40$, and 4×10^7 for the IPM with the same γ and $\beta = 4000/h^4$. Moreover, under h-refinement or p-refinement, the condition number grows faster for the IPMP than for the IPM.

To further compare the IPM and IPMP formulations, Figure 8 plots the errors obtained for velocity and pressure with both methods. Similar accuracy is obtained for the velocity field and the main differences are present in the pressure results. Although both methods provide optimal convergence rates, more accurate results for pressure are obtained with a coupled computation

DOI: 10.1002/fld

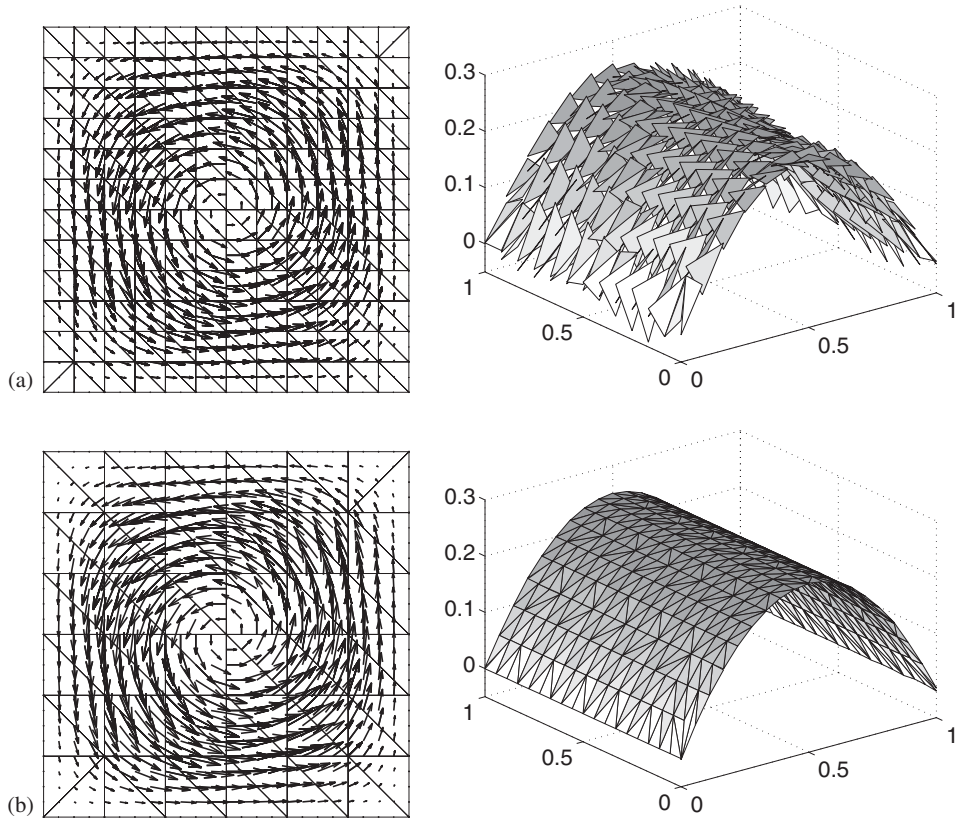

Figure 6. IPMP velocity vectors and pressure field for different orders of approximation: (a) velocity and pressure with degree $k=2$, 256 elements, $\gamma=10$ and $\beta=1000/h^2$ and (b) velocity and pressure with degree $k=4$, 72 elements, $\gamma=40$ and $\beta=4000/h^4$.

of hybrid pressures and velocities, using the IPM formulation. As commented in the previous example in Section 5.2, the computation of pressures as a post-process of velocities with the IPMP represents a saving in computational cost, preserving the accuracy in the velocity field, but with a slightly worse solution for pressure.

5.3. Flow in an idealized porous medium

A fluid in an idealized porous medium is subject to a friction force proportional to the fluid velocity $\mathbf{u}$. This kind of problem is derived from the Stokes equations and it follows Darcy's law. It is valid for slow, viscous flow, such as groundwater flows. The problem to be solved is

$$\begin{aligned} -\nabla\cdot\boldsymbol{\sigma} &= -\alpha\mathbf{u} && \text{in } \widehat{\Omega} \\ \nabla\cdot\mathbf{u} &= 0 && \text{in } \widehat{\Omega} \\ \mathbf{u} &= \mathbf{u}_{\mathrm{D}} && \text{on } \Gamma_{\mathrm{D}} \\ [\![\mathbf{n}\otimes\mathbf{u}]\!] &= \mathbf{0} && \text{on } \Gamma \\ [\![\mathbf{n}\cdot\boldsymbol{\sigma}]\!] &= \mathbf{0} && \text{on } \Gamma \end{aligned}$$

DOI: 10.1002/fld

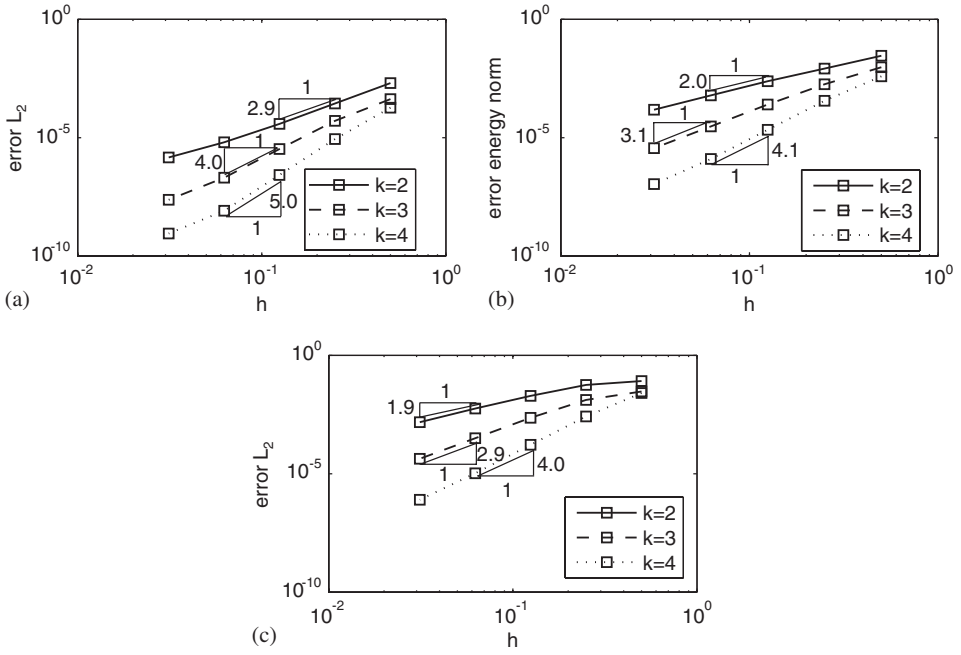

Figure 7. IPMP convergence results with degree $k=2,3,4$ for velocity and degree $k-1$ for pressure, with $\gamma=10,20,40$ and $\beta=1000/h^2, 2000/h^3, 4000/h^4$, respectively: (a) velocity $\mathcal{L}_2$ error; (b) velocity energy error; and (c) pressure $\mathcal{L}_2$ error.

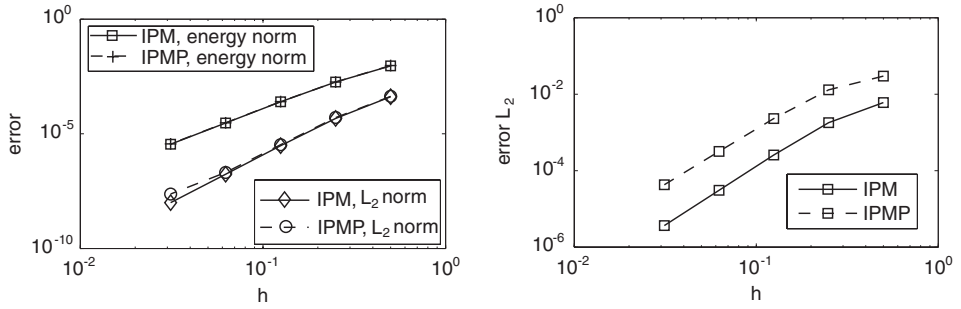

Figure 8. Comparison of the errors obtained with IPM and IPMP, for a cubic approximation of the velocity (left) and a quadratic interpolation of the pressure (right), with $\gamma=20$ and $\beta=2000/h^3$.

where α is the inverse of the local permeability of the medium ($\alpha=0$ for an empty medium and $\alpha=+\infty$ for a solid wall), see [21].

These equations are solved in the computational domain shown in Figure 9, consisting of a long straight channel of height l and length $L=10l$. The porous domain is limited to the central part of length $5l$. The Dirichlet boundary conditions prescribe a parabolic velocity profile at the inlet and at the outlet, and a no-slip condition for the fluid on the channel side. The porous domain is filled

DOI: 10.1002/fld

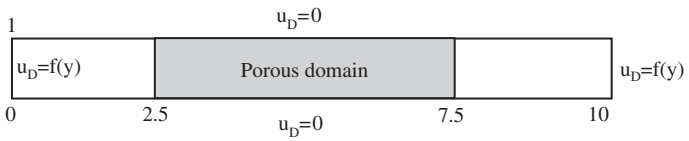

Figure 9. Computational domain. The porous domain is limited to the central part, of length $5l$ and height l.

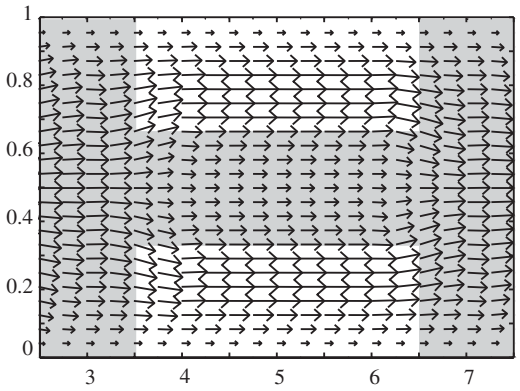

Figure 10. Velocity vectors within the porous domain of length $5l$. The grey part represents a porous material, the white ones an empty domain.

with porous material of arbitrary value $\alpha = 100$ for $2.5 < x < 7.5$ except for two regions verifying

$$x \in]3.5, 6.5[\quad \text{and} \quad y \in]0, \tfrac{1}{3}[\cup]\tfrac{2}{3}, 1[$$

where empty medium is assumed, see white region in Figure 10.

Details of the IPM velocity result in the porous domain are shown in Figure 10, demonstrating the capability of the IPM formulation for the solution of these problem types. As expected, the two empty regions divert the flow away from the center of the channel: the flow tends to go into the empty domains, with higher velocities than the porous region.

6. CONCLUDING REMARKS

Two discontinuous Galerkin (DG) formulations with solenoidal approximation for the simulation of incompressible flow are proposed, with application to the Stokes equation. Following the methodology of the interior penalty method (IPM), and considering a solenoidal and irrotational decomposition of the interpolation space, an efficient DG formulation for the computation of velocities and hybrid pressures (pressures along the element sides) is developed. Moreover, the introduction of a penalty parameter for the weak enforcement of continuity of the normal velocity along element sides leads to an alternative DG formulation where the computation of velocities and pressures is completely decoupled. This second formulation coincides with the formulation

DOI: 10.1002/fld

proposed in [13] and allows to compute the velocity field with no presence of pressure terms; the pressure field can then be obtained as a post-process of the velocity solution.

Numerical experiments demonstrate the applicability of the proposed methods, with optimal convergence rates under h-refinement. The effect of the penalty parameter is also analyzed: as usual in IPM formulations, a penalty of order h^{-1} provides optimal results, whereas the non-consistent penalty in the second formulation must be of order h^{-k}, with k the degree of the approximation. Thus, for large engineering computations this second formulation represents an important save in the number of degrees of freedom in front of the IPM or alternative formulations, but as usual in non-consistent penalty formulations, it may lead to ill-conditioned systems of equations. Moreover, for the same discretization the IPM provides more accurate pressure results than the second formulation.

REFERENCES

1. Crouzeix M, Raviart P-A. Conforming and nonconforming finite element methods for solving the stationary Stokes equations. I. *Revue Française d'Automatique Informatique Recherche Opérationnelle, Série Rouge* 1973; **7**(R-3):33–75.
2. Griffiths DF. An approximately divergence-free 9-node velocity element (with variations) for incompressible flows. *International Journal for Numerical Methods in Fluids* 1981; **1**(4):323–346.
3. Gunzburger MD. *Finite Element Methods for Viscous Incompressible Flows. A Guide to Theory, Practice, and Algorithms*. Academic Press: Boston, MA, 1989.
4. Cockburn B. Discontinuous Galerkin methods for computational fluid dynamics. In *Encyclopedia of Computational Mechanics, vol. 3. Fluids*, Chapter 4, Stein E, de Borst R, Hughes TJR (eds). Wiley: Chichester, 2004; 91–127.
5. Baker GA, Jureidini WN, Karakashian OA. Piecewise solenoidal vector fields and the Stokes problem. *SIAM Journal on Numerical Analysis* 1990; **27**(6):1466–1485.
6. Cockburn B, Gopalakrishnan J. Incompressible finite elements via hybridization. Part I: The Stokes system in two space dimensions. *SIAM Journal on Numerical Analysis* 2005; **43**(4):1627–1650.
7. Toselli A. *hp* discontinuous Galerkin approximations for the Stokes problem. *Mathematical Models and Methods in Applied Sciences* 2002; **12**(11):1565–1597.
8. Karakashian OA, Jureidini WN. A nonconforming finite element method for the stationary Navier–Stokes equations. *SIAM Journal on Numerical Analysis* 1998; **35**(1):93–120.
9. Carrero J, Cockburn B, Schötzau D. Hybridized globally divergence-free LDG methods. Part I: The Stokes problem. *Mathematics of Computation* 2006; **75**:533–563.
10. Cockburn B, Kanschat G, Schötzau D. A note on discontinuous Galerkin divergence-free solutions of the Navier–Stokes equations. *Journal on Scientific Computing* 2007; **31**(1–2):61–73.
11. Arnold DN. An interior penalty finite element method with discontinuous elements. *SIAM Journal on Numerical Analysis* 1982; **19**(4):742–760.
12. Hansbo A, Hansbo P. A finite element method for the simulation of strong and weak discontinuities in solid mechanics. *Computer Methods in Applied Mechanics and Engineering* 2004; **193**(33–35):3523–3540.
13. Hansbo P, Larson MG. Piecewise divergence-free discontinuous Galerkin methods for stokes flow. *Communications in Numerical Methods in Engineering* 2006; DOI: 10.1002/cnm.975.
14. Hansbo P, Larson MG. Discontinuous Galerkin methods for incompressible and nearly incompressible elasticity by Nitsche's method. *Computer Methods in Applied Mechanics and Engineering* 2002; **191**(17–18):1895–1908.
15. Hansbo A, Hansbo P. An unfitted finite element method, based on Nitsche's method, for elliptic interface problems. *Computer Methods in Applied Mechanics and Engineering* 2002; **191**(47–48):5537–5552.
16. Mozolevsky I, Süri E, Bösing PR. Discontinuous Galerkin finite element approximations of the two-dimensional Navier–Stokes equations in stream-function formulation. *Communications in Numerical Methods in Engineering* 2007; **23**(6):447–459.
17. Arnold DN, Brezzi F, Cockburn B, Marini LD. Unified analysis of discontinuous Galerkin methods for elliptic problems. *SIAM Journal on Numerical Analysis* 2002; **39**(5):1749–1779.
18. Babuska I. The finite element method with penalty. *Mathematics of Computation* 1973; **27**:221–228.

19. Brezzi F, Fortin M. *Mixed and Hybrid Finite Element Methods*. Springer: Berlin, 1991.
20. Prudhomme S, Pascal F, Oden J, Romkes A. High-order accurate time-stepping schemes for convection–diffusion problems. *Technical Report 00-27*, TICAM, Austin, TX, 2000.
21. Okkels F, Olesen L, Bruus H. Applications of topology optimization in the design of micro- and nanofluidic systems. *Technical Proceedings of the 2005 NSTI Nanotechnology Conference and Trade Show*, Anaheim, CA, 2005; 575–578.

Int. J. Numer. Meth. Fluids 2008; **57**:1071–1092
DOI: 10.1002/fld

Discontinuous Galerkin methods for the Navier-Stokes equations using solenoidal approximations

A. Montlaur, S. Fernández-Méndez and A. Huerta

International Journal for Numerical Methods in Fluids,

Accepted for publication, 2009

INTERNATIONAL JOURNAL FOR NUMERICAL METHODS IN FLUIDS
Int. J. Numer. Meth. Fluids 2007; **00**:1–19 *Prepared using* fldauth.cls *[Version: 2002/09/18 v1.01]*

Discontinuous Galerkin methods for the Navier-Stokes equations using solenoidal approximations

A. Montlaur[1,2], S. Fernandez-Mendez[1,3], J. Peraire[4] and A. Huerta[1,3i]

[1] *Laboratori de Càlcul Numèric (LaCàN), www-lacan.upc.edu*
Universitat Politècnica de Catalunya
Jordi Girona 1-3, 08034 Barcelona, Spain
[2] *Escola Politècnica Superior de Castelldefels*
[3] *E.T.S. d'Enginyers de Camins, Canals i Ports de Barcelona*
[4] *Aerospace Computational Design Laboratory, Department of Aeronautics and Astronautics*
Massachusetts Institute of Technology, Cambridge, MA 02139, USA

SUMMARY

An Interior Penalty Method and a Compact Discontinuous Galerkin method are proposed and compared for the solution of the steady incompressible Navier-Stokes equations. Both compact formulations can be easily applied using high-order piecewise divergence-free approximations, leading to two uncoupled problems: one associated to velocity and hybrid pressure, and the other one only concerned with the computation of pressures in the elements interior. Numerical examples compare efficiency and accuracy of both proposed methods. Copyright © 2007 John Wiley & Sons, Ltd.

KEY WORDS: Compact Discontinuous Galerkin; Interior Penalty Method; Navier-Stokes; high-order; solenoidal; incompressible; hybrid pressure

1. INTRODUCTION

Recently several authors have focused their attention on *Discontinuous Galerkin* (DG) formulations for computational fluid dynamics [1], and in particular for incompressible flow. Divergence-free high-order approximations are easily defined within a DG framework for incompressible problems. Namely, a divergence-free polynomial base is considered in each element. The divergence-free approach induces an important decrement in the number of degrees of freedom with the corresponding reduction in computational cost. Following this idea, in [2, 3, 4, 5, 6] Stokes equations are solved using a decomposition of the approximation

[i]Correspondence to: Departament de Matemàtica Aplicada III, E.T.S. Ingenieros de Caminos, Universitat Politècnica de Catalunya, Jordi Girona 1, E-08034 Barcelona, Spain. e-mail: antonio.huerta@upc.edu

Contract/grant sponsor: Ministerio de Educación y Ciencia; contract/grant number: BIA2007-66965 and DPI2007-62395

Contract/grant sponsor: Generalitat de Catalunya AGAUR; contract/grant number: 2005SGR917

Received
Revised

space for the velocity field as direct sum of a solenoidal space and an irrotational space. This allows to split the DG weak form in two uncoupled problems: the first one solves for velocities and hybrid pressures (pressure along the mesh sides/faces) and the second one allows the computation of pressure in the interior of the elements.

Many DG methods have recently been developed in the framework of computational fluid dynamics, such as the Local Discontinuous Galerkin (LDG) method [7], the Compact Discontinuous Galerkin (CDG) method [8], or the Interior Penalty Method (IPM) [6]. LDG proposes a mixed formulation with vorticity, velocity and pressure. Lifting operators are introduced to substitute vorticity, thus leading to a velocity-pressure formulation. LDG has been successfully analyzed and applied to Stokes, Oseen and Navier-Stokes equations, see for instance [7]. However, one major drawback of LDG is the loss of compactness due to the introduction of lifting factors. That is, the LDG stencil goes beyond immediate neighbors, in front of the usual DG stencil where degrees of freedom in one element are connected only to those in the neighboring elements. To avoid this loss of compactness, Compact Discontinuous Galerkin (CDG) was introduced in [8] with application to elliptic problems. CDG is very similar to LDG but it eliminates coupling between degrees of freedom of non-neighboring elements by means of alternative local lifting operators. Another possible compact formulation is obtained when using an Interior Penalty Method (IPM), which was first introduced by Arnold [9] for second-order parabolic equations. An IPM with piecewise solenoidal approximation is proposed for the solution of incompressible Stokes equations in [6].

IPM and CDG have many points in common, both methods inducing compact formulations and leading to symmetric and coercive bilinear forms for self-adjoint operators. Nevertheless, one of the most remarkable differences is that the IPM formulation does not involve lifting operators, leading to a much simpler and straight-forward implementation, with a non-negligible reduction in computational cost. To further compare these methods, IPM and CDG formulations are derived in this paper for the solution of the incompressible Navier-Stokes equations. For IPM, the rationale proposed in [6] in the context of Stokes equations is extended to Navier-Stokes equations. The CDG formulation is derived following the basis of the method for elliptic problems presented in [8]. Both compact formulations can be easily applied using high-order piecewise divergence-free approximations.

The contributions of this paper are presented as follows. The DG formulations for the solution of the incompressible Navier-Stokes equations, with Dirichlet and Neumann boundary conditions, are presented in Section 2.2 for IPM, and in Section 2.3 for CDG. Particularization of the two weak forms with a splitting of the velocity space into solenoidal and irrotational parts is detailed in Section 2.4. Numerical tests show the applicability of both methodologies (IPM and CDG) and compare their accuracy in Section 3.

2. THE NAVIER-STOKES PROBLEM AND TWO ALTERNATIVE FORMULATIONS

2.1. Problem statement and definitions

Let $\Omega \subset \mathbb{R}^{\mathtt{n_{sd}}}$ be an open bounded domain, with boundary $\partial\Omega$, and $\mathtt{n_{sd}}$ the number of spatial dimensions. The strong form for the homogeneous steady incompressible Navier-Stokes

problem can be written as:

$$-2\boldsymbol{\nabla}\cdot(\nu\boldsymbol{\nabla}^{\mathtt{S}}\boldsymbol{u})+\boldsymbol{\nabla}p+(\boldsymbol{u}\cdot\boldsymbol{\nabla})\boldsymbol{u}=\boldsymbol{f} \qquad \text{in } \Omega \tag{1a}$$

$$\boldsymbol{\nabla}\cdot\boldsymbol{u}=0 \qquad \text{in } \Omega \tag{1b}$$

$$\boldsymbol{u}=\boldsymbol{u}_D \qquad \text{on } \Gamma_D \tag{1c}$$

$$-p\boldsymbol{n}+2\nu(\boldsymbol{n}\cdot\boldsymbol{\nabla}^{\mathtt{S}})\boldsymbol{u}=\boldsymbol{t} \qquad \text{on } \Gamma_N \tag{1d}$$

where $\partial\Omega=\overline{\Gamma}_D\cup\overline{\Gamma}_N$, $\Gamma_D\cap\Gamma_N=\emptyset$, $\boldsymbol{f}\in\mathcal{L}_2(\Omega)$ is a source term, $\boldsymbol{u}$ is the flux velocity and p its pressure, ν is the kinematic viscosity, $\boldsymbol{n}$ is the exterior unit normal vector, and $\boldsymbol{\nabla}^{\mathtt{S}}=\frac{1}{2}(\boldsymbol{\nabla}+\boldsymbol{\nabla}^T)$. In (1a), the constant density has been absorbed into the pressure.

Moreover, suppose that Ω is partitioned in $\mathtt{n_{el}}$ disjoint subdomains Ω_i,

$$\overline{\Omega}=\bigcup_{i=1}^{\mathtt{n_{el}}}\overline{\Omega}_i,\quad \Omega_i\cap\Omega_j=\emptyset \text{ for } i\neq j,$$

with piecewise linear boundaries $\partial\Omega_i$, which define an internal interphase Γ

$$\Gamma:=\Big[\bigcup_{i=1}^{\mathtt{n_{el}}}\partial\Omega_i\Big]\backslash\partial\Omega.$$

The *jump* $[\![\cdot]\!]$ and *mean* $\{\cdot\}$ operators are defined along the interface Γ using values from the elements to the left and to the right of the interface (say, Ω_i and Ω_j) and are also extended along the exterior boundary (only values in Ω are employed), namely

$$[\![\circledcirc]\!]=\begin{cases}\circledcirc_i+\circledcirc_j & \text{on } \Gamma,\\ \circledcirc & \text{on } \partial\Omega,\end{cases}\quad\text{and}\quad \{\circledcirc\}=\begin{cases}\kappa_i\,\circledcirc_i+\kappa_j\circledcirc_j & \text{on } \Gamma,\\ \circledcirc & \text{on } \partial\Omega.\end{cases}$$

Usually $\kappa_i=\kappa_j=1/2$ but, in general, these two scalars are only required to verify $\kappa_i+\kappa_j=1$, see for instance [10]. The major difference between the mean and the jump operator is that the latter always involves the normal to the interface or to the domain. For instance, given two contiguous subdomains Ω_i and Ω_j their exterior unit normals are denoted respectively $\boldsymbol{n}_i$ and $\boldsymbol{n}_j$ (recall that $\boldsymbol{n}_i=-\boldsymbol{n}_j$) and along $\partial\Omega$ the exterior unit normal is denoted by $\boldsymbol{n}$; the jump is then

$$[\![p\,\boldsymbol{n}]\!]=\begin{cases}p_i\,\boldsymbol{n}_i+p_j\,\boldsymbol{n}_j=\boldsymbol{n}_i(p_i-p_j) & \text{on } \Gamma\\ p\,\boldsymbol{n} & \text{on } \partial\Omega\end{cases}$$

for scalars, see [6] for vectors or tensors.

The following discrete finite element spaces are also introduced

$$\boldsymbol{\mathcal{V}}^h=\{\boldsymbol{v}\in[\mathcal{L}_2(\Omega)]^{\mathtt{n_{sd}}}\ ;\ \boldsymbol{v}|_{\Omega_i}\in[\mathcal{P}^k(\Omega_i)]^{\mathtt{n_{sd}}}\quad\forall\Omega_i\}$$
$$\mathcal{Q}^h=\{q\in[\mathcal{L}_2(\Omega)]\ ;\ q|_{\Omega_i}\in[\mathcal{P}^{k-1}(\Omega_i)]\quad\forall\Omega_i\}$$

where $\mathcal{P}^k(\Omega_i)$ is the space of polynomial functions of degree at most $k\geq 1$ in Ω_i.

Finally, in the following equations $\big(\cdot,\cdot\big)$ denotes the $\mathcal{L}_2$ scalar product in Ω, that is

$$\big(p,q\big)=\int_\Omega p\,q\,d\Omega \qquad \text{for scalars,}$$

$$\big(\boldsymbol{u},\boldsymbol{v}\big) = \int_\Omega \boldsymbol{u}\cdot\boldsymbol{v}\,d\Omega \qquad \text{for vectors,}$$
$$\big(\boldsymbol{\sigma},\boldsymbol{\tau}\big) = \int_\Omega \boldsymbol{\sigma}:\boldsymbol{\tau}\,d\Omega \qquad \text{for second order tensors.}$$

Analogously, $\big(\cdot,\cdot\big)_\Upsilon$ denotes the $\mathcal{L}_2$ scalar product in any domain $\Upsilon \subset \Gamma \cup \partial\Omega$. For instance,

$$\big(p,q\big)_\Upsilon = \int_\Upsilon p\,q\,d\Gamma$$

for scalars.

2.2. Interior Penalty Method

Here, the Interior Penalty approach presented in [6] for the Stokes equations, is extended to the Navier-Stokes equations. The weak form containing the nonlinear convection becomes, find $\boldsymbol{u}_h \in \boldsymbol{\mathcal{V}}^h$ and $p_h \in \mathcal{Q}^h$ such that

$$\begin{aligned} a_{\mathtt{IP}}\big(\boldsymbol{u}_h,\boldsymbol{v}\big) + c\big(\boldsymbol{u}_h;\boldsymbol{u}_h,\boldsymbol{v}\big) + b\big(\boldsymbol{v},p_h\big) + \big(\{p_h\},[\![\boldsymbol{n}\cdot\boldsymbol{v}]\!]\big)_{\Gamma\cup\Gamma_D} &= l_{\mathtt{IP}}\big(\boldsymbol{v}\big) \qquad \forall\,\boldsymbol{v}\in\boldsymbol{\mathcal{V}}^h,\\ b\big(\boldsymbol{u}_h,q\big) + \big(\{q\},[\![\boldsymbol{n}\cdot\boldsymbol{u}_h]\!]\big)_{\Gamma\cup\Gamma_D} &= \big(q,\boldsymbol{n}\cdot\boldsymbol{u}_D\big)_{\Gamma_D} \qquad \forall\,q\in\mathcal{Q}^h, \end{aligned} \tag{2}$$

where the following forms must be defined,

$$\begin{aligned} a_{\mathtt{IP}}\big(\boldsymbol{u},\boldsymbol{v}\big) := \big(2\nu\boldsymbol{\nabla}^{\mathtt{S}}\boldsymbol{u},\boldsymbol{\nabla}^{\mathtt{S}}\boldsymbol{v}\big) + C_{11}\big([\![\boldsymbol{n}\otimes\boldsymbol{u}]\!],[\![\boldsymbol{n}\otimes\boldsymbol{v}]\!]\big)_{\Gamma\cup\Gamma_D}\\ - \big(2\nu\{\boldsymbol{\nabla}^{\mathtt{S}}\boldsymbol{u}\},[\![\boldsymbol{n}\otimes\boldsymbol{v}]\!]\big)_{\Gamma\cup\Gamma_D} - \big([\![\boldsymbol{n}\otimes\boldsymbol{u}]\!],2\nu\{\boldsymbol{\nabla}^{\mathtt{S}}\boldsymbol{v}\}\big)_{\Gamma\cup\Gamma_D}, \end{aligned} \tag{3a}$$

$$l_{\mathtt{IP}}\big(\boldsymbol{v}\big) := \big(\boldsymbol{f},\boldsymbol{v}\big) + \big(\boldsymbol{t},\boldsymbol{v}\big)_{\Gamma_N} + C_{11}\big(\boldsymbol{u}_D,\boldsymbol{v}\big)_{\Gamma_D} - \big(\boldsymbol{n}\otimes\boldsymbol{u}_D,2\nu\boldsymbol{\nabla}^{\mathtt{S}}\boldsymbol{v}\big)_{\Gamma_D}, \tag{3b}$$

$$\begin{aligned} c\big(\boldsymbol{w};\boldsymbol{u},\boldsymbol{v}\big) := -\big((\boldsymbol{w}\cdot\boldsymbol{\nabla})\boldsymbol{v},\boldsymbol{u}\big) + \sum_{i=1}^{\mathtt{n_{el}}}\int_{\partial\Omega_i\setminus\Gamma_N}\frac{1}{2}\left[(\boldsymbol{w}\cdot\boldsymbol{n}_i)(\boldsymbol{u}^{ext}+\boldsymbol{u}) - |\boldsymbol{w}\cdot\boldsymbol{n}_i|\,(\boldsymbol{u}^{ext}-\boldsymbol{u})\right]\cdot\boldsymbol{v}d\Gamma\\ + \int_{\Gamma_N}(\boldsymbol{w}\cdot\boldsymbol{n})\boldsymbol{u}\cdot\boldsymbol{v}d\Gamma, \end{aligned} \tag{4a}$$

and

$$b\big(\boldsymbol{v},p\big) := -\int_\Omega q\,\boldsymbol{\nabla}\cdot\boldsymbol{v}\,d\Omega. \tag{4b}$$

The penalty parameter, a positive scalar C_{11} of order $\mathcal{O}(h^{-1})$, must be large enough to ensure coercivity of the bilinear form $a_{\mathtt{IP}}\big(\cdot,\cdot\big)$, see [6]. The characteristic mesh size is denoted by h. A standard upwind numerical flux, see for instance [11], is used for the definition of the convective term $c\big(\cdot;\cdot,\cdot\big)$. In (4a), $\boldsymbol{u}^{ext}$ denotes the exterior trace of $\boldsymbol{u}$ taken over the side/face under consideration, that is

$$\boldsymbol{u}^{ext}(\boldsymbol{x}) = \lim_{\varepsilon\to 0^+}\boldsymbol{u}(\boldsymbol{x}+\varepsilon\boldsymbol{n}_i) \qquad \text{for } \boldsymbol{x}\in\partial\Omega_i.$$

2.3. Compact Discontinuous Galerkin formulation

This section shows the application of CDG to the solution of the Navier-Stokes equations. As usual in CDG [8], two local lifting operators are defined on interior and Dirichlet sides/faces. For $\Gamma_e \subset \Gamma \cup \Gamma_D$, the lifting $r^e : [\mathcal{L}_2(\Gamma_e)]^{\mathtt{n}_{\mathtt{sd}}^2} \to \boldsymbol{\Sigma}^h$ is defined by

$$\int_\Omega r^e(\boldsymbol{\sigma}) : \boldsymbol{\tau}\, d\Omega = \int_{\Gamma_e} \boldsymbol{\sigma} : \{\boldsymbol{\tau}\} d\Gamma \quad \forall \boldsymbol{\tau} \in \boldsymbol{\Sigma}^h, \tag{5}$$

where $\boldsymbol{\Sigma}^h = \{\boldsymbol{\tau} \in [\mathcal{L}_2(\Omega)]^{\mathtt{n}_{\mathtt{sd}}^2} \ ; \ \boldsymbol{\tau}|_{\Omega_i} \in [\mathcal{P}^k(\Omega_i)]^{\mathtt{n}_{\mathtt{sd}}^2} \ i = 1, \ldots, \mathtt{n}_{\mathtt{el}}\}$. The second lifting, $s^e : [\mathcal{L}_2(\Gamma_e)]^{\mathtt{n}_{\mathtt{sd}}} \to \boldsymbol{\Sigma}^h$, is such that $s^e(\boldsymbol{v}) = \mathbf{0}\ \forall \boldsymbol{v} \in [\mathcal{L}_2(\Gamma_e)]^{\mathtt{n}_{\mathtt{sd}}}$ for $\Gamma_e \subset \Gamma_D$, and is defined by

$$\int_\Omega s^e(\boldsymbol{v}) : \boldsymbol{\tau}\, d\Omega = \int_{\Gamma_e} \boldsymbol{v} \cdot [\![\boldsymbol{n} \cdot \boldsymbol{\tau}]\!] d\Gamma \quad \forall \boldsymbol{\tau} \in \boldsymbol{\Sigma}^h,$$

for all interior sides $\Gamma_e \subset \Gamma$.

The extension of CDG to Navier-Stokes equations combines the rationale detailed in [8] for the second-order differential operators and the one proposed in [7, 12] for the first order ones. The CDG scheme becomes: find $\boldsymbol{u}_h \in \boldsymbol{\mathcal{V}}^h$ and $p_h \in \mathcal{Q}^h$ such that

$$\begin{aligned} a_{\mathtt{CDG}}(\boldsymbol{u}_h, \boldsymbol{v}) + c(\boldsymbol{u}_h; \boldsymbol{u}_h, \boldsymbol{v}) + b(\boldsymbol{v}, p_h) + \big(\{p_h\}, [\![\boldsymbol{n} \cdot \boldsymbol{v}]\!]\big)_{\Gamma \cup \Gamma_D} &= l_{\mathtt{CDG}}(\boldsymbol{v}) \qquad \forall\, \boldsymbol{v} \in \boldsymbol{\mathcal{V}}^h, \\ b(\boldsymbol{u}_h, q) + \big(\{q\}, [\![\boldsymbol{n} \cdot \boldsymbol{u}_h]\!]\big)_{\Gamma \cup \Gamma_D} &= \big(q, \boldsymbol{n} \cdot \boldsymbol{u}_D\big)_{\Gamma_D} \quad \forall\, q \in \mathcal{Q}^h, \end{aligned} \tag{6}$$

where the forms $c(\cdot;\cdot,\cdot)$ and $b(\cdot,\cdot)$ are already defined in (4), and the two new forms are

$$\begin{aligned} a_{\mathtt{CDG}}(\boldsymbol{u}, \boldsymbol{v}) := a_{\mathtt{IP}}(\boldsymbol{u}, \boldsymbol{v}) &- \big(2\nu \boldsymbol{C}_{12} \otimes [\![\boldsymbol{n} \cdot \boldsymbol{\nabla}^{\mathtt{S}} \boldsymbol{v}]\!], [\![\boldsymbol{n} \otimes \boldsymbol{u}]\!]\big)_\Gamma - \big(2\nu \boldsymbol{C}_{12} \otimes [\![\boldsymbol{n} \cdot \boldsymbol{\nabla}^{\mathtt{S}} \boldsymbol{u}]\!], [\![\boldsymbol{n} \otimes \boldsymbol{v}]\!]\big)_\Gamma \\ &+ \sum_{\Gamma_e \subset \Gamma \cup \Gamma_D} \Big(2\nu \big(r^e([\![\boldsymbol{n} \otimes \boldsymbol{u}]\!]) + s^e(\boldsymbol{C}_{12} \cdot [\![\boldsymbol{n} \otimes \boldsymbol{u}]\!])\big), r^e([\![\boldsymbol{n} \otimes \boldsymbol{v}]\!]) + s^e(\boldsymbol{C}_{12} \cdot [\![\boldsymbol{n} \otimes \boldsymbol{v}]\!])\Big) \end{aligned} \tag{7a}$$

$$l_{\mathtt{CDG}}(\boldsymbol{v}) := l_{\mathtt{IP}}(\boldsymbol{v}) + \sum_{\Gamma_e \subset \Gamma_D} \Big(2\nu\, r^e(\boldsymbol{n} \otimes \boldsymbol{v}), r^e(\boldsymbol{n} \otimes \boldsymbol{u}_D)\Big) \tag{7b}$$

being $a_{\mathtt{IP}}(\cdot,\cdot)$ and $l_{\mathtt{IP}}(\cdot)$ the IPM forms defined in (3). The CDG forms have two parameters, C_{11} and $\boldsymbol{C}_{12}$. The former, C_{11}, as in IPM, is a non-negative parameter of order $\mathcal{O}(h^{-1})$. The latter, is an additional vector, $\boldsymbol{C}_{12} \in \mathbb{R}^{\mathtt{n}_{\mathtt{sd}}}$, which is defined for each interior side/face of the domain according to

$$\boldsymbol{C}_{12} = \frac{1}{2}(S_{ij}\boldsymbol{n}_i + S_{ji}\boldsymbol{n}_j)$$

where $S_{ij} \in \{0, 1\}$ denotes the switch associated with element Ω_i on the side/face that element Ω_i shares with element Ω_j. There are several possible choices of the switches, always satisfying $S_{ij} + S_{ji} = 1$, see [8, 13] for details.

Remark 1. *In CDG, $C_{11} = 0$ may be considered on Γ, see [8]. However, on the Dirichlet boundary it must be positive, $C_{11} > 0$, to treat properly boundary conditions.*

Remark 2. *Lifting operators in CDG are associated to individual sides/faces, and therefore there are no connectivities between non-neighbor elements. This is also the case for IPM, but not for LDG, see [8], as can be seen in Figure 1. IPM and CDG never connect non-neighboring elements, whereas LDG may connect some non-neighboring elements.*

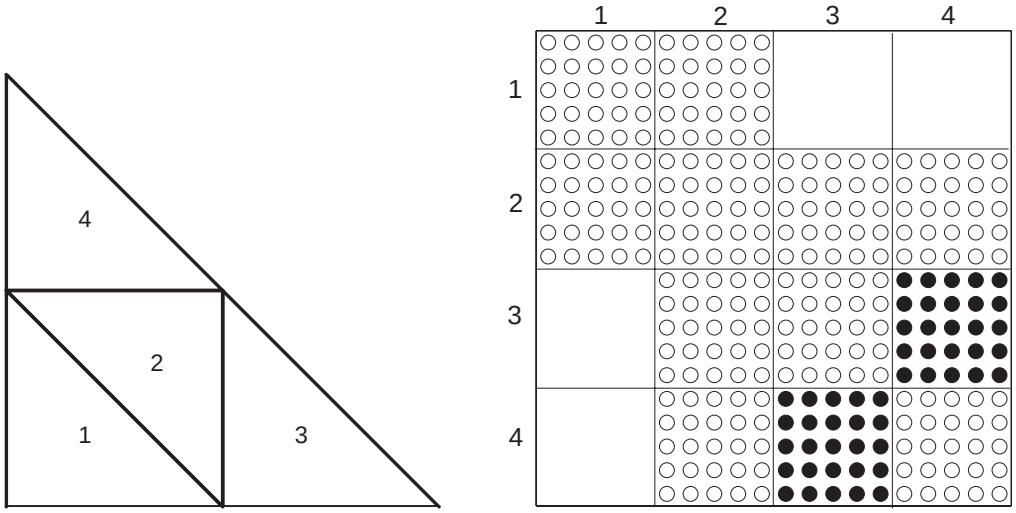

Figure 1. Sparsity structure of the diffusion matrix for four triangles with quadratic velocity. IPM and CDG (∘) are both compact in the sense that they only connect neighboring triangles, whereas LDG (∘ and •) is non-compact and connects some non-neighboring triangles (3 and 4).

Remark 3. *It is worth noting that the CDG weak form can be written as the IPM weak form plus some extra terms, mainly involving CDG lifting operators, see equations* (6) *and* (7)*. The implementation of these extra lifting terms in CDG requires computing several elemental matrices, matrix inversions and products, for every side/face (see Appendix I.1). Thus, in addition to the implementation effort, lifting terms represent a clearly non-negligible increase in the computational cost relative to IPM. This is also the case for transient problems and implies a non-negligible burden mostly for explicit time integrators. Auxiliary variables for the liftings have to be stored and computed (solving linear systems of equations in each element) at every time step.*

2.4. DG formulations with solenoidal approximations

Following [3, 2, 4, 6], the velocity space $\boldsymbol{\mathcal{V}}^h$ is split into direct sum of a solenoidal part and an irrotational part $\boldsymbol{\mathcal{V}}^h = \boldsymbol{\mathcal{S}}^h \oplus \boldsymbol{\mathcal{I}}^h$, where

$$\boldsymbol{\mathcal{S}}^h = \left\{ \boldsymbol{v} \in [\mathcal{H}^1(\Omega)]^{\mathtt{n_{sd}}} \mid \boldsymbol{v}|_{\Omega_i} \in [\mathcal{P}^k(\Omega_i)]^{\mathtt{n_{sd}}},\ \boldsymbol{\nabla} \cdot \boldsymbol{v}|_{\Omega_i} = 0 \text{ for } i = 1, \dots, \mathtt{n_{el}} \right\},$$
$$\boldsymbol{\mathcal{I}}^h \subset \left\{ \boldsymbol{v} \in [\mathcal{H}^1(\Omega)]^{\mathtt{n_{sd}}} \mid \boldsymbol{v}|_{\Omega_i} \in [\mathcal{P}^k(\Omega_i)]^{\mathtt{n_{sd}}},\ \boldsymbol{\nabla} \times \boldsymbol{v}|_{\Omega_i} = \boldsymbol{0} \text{ for } i = 1, \dots, \mathtt{n_{el}} \right\}.$$

For instance, a solenoidal base in a 2D triangle for an approximation of degree $k = 2$ is

$$\boldsymbol{\mathcal{S}}^h = \left\langle \begin{pmatrix} 1 \\ 0 \end{pmatrix}, \begin{pmatrix} 0 \\ 1 \end{pmatrix}, \begin{pmatrix} 0 \\ x \end{pmatrix}, \begin{pmatrix} x \\ -y \end{pmatrix}, \begin{pmatrix} y \\ 0 \end{pmatrix}, \begin{pmatrix} 0 \\ x^2 \end{pmatrix}, \begin{pmatrix} 2xy \\ -y^2 \end{pmatrix}, \begin{pmatrix} x^2 \\ -2xy \end{pmatrix}, \begin{pmatrix} y^2 \\ 0 \end{pmatrix} \right\rangle, \tag{8}$$

and an irrotational base for $k = 2$ is

$$\boldsymbol{\mathcal{I}}^h = \left\langle \begin{pmatrix} x \\ 0 \end{pmatrix}, \begin{pmatrix} x^2 \\ 0 \end{pmatrix}, \begin{pmatrix} 0 \\ y^2 \end{pmatrix} \right\rangle,$$

see for example [3] for the construction of these basis.

Under these circumstances, the IPM problem (2) can be split in two *uncoupled* problems. The first one solves for *divergence-free* velocities and *hybrid pressures*: find $\boldsymbol{u}_h \in \boldsymbol{\mathcal{S}}^h$ and $\tilde{p}_h \in \boldsymbol{P}^h$ solution of

$$\begin{cases} a_{\mathtt{IP}}(\boldsymbol{u}_h, \boldsymbol{v}) + c(\boldsymbol{u}_h; \boldsymbol{u}_h, \boldsymbol{v}) + \left(\tilde{p}_h, [\![\boldsymbol{n}\cdot\boldsymbol{v}]\!]\right)_{\Gamma\cup\Gamma_D} = l_{\mathtt{IP}}(\boldsymbol{v}) & \forall \boldsymbol{v} \in \boldsymbol{\mathcal{S}}^h, \\ \left(\tilde{q}, [\![\boldsymbol{n}\cdot\boldsymbol{u}_h]\!]\right)_{\Gamma\cup\Gamma_D} = \left(\tilde{q}, \boldsymbol{n}\cdot\boldsymbol{u}_D\right)_{\Gamma_D} & \forall \tilde{q} \in \boldsymbol{P}^h, \end{cases} \tag{9}$$

with the forms defined in (3) and (4).

The space of hybrid pressures (pressures along the sides in 2D or faces in 3D) is simply:

$$\boldsymbol{P}^h := \left\{ \tilde{p} \mid \tilde{p} : \Gamma \cup \Gamma_D \longrightarrow \mathbb{R} \ \text{ and } \ \tilde{p} = [\![\boldsymbol{n}\cdot\boldsymbol{v}]\!] \ \text{ for some } \ \boldsymbol{v} \in \boldsymbol{\mathcal{S}}^h \right\}. \tag{10}$$

In fact, reference [2] demonstrates that $\boldsymbol{P}^h$ corresponds to piecewise polynomial pressures in the element sides in 2D or faces in 3D.

The second problem, which requires the solution of the previous one, evaluates the "interior" pressures: find $p_h \in \mathcal{Q}^h$ such that

$$b(\boldsymbol{v}, p_h) = l_{\mathtt{IP}}(\boldsymbol{v}) - a_{\mathtt{IP}}(\boldsymbol{u}_h, \boldsymbol{v}) - \left(\tilde{p}_h, [\![\boldsymbol{n}\cdot\boldsymbol{v}]\!]\right)_{\Gamma\cup\Gamma_D} - c(\boldsymbol{u}_h; \boldsymbol{u}_h, \boldsymbol{v}) \quad \forall \boldsymbol{v} \in \boldsymbol{\mathcal{I}}^h. \tag{11}$$

It is important to note that equation (11) can be solved element by element and pressure is its only unknown.

Analogously, using the velocity space decomposition $\boldsymbol{\mathcal{V}}^h = \boldsymbol{\mathcal{S}}^h \oplus \boldsymbol{\mathcal{I}}^h$, the CDG scheme proposed in (6) is also split in two uncoupled problems. For instance, the first problem for CDG is: find $\boldsymbol{u}_h \in \boldsymbol{\mathcal{S}}^h$ and $\tilde{p}_h \in \boldsymbol{P}^h$ solution of

$$\begin{cases} a_{\mathtt{CDG}}(\boldsymbol{u}_h, \boldsymbol{v}) + c(\boldsymbol{u}_h; \boldsymbol{u}_h, \boldsymbol{v}) + \left(\tilde{p}_h, [\![\boldsymbol{n}\cdot\boldsymbol{v}]\!]\right)_{\Gamma\cup\Gamma_D} = l_{\mathtt{CDG}}(\boldsymbol{v}) & \forall \boldsymbol{v} \in \boldsymbol{\mathcal{S}}^h, \\ \left(\tilde{q}, [\![\boldsymbol{n}\cdot\boldsymbol{u}_h]\!]\right)_{\Gamma\cup\Gamma_D} = \left(\tilde{q}, \boldsymbol{n}\cdot\boldsymbol{u}_D\right)_{\Gamma_D} & \forall \tilde{q} \in \boldsymbol{P}^h, \end{cases} \tag{12}$$

with the forms defined in (7).

A major advantage of solenoidal spaces is the reduction in the number of degrees of freedom (dof) for the DG solution. Table I and Figure 2 show the number of dof for a typical finite element mesh corresponding to a continuous Galerkin (cG) discretization, a discontinuous Galerkin nodal interpolation (DG), and a discontinuous Galerkin solenoidal approximation (DGS).

	2D	3D
cG	$\frac{3}{2}k^2 + \frac{1}{2}k$	$\frac{2}{3}k^3 + \frac{1}{2}k^2 + \frac{1}{3}k$
DG	$\frac{3}{2}k^2 + \frac{7}{2}k + 2$	$\frac{2}{3}k^3 + \frac{7}{2}k^2 + \frac{35}{6}k + 3$
DGS	$\frac{1}{2}k^2 + 4k + 2$	$\frac{1}{3}k^3 + \frac{7}{2}k^2 + \frac{37}{6}k + 3$

Table I. Comparison of total number of dof, divided by the number of elements, for a typical finite element mesh corresponding to a continuous Galerkin (cG) discretization, a discontinuous Galerkin nodal interpolation (DG), and a discontinuous Galerkin solenoidal approximation (DGS), with order k for velocity and $k-1$ for pressure, in $2D$ and $3D$.

Some hypothesis have been taken to obtain the formulas in Table I. For a typical k^{th} order continuous Galerkin finite element mesh, the number of nodes is approximated by $\frac{1}{2}k^2\mathtt{n_{el}}$ in

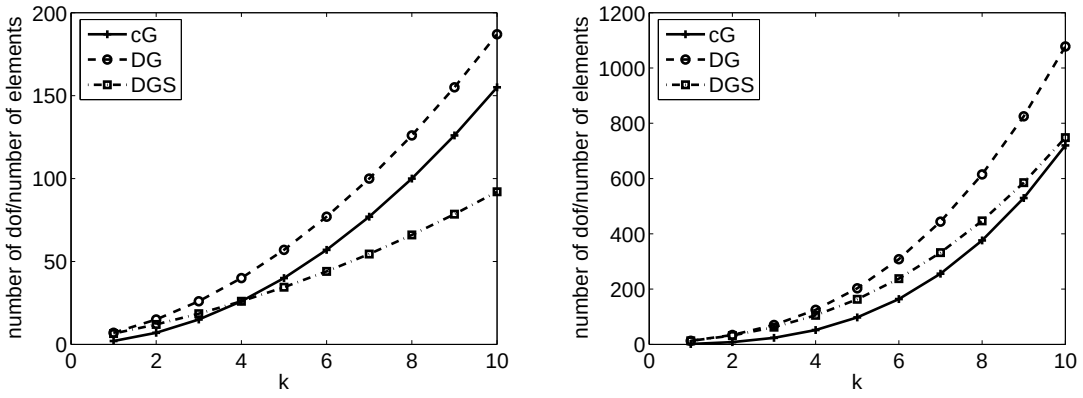

(a) $2D$ (b) $3D$

Figure 2. Comparison of the total number of dof, divided by the number of elements, for a typical finite element mesh corresponding to a continuous Galerkin (cG) discretization, a discontinuous Galerkin nodal interpolation (DG), and a discontinuous Galerkin solenoidal approximation (DGS), in $2D$ (a) and $3D$ (b), with order k for velocity and $k-1$ for pressure.

$2D$, and $\frac{1}{6}k^3\mathtt{n_{el}}$ in 3D, where $\mathtt{n_{el}}$ is the number of elements. In addition, note that for cG and DG, the number of dof for velocities and interior pressures is contemplated, whereas for the DG solenoidal approximation the number of dof for velocities and hybrid pressures is considered. In this case, in order to count the dof for hybrid pressures, the number of sides in a $2D$ finite element mesh is approximated by $\frac{3}{2}\mathtt{n_{el}}$, and the number of faces in a $3D$ mesh is approximated by $2\mathtt{n_{el}}$.

Figure 2 shows the important reduction in dof when using a solenoidal approximation with hybrid pressures in a DG formulation. Moreover, compared with cG, the DG solenoidal approximation leads to less dof in 2D, and to a competitive number of dof in 3D. From the formulas giving the number of dof in Table I other conclusions can also be derived. The coefficient of the leading term in the dof formula is the same for cG and standard DG, and it is greater than the corresponding coefficient for solenoidal DG. Thus, cG and standard DG behave similarly when increasing k, whereas the growth of the number of dof of the solenoidal DG method is much slower.

It is worth mentioning that an additional reduction in the number of dof can be achieved introducing a non-consistent penalty parameter, to weakly enforce continuity of normal velocities along element sides/faces. Following the rationale in [6], alternative DG formulations can be derived, where the computation of velocity and pressure is completely decoupled, with an apparent reduction in computational cost. Nevertheless, as usual in non-consistent penalty formulations, it may lead to ill-conditioned systems of equations, see [6] for details.

3. NUMERICAL EXAMPLES

IPM and CDG with solenoidal approximation are compared for the steady incompressible Navier-Stokes equations in this section. In all examples, a structured mesh of triangles is used,

with interpolation of order k and $k-1$ for velocity and pressure respectively.

3.1. Condition number of the diffusion matrix

The influence of the C_{11} parameter on the condition number of the diffusion matrix — the discretization of the bilinear form $a_{\texttt{CDG}}(\cdot,\cdot)$ for CDG or $a_{\texttt{IP}}(\cdot,\cdot)$ for IPM — is studied next. Figure 3 shows the evolution of the condition number for a regular structured mesh with $h = 1/8$ and degree $k = 4$.

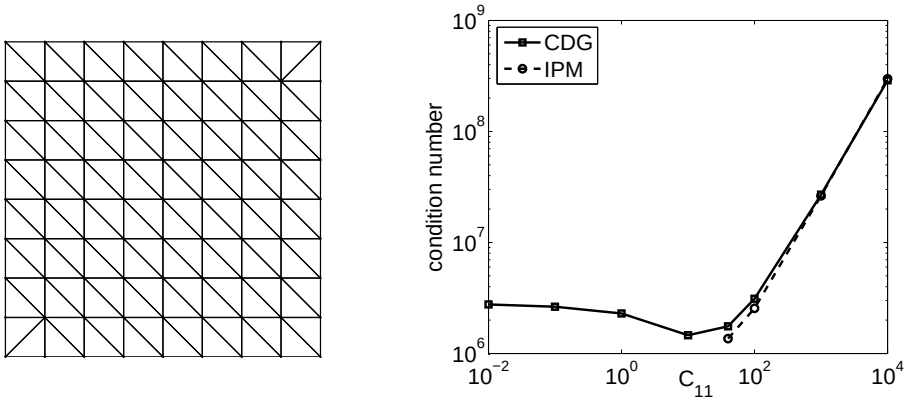

Figure 3. Structured mesh for $h = 1/8$ and dependency of the condition number of the diffusion matrix on the stabilization parameter C_{11}, for CDG and IPM, with a fourth order approximation of the velocity ($k = 4$).

For $C_{11} \geq 40h^{-1}$, i.e for C_{11} large enough to ensure coercivity of the IPM bilinear form, similar condition numbers are obtained with both methods. Figure 3 also shows that CDG (and it would also be the case for LDG) allows to choose a value of C_{11} as small as wanted, see [8]. Nevertheless, the condition number is rather constant for small value of C_{11}, and the minimum value of the condition number is more or less the same for CDG and for IPM. Thus, the flexibility of CDG for the choice of C_{11} does not imply any advantage in front of IPM for the conditioning of the matrix.

3.2. Driven cavity example

A standard benchmark test for the Navier-Stokes equations is now considered. A plane flow of an isothermal fluid in a lid-driven cavity is modelled in a 2D square domain $\Omega =]0,1[\times]0,1[$, with zero body force and one moving wall. A continuous velocity

$$\boldsymbol{u} = \begin{cases} (10x, 0)^T & \text{for } 0 \leq x \leq 0.1 \\ (1, 0)^T & \text{for } 0.1 \leq x \leq 0.9 \\ (10 - 10x, 0)^T & \text{for } 0.9 \leq x \leq 1 \end{cases}$$

is imposed on the exterior upper boundary $\{y = 1\}$, and a zero velocity $\boldsymbol{u} = (0, 0)^T$ is enforced on the three other sides.

Figure 4 shows the velocity streamlines, which fit to the expected solution. The main vortex moves toward the center of the cavity for increasing Reynolds number, both CDG and IPM

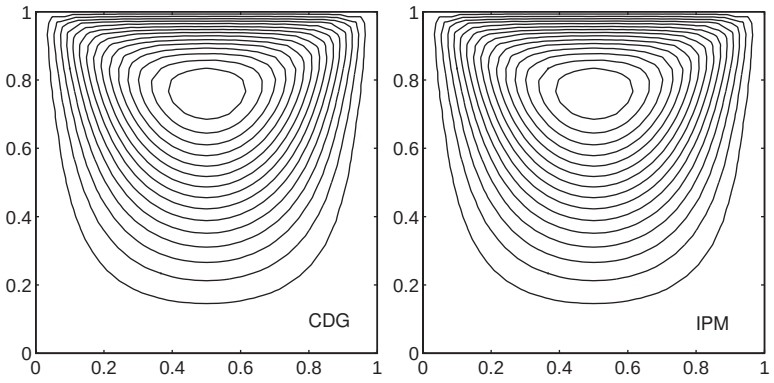

(a) $Re = 1$

(b) $Re = 400$

Figure 4. Velocity streamlines for CDG (left) and IPM (right), for $Re = 1$ (a) and $Re = 400$ (b), $k = 2$, $h = 0.0667$, $C_{11} = 10h^{-1}$.

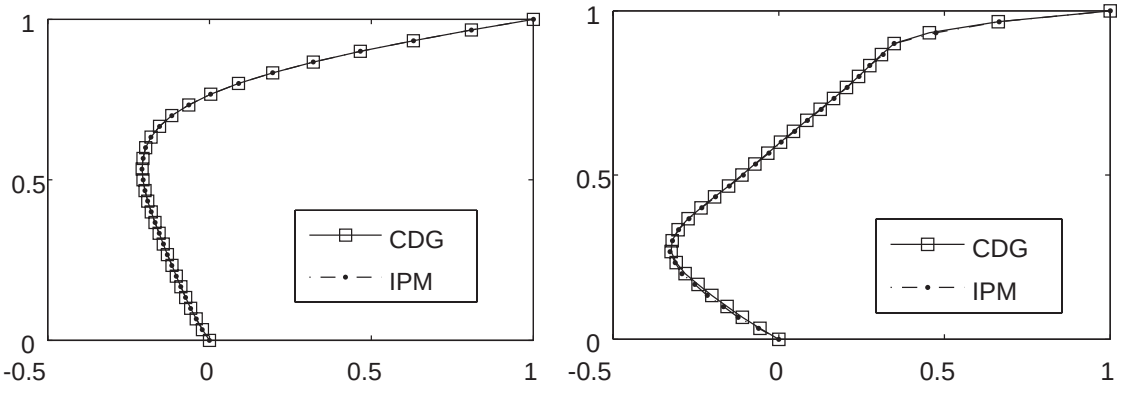

(a) $Re = 1$

(b) $Re = 400$

Figure 5. Velocity profiles at the vertical centerline for CDG and IPM, for $Re = 1$ (a) and $Re = 400$ (b), $k = 2$, $h = 0.0667$, $C_{11} = 10h^{-1}$.

giving very similar results. To further compare them, velocity profiles at the vertical centerline are shown in Figure 5 for $Re = 1$, 400. First, it can be noticed that as the Reynolds number increases, the boundary layers are more obvious and the variations in the velocity are sharper. Second, results for CDG and IPM are again almost identical. To compare more precisely the accuracy of both methods, an analytical example is taken in the next section.

3.3. Analytical example

An example with analytical solution is considered next. The steady incompressible Navier-Stokes equations are solved in a 2D square domain $\Omega =]0,1[\times]0,1[$ with Dirichlet boundary conditions on three sides, and Neumann boundary condition on the fourth side $\{x = 0\}$. A body force

$$\boldsymbol{f} = \begin{pmatrix} -4\nu(-1+2y)(y^2-6xy^2+6x^2y^2-y+6xy-6x^2y+3x^2-6x^3+3x^4) \\ +1-2x+4x^3y^2(2y^2-2y+1)(y-1)^2(-1+2x)(x-1)^3 \\ 4\nu(-1+2x)(x^2-6x^2y+6x^2y^2-x+6xy-6xy^2+3y^2-6y^3+3y^4) \\ +4x^2y^3(-1+2y)(y-1)^3(2x^2-2x+1)(x-1)^2 \end{pmatrix}$$

is imposed in order to have the polynomial exact solution

$$\boldsymbol{u} = \begin{pmatrix} x^2(1-x)^2(2y-6y^2+4y^3) \\ -y^2(1-y)^2(2x-6x^2+4x^3) \end{pmatrix},$$

$$p = x(1-x).$$

Fourth order approximation for velocity and cubic approximation for pressure (i.e. $k = 4$) are considered.

The influence of C_{11} on the accuracy of CDG is analyzed. Figure 6 shows the results for velocity, hybrid pressure and interior pressure $\mathcal{L}_2$-errors with $hC_{11} = 1, 10, 40$ and $C_{11}^* = 0$, which denotes $C_{11} = 0$ on interior faces and $C_{11} = h^{-1}$ on the Dirichlet boundary, see Remark 1. Optimal convergence is obtained in all cases, with similar accuracy, though larger values $C_{11} = 10h^{-1}$ or $C_{11} = 40h^{-1}$ give slightly worse results for velocity and hybrid pressure errors, but slightly better results for pressure error.

CDG and IPM are compared from an accuracy point of view in Figure 7. $C_{11} = 40h^{-1}$ is considered for both methods. Note that, as seen in Figure 6, $C_{11} = 40h^{-1}$ provides accurate results for CDG, and it is also close to the minimum value that ensures coercivity of the IPM bilinear form. With this selection of C_{11}, similar results are obtained: both methods reach optimal convergence rates for velocity and hybrid pressure, with similar accuracy.

4. CONCLUSIONS

An IPM and a CDG formulation for solving the steady incompressible Navier-Stokes equations are proposed. Both methods can be easily applied using high-order piecewise divergence-free approximations, leading to two uncoupled problems: one for velocities and hybrid pressures, and one for an element-by-element computation of pressure in the interior of the elements.

Although both formulations are derived from different rationales, CDG can be written as the IPM formulation plus some extra terms, some of them related to lifting operators. These

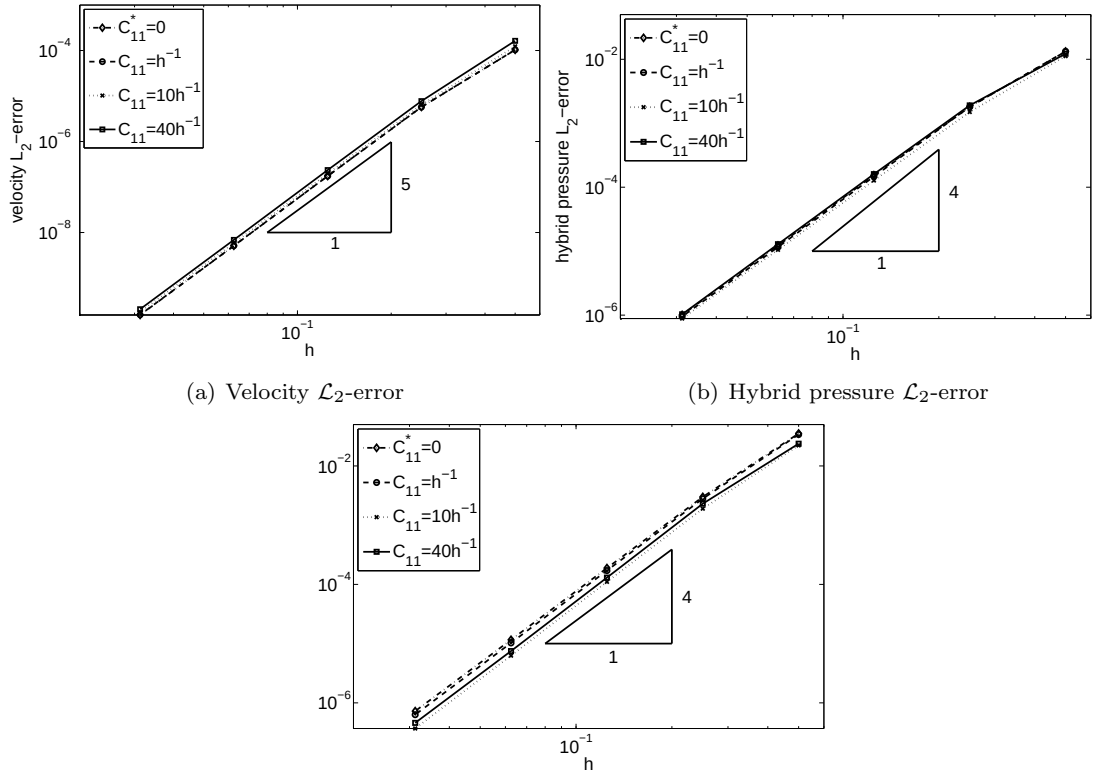

(a) Velocity $\mathcal{L}_2$-error

(b) Hybrid pressure $\mathcal{L}_2$-error

(c) Interior pressure $\mathcal{L}_2$-error

Figure 6. Comparison of $\mathcal{L}_2$-errors obtained with CDG for different values of C_{11}, for a fourth order approximation of the velocity and a cubic interpolation of hybrid and interior pressures.

extra terms allow more flexibility in the choice of the C_{11} parameter, which can even be set as $C_{11} = 0$ for all internal sides/faces in CDG, whereas it has to be taken big enough in the whole domain to ensure coercivity of the bilinear form of IPM.

Though the bilinear form of CDG introduces more terms, the stencil is the same in both methods, and both formulations present the major advantage –relative to LDG for example– that they are compact formulations: degrees of freedom of one element are only connected to those of immediate neighbors.

Numerical experiments reveal that IPM and CDG present similar results for the condition number of the diffusion matrix, and for the accuracy of the numerical solution, both reaching optimal convergence rates for velocity and pressure.

Thus, the main differences between both methods are that CDG is less sensitive to the selection of the penalty parameter (tuning of C_{11} is almost eliminated), but it has the major disadvantage of the implementation and computation of the lifting operators. That is, IPM leads to a simpler and straight-forward implementation, avoiding the extra computational cost associated to CDG or LDG liftings.

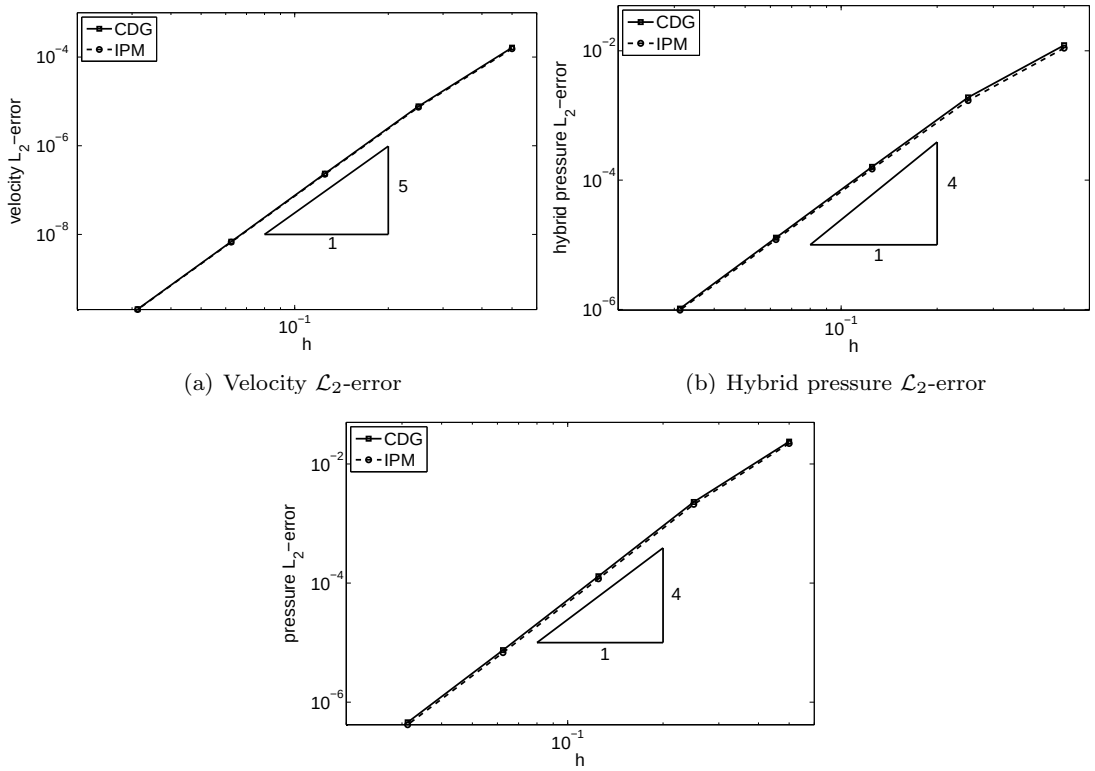

(a) Velocity $\mathcal{L}_2$-error

(b) Hybrid pressure $\mathcal{L}_2$-error

(c) Interior pressure $\mathcal{L}_2$-error

Figure 7. Comparison of $\mathcal{L}_2$-errors obtained with CDG and IPM, for a fourth order approximation of the velocity and a cubic interpolation of hybrid and interior pressures, with $C_{11} = 40h^{-1}$.

APPENDIX

I.1. Implementation of lifting operators

CDG introduces the concept of lifting operators, whose implementation is not trivial. As an example, the discretization of the lifting product $\int_\Omega r^e([\![\boldsymbol{n} \otimes \boldsymbol{u}]\!]) : r^e([\![\boldsymbol{n} \otimes \boldsymbol{v}]\!])d\Omega$ in (7a) is commented next.

In the following, solenoidal vector functions are discretized in each element Ω_k (for $k = 1, \ldots, \mathtt{n_{el}}$) with a solenoidal vector basis $\boldsymbol{\phi}_i^k$ (see section 2.4) as

$$\boldsymbol{v} = \sum_{i=1}^{\mathtt{n_{bf}}} \boldsymbol{\phi}_i^k \mathrm{v}_i^k \quad \text{in } \Omega_k$$

with some scalar coefficients v_i^k, where $\mathtt{n_{bf}}$ is the number of basis functions in each element. The solenoidal discrete space in Ω_k is denoted as $\boldsymbol{\mathcal{S}}(\Omega_k) :=< \boldsymbol{\phi}_i^k >_{i=1}^{\mathtt{n_{bf}}}$. The corresponding space of tensor functions is $\boldsymbol{\nabla^{\mathtt{S}}\mathcal{S}}(\Omega_k)$, and therefore, a tensor $\boldsymbol{\tau} \in \boldsymbol{\nabla^{\mathtt{S}}\mathcal{S}}(\Omega_k)$ will be expressed as $\boldsymbol{\tau} = \sum_{i=1}^{\mathtt{n_{tf}}} \boldsymbol{\psi}_i^k \boldsymbol{\tau}_i^k$ in Ω_k, with constant vectors $\boldsymbol{\tau}_i^k \in \mathbb{R}$, $\boldsymbol{\psi}_i^k \in \boldsymbol{\nabla^{\mathtt{S}}\mathcal{S}}(\Omega_k)$ and

$\mathtt{n_{tf}} = \dim\left\{\boldsymbol{\nabla}^{\mathtt{S}}\boldsymbol{\mathcal{S}}(\Omega_k)\right\}$. For instance, for $k = 2$ a solenoidal basis is detailed in (8) and a tensor basis of $\boldsymbol{\nabla}^{\mathtt{S}}\boldsymbol{\mathcal{S}}(\Omega_k)$ is

$$\left\langle \begin{pmatrix} 0 & \frac{1}{2} \\ \frac{1}{2} & 0 \end{pmatrix}, \begin{pmatrix} 1 & 0 \\ 0 & -1 \end{pmatrix}, \begin{pmatrix} 0 & x \\ x & 0 \end{pmatrix}, \begin{pmatrix} 2y & x \\ x & -2y \end{pmatrix}, \begin{pmatrix} 2x & -y \\ -y & -2x \end{pmatrix}, \begin{pmatrix} 0 & y \\ y & 0 \end{pmatrix} \right\rangle.$$

Moreover, for every side Γ_e, or face in 3D, $\ell(e,1)$ and $\ell(e,2)$ respectively denote the numbers of the first element (left element) and the second element (right element) sharing the side. Figure 8 shows an example where side Γ_{13} is shared by elements Ω_{37} and Ω_{22}, thus for this side $\ell(13,1) = 37$ and $\ell(13,2) = 22$.

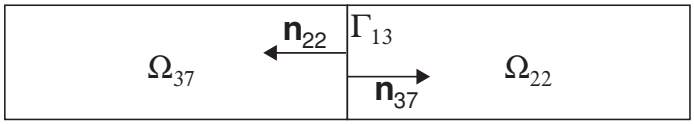

Figure 8. Elements Ω_{37} and Ω_{22} share face Γ_{13}; $\boldsymbol{n}_{37}$ and $\boldsymbol{n}_{22}$ are respectively exterior unit normals to Ω_{37} and Ω_{22}.

In CDG, lifting terms are implemented with a loop in sides (faces in 3D). Thus, let us consider a side $\Gamma_e = \overline{\Omega}_{\ell(e,1)} \cap \overline{\Omega}_{\ell(e,2)}$. The lifting operator associated to side Γ_e, r^e, is zero outside $\Omega_{\ell(e,1)} \cup \Omega_{\ell(e,2)}$. Thus, the lifting term appearing in the bilinear form can be expressed as a sum of integrals in $\Omega_{\ell(e,1)}$ and $\Omega_{\ell(e,2)}$,

$$\begin{aligned}\int_\Omega r^e(\llbracket \boldsymbol{n} \otimes \boldsymbol{u} \rrbracket) : r^e(\llbracket \boldsymbol{n} \otimes \boldsymbol{v} \rrbracket) d\Omega \\ = \int_{\Omega_{\ell(e,1)}} r^e(\llbracket \boldsymbol{n} \otimes \boldsymbol{u} \rrbracket) : r^e(\llbracket \boldsymbol{n} \otimes \boldsymbol{v} \rrbracket) d\Omega + \int_{\Omega_{\ell(e,2)}} r^e(\llbracket \boldsymbol{n} \otimes \boldsymbol{u} \rrbracket) : r^e(\llbracket \boldsymbol{n} \otimes \boldsymbol{v} \rrbracket) d\Omega,\end{aligned}$$

requiring the computation of r^e only in $\Omega_{\ell(e,1)}$ and $\Omega_{\ell(e,2)}$. In fact, given the discontinuous nature of the test functions $\boldsymbol{\tau}$ in (5), the lifting can be computed separately in each one of the two elements. For instance, taking test functions $\boldsymbol{\tau}$ with support in $\Omega_{\ell(e,1)}$, first equation in (5) is particularized as

$$\int_{\Omega_{\ell(e,1)}} r^e(\llbracket \boldsymbol{n} \otimes \boldsymbol{u} \rrbracket) : \boldsymbol{\tau}\, d\Omega = \frac{1}{2} \int_{\Gamma_e} \llbracket \boldsymbol{n} \otimes \boldsymbol{u} \rrbracket : \boldsymbol{\tau} d\Gamma \quad \forall \boldsymbol{\tau} \in \boldsymbol{\nabla}^{\mathtt{S}}\boldsymbol{\mathcal{S}}(\Omega_{\ell(e,1)}), \tag{13}$$

which can be interpreted as a formula for computing the lifting in the first element, i.e $r^e|_{\Omega_{\ell(e,1)}}$. Discretization of (13) leads to the matrix equation

$$\mathbf{M}^{\Omega_{\ell(e,1)}}\, \mathbf{r}_{\boldsymbol{u}}^{e,1} = \mathbf{S}_{11}^e\, \mathbf{u}^{\ell(e,1)} + \mathbf{S}_{21}^e\, \mathbf{u}^{\ell(e,2)} \tag{14}$$

where $\mathbf{u}^{\ell(e,1)}$ and $\mathbf{u}^{\ell(e,2)}$ are vectors containing the coefficients of the interpolation of $\boldsymbol{u}$ in $\Omega_{\ell(e,1)}$ and $\Omega_{\ell(e,2)}$ respectively, $\mathbf{r}_{\boldsymbol{u}}^{e,1}$ is a vector containing the coefficients corresponding to the lifting of $\llbracket \boldsymbol{n} \otimes \boldsymbol{u} \rrbracket$ in the first element, that is

$$r^e(\llbracket \boldsymbol{n} \otimes \boldsymbol{u} \rrbracket) = \sum_{i=1}^{\mathtt{n_{tf}}} \boldsymbol{\psi}_i^{\ell(e,1)} (\mathbf{r}_{\boldsymbol{u}}^{e,1})_i \quad \text{in } \Omega_{\ell(e,1)},$$

and $\mathbf{M}^{\Omega_k}$ (for $k = 1, \ldots, \mathtt{n_{el}}$) and $\mathbf{S}^e_{\alpha\beta}$ (for $\alpha, \beta = 1, 2$) are block matrices given by

$$[\mathbf{M}^{\Omega_k}]_{ij} = \int_{\Omega_k} \boldsymbol{\psi}^k_i : \boldsymbol{\psi}^k_j \, d\Omega, \quad \text{for } i, j = 1 \ldots \mathtt{n_{tf}}$$
$$[\mathbf{S}^e_{\alpha\beta}]_{ij} = \frac{1}{2} \int_{\Gamma_e} \boldsymbol{\psi}^{\ell(e,\beta)}_i : (\boldsymbol{n}_{\ell(e,\alpha)} \otimes \boldsymbol{\phi}^{\ell(e,\alpha)}_j) \, d\Gamma, \quad \text{for } i = 1 \ldots \mathtt{n_{tf}} \text{ and } j = 1 \ldots \mathtt{n_{bf}}.$$

For illustration purposes, note that for the example in Figure 8, exterior normal vectors appearing in the definition of $\mathbf{S}^e_{\alpha\beta}$ are $\boldsymbol{n}_{\ell(e,1)} = \boldsymbol{n}_{37}$ and $\boldsymbol{n}_{\ell(e,2)} = \boldsymbol{n}_{22}$, that is, exterior unit normals to Ω_{37} and Ω_{22} respectively.

Analogously, the lifting in $\Omega_{\ell(e,2)}$ is determined by

$$\mathbf{M}^{\Omega_{\ell(e,2)}} \, \mathbf{r}^{e,2}_{\boldsymbol{u}} = \mathbf{S}^e_{12} \, \mathbf{u}^{\ell(e,1)} + \mathbf{S}^e_{22} \, \mathbf{u}^{\ell(e,2)},$$

where $\mathbf{r}^{e,2}_{\boldsymbol{u}}$ is the vector containing the coefficients corresponding to the lifting $r^e([\![\boldsymbol{n} \otimes \boldsymbol{u}]\!])$ in $\Omega_{\ell(e,2)}$.

Now, using the discretization of the lifting (14), the contribution of the first element $\Omega_{\ell(e,1)}$ to the lifting product appearing in the CDG weak form corresponds to

$$\int_{\Omega_{\ell(e,1)}} r^e([\![\boldsymbol{n} \otimes \boldsymbol{v}]\!]) : r^e([\![\boldsymbol{n} \otimes \boldsymbol{u}]\!]) \, d\Omega = (\mathbf{r}^{e,1}_{\boldsymbol{v}})^T \mathbf{M}^{\Omega_{\ell(e,1)}} \mathbf{r}^{e,1}_{\boldsymbol{u}}$$
$$= \left(\mathbf{S}^e_{11} \, \mathbf{v}^{\ell(e,1)} + \mathbf{S}^e_{21} \, \mathbf{v}^{\ell(e,2)} \right)^T (\mathbf{M}^{\Omega_{\ell(e,1)}})^{-1} \left(\mathbf{S}^e_{11} \, \mathbf{u}^{\ell(e,1)} + \mathbf{S}^e_{21} \, \mathbf{u}^{\ell(e,2)} \right).$$

Finally, following the same derivation for the second element, and summing the contribution of both elements, the lifting product appearing in the CDG weak form for the e-th side Γ_e corresponds to

$$\int_{\Omega} r^e([\![\boldsymbol{n} \otimes \boldsymbol{v}]\!]) : r^e([\![\boldsymbol{n} \otimes \boldsymbol{u}]\!]) \, d\Omega = (\mathbf{v}^{\ell(e,1)})^T \mathbf{K}^e_{11} \mathbf{u}^{\ell(e,1)} + (\mathbf{v}^{\ell(e,1)})^T \mathbf{K}^e_{12} \mathbf{u}^{\ell(e,2)}$$
$$+ (\mathbf{v}^{\ell(e,2)})^T \mathbf{K}^e_{22} \mathbf{u}^{\ell(e,2)} + (\mathbf{v}^{\ell(e,2)})^T (\mathbf{K}^e_{12})^T \mathbf{u}^{\ell(e,1)}$$

with matrices given by

$$\mathbf{K}^e_{\alpha\beta} = (\mathbf{S}^e_{\alpha 1})^T (\mathbf{M}^{\Omega_{\ell(e,1)}})^{-1} \mathbf{S}^e_{\beta 1} + (\mathbf{S}^e_{\alpha 2})^T (\mathbf{M}^{\Omega_{\ell(e,2)}})^{-1} \mathbf{S}^e_{\beta 2}$$

for $\alpha, \beta = 1, 2$.

Thus, implementing a lifting term implies computing three matrices for each face Γ_e, to be assembled in rows and columns corresponding to elements sharing this face, i.e elements (matrix blocks) with indexes $\ell(e,1)$ and $\ell(e,2)$.

Note that computing these matrices involves several elemental matrices, matrix inversions and products, with a clearly non-negligible increase in computational cost. Moreover, for transient problems solved with explicit time integrators, implementing the lifting also represents an important increase in computational cost: auxiliary variables for liftings have to be stored and computed (solving linear systems of equations in each element) at every time step.

REFERENCES

1. B. Cockburn, *Discontinuous Galerkin methods for Computational Fluid Dynamics*, vol. 3 Fluids. Chichester: John Wiley & Sons, 2004.
2. B. Cockburn and J. Gopalakrishnan, "Incompressible finite elements via hybridization. Part I: the Stokes system in two space dimensions," *SIAM J. Numer. Anal.*, vol. 43, no. 4, pp. 1627–1650, 2005.
3. G. A. Baker, W. N. Jureidini, and O. A. Karakashian, "Piecewise solenoidal vector fields and the Stokes problem," *SIAM J. Numer. Anal.*, vol. 27, no. 6, pp. 1466–1485, 1990.
4. J. Carrero, B. Cockburn, and D. Schötzau, "Hybridized globally divergence-free LDG methods. Part I: The Stokes problem," *Math. Comp.*, vol. 75, no. 254, pp. 533–563, 2005.
5. P. Hansbo and M. G. Larson, "Piecewise divergence-free Discontinuous Galerkin methods for Stokes flow," *Commun. Numer. Meth. Eng.*, vol. 24, no. 5, pp. 355–366, 2008.
6. A. Montlaur, S. Fernandez-Mendez, and A. Huerta, "A discontinuous Galerkin method with divergence-free interpolation for the incompressible Stokes equations," *Int. J. Numer. Methods Fluids*, vol. 57, no. 9, pp. 1071–1092, 2008.
7. D. S. B. Cockburn, G. Kanschat, "The local discontinuous Galerkin method for linearized incompressible fluid flow: a review," *Computers and Fluids*, vol. 34, pp. 491–506, 2005.
8. J. Peraire and P.-O. Persson, "The Compact Discontinuous Galerkin (CDG) method for elliptic problems," *SIAM J. Sci. Stat. Comput.*, vol. 30, no. 4, pp. 1806–1824, 2008.
9. D. N. Arnold, "An interior penalty finite element method with discontinuous elements," *SIAM J. Numer. Anal.*, vol. 19, no. 4, pp. 742–760, 1982.
10. A. Hansbo and P. Hansbo, "A finite element method for the simulation of strong and weak discontinuities in solid mechanics," *Comput. Meth. Appl. Mech. Eng.*, vol. 193, no. 33-35, pp. 3523–3540, 2004.
11. G. Kanschat and D. Schötzau, "Energy norm a posteriori error estimation for divergence-free discontinuous Galerkin approximations of the Navier-Stokes equations," *Int. J. Numer. Methods Fluids*, vol. 57, no. 9, pp. 1093 – 1113, 2008.
12. B. Cockburn, G. Kanschat, and D. Schötzau, "A locally conservative LDG method for the incompressible Navier-Stokes equations," *Math. Comp.*, vol. 74, no. 251, pp. 1067–1095, 2005.
13. B. Cockburn, G. Kanschat, I. Perugia, and D. Schötzau, "Superconvergence of the Local Discontinuous Galerkin method for elliptic problems on cartesian grids," *SIAM J. Numer. Anal.*, vol. 39, no. 1, pp. 264–285, 2001.